Molecularly Imprinted Materials—Sensors and Other Devices

Molecularly Imprinted Materials—Sensors and Other Devices

Symposia held April 2–5, 2002, San Francisco, California, U.S.A.

EDITORS (SYMPOSIUM M):

Kenneth J. Shea
University of California at Irvine
Irvine, California, U.S.A.

Mingdi Yan
Portland State University
Portland, Oregon, U.S.A.

M. Joseph Roberts
NAVAIR
China Lake, California, U.S.A.

ORGANIZERS (SYMPOSIUM O):

Paul S. Cremer
Texas A&M University
College Station, Texas, U.S.A.

Richard M. Crooks
Texas A&M University
College Station, Texas, U.S.A.

Michael J. Sailor
University of California at San Diego
La Jolla, California, U.S.A.

20021122 002

|M|R|S|

Materials Research Society
Warrendale, Pennsylvania

Single article reprints from this publication are available through
University Microfilms Inc., 300 North Zeeb Road, Ann Arbor, Michigan 48106

CODEN: MRSPDH

Published by:

Manufactured in the United States of America

CONTENTS

SYMPOSIUM M

SYNTHESIS AND
CHARACTERIZATION

MICROFABRICATION AND
SILICA IMPRINTING

*Invited Paper

*Invited Paper

SYMPOSIUM O

SENSOR ARRAYS AND DEVICES

SENSING WITH NANOPARTICLES

SENSING WITH BILAYERS, CELLS, AND POLYMERS

SENSING WITH SILICON

PREFACE

This symposium proceedings contains papers presented at Symposium M, "Molecularly Imprinted Materials," and Symposium O, "Chemical and Biological Sensors—Materials and Devices," held April 2-5 at the 2002 MRS Spring Meeting in San Francisco, California.

Symposium M was the first of its kind at a Materials Research Society Meeting. The symposium consisted of 17 talks and 15 posters and brought together a number of scientists in the field to discuss the current state of the art in molecular imprinting. Topics included microfabrication, imprinted membranes and nanoparticles, covalent and non-covalent methods of molecular imprinting, separate technology, and sensor applications.

Symposium O contained 45 presentations that covered topics that included microfluidics and sensing systems, sensor arrays and devices, sensing with nanoparticles, monolayers, bilayers, cells, and silicon.

Kenneth J. Shea
Mingdi Yan
M. Joseph Roberts

September 2002

ACKNOWLEDGMENTS

MATERIALS RESEARCH SOCIETY SYMPOSIUM PROCEEDINGS

MATERIALS RESEARCH SOCIETY SYMPOSIUM PROCEEDINGS

Prior Materials Research Society Symposium Proceedings available by contacting Materials Research Society

SYMPOSIUM M

Synthesis and Characterization

Development of Improved Crosslinking Monomers for Molecularly Imprinted Materials.

David A. Spivak and Martha Sibrian-Vazquez
Department of Chemistry
Louisiana State University
Baton Rouge, LA 70803

ABSTRACT

Molecular imprinting involves the self-assembled complexation of a substrate to functional monomers to form a pre-polymer complex which is "locked-in" to place by copolymerization with an excess of crosslinking monomer. Removal of the template leaves binding or catalytic sites that are complementary in size, shape, and functionality to the template. Most of the research in molecularly imprinted materials has focused on choice of substrate or functional monomer of the pre-polymer complex. The cross-linking monomers have primarily been EGDMA or DVB, which are commercially available. Redirecting focus on the design of crosslinking monomers for molecular imprinting, we have developed new classes of crosslinked polymers to optimize the performance of molecularly imprinted polymers. The design of the new crosslinking monomers has followed two strategies: (1) development of new crosslinked materials for formation of the supporting matrix, and (2) development of crosslinking monomers that simultaneously serve as the functional monomer. The details of the design, synthesis, polymerization and performance of these new crosslinking monomers for molecularly imprinted polymers will be reported.

INTRODUCTION

Currently, cross-linking monomers for molecularly imprinted polymers (MIPs) have primarily been EGDMA or DVB, which are commercially available.[1-2] One benefit of using these monomers is that they are inexpensive and readily available in large quantities. This is important for applications that would require large amounts of material such as industrial catalytic reactors or separations on the industrial scale. However, many future applications of imprinted polymers are envisioned in the fields of microfabricated sensors and microseparations that will only require small amounts of material. Therefore, economic price considerations of the imprinting materials is less of a concern. Instead, materials with the best performance possible are the target for microfabricated and nanofabricated devices.

Most of the research in molecularly imprinted materials has focused on choice of substrate or functional monomer of the pre-polymer complex. However, approximately 80-90% of the imprinted polymers are composed of the crosslinking monomer, with the remaining 10-20% comprised of functional monomer. The large percentage of crosslinking monomer materials in imprinted polymers affords the possibility of a commensurate improvement in polymer properties. Redirecting focus on the design of crosslinking monomers for molecular imprinting, we have developed new classes of crosslinked polymers to optimize the performance of molecularly imprinted polymers.

EXPERIMENTAL DETAILS

Preparation of Dansyl-L-phenylalanine imprinted polymer using novel crosslinking monomer N,O-bismethacryloyl ethanolamine (NOBE). The following procedure was used for imprinted polymers employing the new cross-linking monomers. In a 13 x 100 mm test tube, (0.064g, 0.16 mmol) of dansyl-L-phenylalanine was dissolved in 1.5 mL of ACN. To this solution was added (1.3g, 6.6 mmol) of **NOBE**, (0.113g, 1.32 mmol) of MAA, and (0.021g, 0.13 mmol) of AIBN. For comparison to traditionally formulated imprinted polymers, another polymer was imprinted using the formulation above, substituting EGDMA as the crosslinking monomer. The solution was purged by bubbling nitrogen gas into the mixture for 5 minutes, then capped and sealed with teflon tape and parafilm. The samples were inserted into a photochemical turntable reactor (ACE Glass Inc.) which was immersed in a constant temperature bath. A standard laboratory UV light source (a Canrad-Hanovia medium pressure 450 W mercury arc lamp) jacketed in a borosilicate double-walled immersion well was placed at the center of the turntable. The polymerization was initiated photochemically at 20°C and the temperature maintained by both the cooling jacket surrounding the lamp and the constant temperature bath holding the entire apparatus. The polymerization was allowed to proceed for 10 h, then used for chromatographic experiments.

Preparation of S-(-)-nicotine imprinted polymer using functionalized crosslinking monomer N,O-bismethacryloyl aspartic acid (NOAA). In a borosilicate scintillation vial, (0.0454g, 0.28 mmol) of S-(+)-Nicotine was dissolved in 0.95 mL methylene chloride. To this solution was added (0.991g, 5.0 mmol) EGDMA, (0.135g, 0.53 mmol) of functional monomer **NOAA**, and (0.105g, 0.64 mmol) AIBN. The control polymer was formulated in a similar fashion, without introduction of a template molecule. For comparison to traditionally formulated imprinted polymers, another polymer was imprinted using the formulation above, only substituting (0.045g, 0.53 mmol) methacrylic acid (MAA) in place of the aspartic acid functional monomer. The solution was purged by bubbling nitrogen gas into the mixture for 5 minutes, then capped and sealed with teflon tape and parafilm. The samples were inserted into a photochemical turntable reactor (ACE Glass Inc.) which was immersed in a constant temperature bath. A standard laboratory UV light source (a Canrad-Hanovia medium pressure 450 W mercury arc lamp) jacketed in a borosilicate double-walled immersion well was placed at the center of the turntable. The polymerization was initiated photochemically at 20°C and the temperature maintained by both the cooling jacket surrounding the lamp and the constant temperature bath holding the entire apparatus. The polymerization was allowed to proceed for 10 h, then used for chromatographic experiments.

Chromatographic Experiments. The polymers were ground using a mortar and pestle, the particles were sized using U.S.A. Standard Testing Sieves (VWR), and the fraction between 20-25 µm was collected. The particles were slurry packed, using a Beckman 1108 Solvent Delivery Module, into stainless steel columns (length, 7.5 cm, i.d. 2.1 mm) to full volume for chromatographic experiments. The polymers were then washed on line for 12 hours using acetonitrile/acetic acid: 90/10, at a flow rate of 0.1 mL/min to remove the template. HPLC analyses were performed isocratically at room temperature (21°C) using a Hitachi L-7100 pump

with a Hitachi L-7400 detector. The flow rate, UV detector wavelength, substrate and substrate concentration are provided with the tables in the text. The void volume was determined using acetone as an inert substrate. The separation factors (α) were measured as the ratio of capacity factors (k'_S/k'_R). The capacity factors were determined by the relation $k' = (R_v - D_v) / D_v$, where R_v is the retention volume of the substrate, and D_v is the void volume.

DISCUSSION

Two types of novel crosslinking monomers are currently being investigated by our lab. First, crosslinking monomers are used for copolymerization of the pre-polymer complex forming the the required highly-crosslinked network polymer. In this case, the crosslinker provides the matrix material that holds the functional monomers provided in place. Wulff and coworkers have shown that maximization of crosslinker improves the quality of imprinted polymers. This often leads to finding a balance between crosslinker and non-crosslinking functional monomers, in order to optimize the performance of imprinted polymers. Too much of one or the other can lead to undesirable results. Therefore, it is postulated that properties of molecularly imprinted materials could be enhanced by combining the crosslinking and functional properties needed into one monomer. This is the second type of monomer format currently being investigated by our laboratory.

An example of the first type of monomer is N,O-bismethacryloyl ethanolamine (**NOBE**), shown in figure 1. The structure of this monomer is similar to the commonly used ethyleneglycol dimethacrylate (**EGDMA**); however, it incorporates an acrylamide group instead of a methacrylate group that may provide different binding interactions with template molecules, and different polymer morphology characteristics.
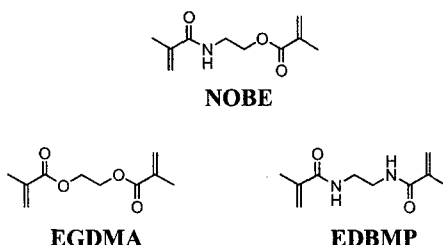
NOBE

EGDMA **EDBMP**

Figure 1. Example of crosslinking monomers: **NOBE** = novel crosslinking monomer N,O-bismethacryloyl ethanolamine; **EGDMA** = ethylene glycol dimethacrylate; **EDBMP** = N,N'-1,2 ethanediylbis(2-methyl-2-propenamide).

Furthermore, **NOBE** is soluble in non-polar organic solvents such as acetonitrile and chloroform or methylene chloride, versus the similar **EDBMP** reported in the literature to be insoluble in these solvents.[3] To test the performance of **NOBE**, polymers were imprinted with Dansyl-L-phenylalanine as illustrated in scheme 1, with chloroform as the solvent. An HPLC column
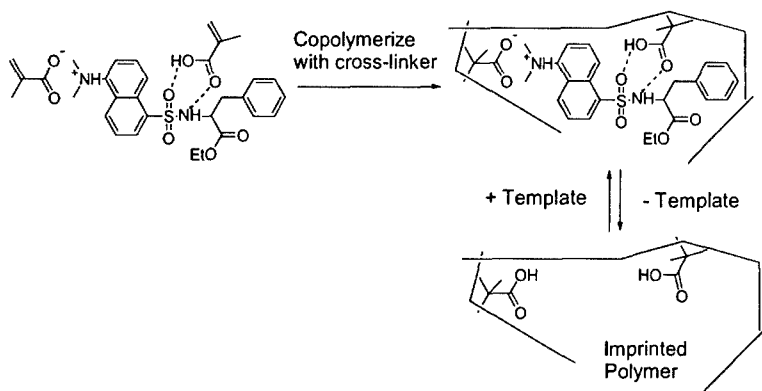
Scheme 1. Outline of strategy for imprinting Dansyl-L-phenylalanine.

made with this polymer was compared to a column made with **EGDMA** under the same conditions, and the results are shown in table 1. The new crosslinking monomer provided polymers with increased binding affinity versus polymers formed with **EGDMA**, verified by the large increase in capacity factors. More important, increased chiral selectivity was seen under these conditions for the L enantiomer of Dansylphenylalanine, versus the D enantiomer.

Table 1. Binding data for Dansyl-L-phenylalanine imprinted polymers.[*]

Entry	Crosslinking Monomer	k'_L	k'_D	α
1	**NOBE**	1.5	0.8	1.9
2	**EGDMA**	0.1	0.1	1.0

[*] Mobile phase = 99/1: MeCN/HOAc, flow rate = 1.0 mL/min, substrate samples consisted of 5 μL injections of a 0.1 mM Dansyl-L-phe substrate concentration, detection at λ = 330 nm.

An example of the second type of monomer is N,O-bismethacryloyl aspartic acid (**NOAA**) shown in figure 2. Inspired by proteins in nature that are responsible for molecular recognition and catalysis, functional crosslinking monomer **NOAA** was designed based on the amino acid aspartic acid. Polymers were synthesized using both the **NOAA** functional monomer and with the traditionally employed methacrylic acid (**MAA**) for comparison. Polymers were imprinted

8
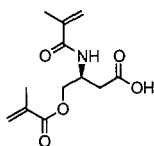
NOAA

Figure 2. Example of a functionalized crosslinking monomer, N,O-bismethacryloyl aspartic acid (**NOAA**).

with the naturally occuring S enantiomer of nicotine as the template, and the results for binding of both enantiomers of nicotine are shown in table 2. Looking at the table, enantioselectivity is enhanced by almost an order of magnitude for polymer made with functional monomer **NOAA** versus traditional methacrylic acid (**MAA**) functionalized polymers. The increase is postulated to arise primarily from using a crosslinking carboxylic acid functional monomer versus the non-crosslinking methacrylic acid, with minor enhancement to binding from the amide moiety as precedented by the **NOBE** data above.

Table 2. Binding data for S-(-)-nicotine imprinted polymers.[*]

Entry	Crosslinking Monomer	k'_S	k'_R	α
1	**NOAA**	4.0	0.2	20.0
2	**MAA**	0.7	0.2	3.5

[*] Mobile phase = 99/1: MeCN/HOAc, flow rate = 0.1 mL/min, substrate samples consisted of 10 μL injections of a 1.0 S-(-)-nicotine substrate concentration, detection at λ = 262 nm.

In addition to increased crosslinking, the polymers made with the new monomers more closely resemble protein matrices that perform molecular recognition functions seen in enzymes and antibodies, which may account for increased binding characteristics. The increased performance of these new materials is anticipated to improve the role of imprinted polymers for sensors, catalysts and separation science.

REFERENCES

1. B. Sellergren, Ed., *Molecularly Imprinted Polymers. Man-Made Mimics of Antibodies and their Application in Analytical Chemistry* (Elsevier Science, Amsterdam, The Netherlands, 2000).

2. G. Wulff, Angew. Chem. Int. Ed. **34**, 1812 (1995).

3. Shea, K.J., Stoddard, G.J., Shavelle, D.M., Wakui, F., Choate, R.M., Macromolecules, **23**, 4497 (1990).

M1.3

Molecularly Imprinted Polymers (MIPs) Against Uracils : Functional Monomer Design, Monomer-Template Interactions In Solution And MIP Performance In Chromatography

Andrew J. Hall[1], Panagiotis Manesiotis, Jakob T. Mossing and Börje Sellergren
Institut für Anorganische Chemie und Analytische Chemie, Johannes Gutenberg-Universität,
Duesbergweg 10-14, D-55099 Mainz, Germany.

ABSTRACT

The interaction of N^1-substituted uracils (cyclohexyl (1) and benzyl (2)) with three polymerisable recognition elements, the novel monomers 9-(3/4-vinylbenzyl)adenine (3) and 2,6-diamino-9-(3/4-vinylbenzyl)purine (4) and the previously synthesised monomer 2,6-bis(acrylamido)pyridine (5), has been studied via ^{1}H NMR in deuterio-chloroform solution. MIPs against (2) have been prepared using each of the monomers and tested in the chromatographic mode. The effect of the number and type of hydrogen bonds formed between the templates and the functional monomers is reflected in the values of the apparent association constants obtained from the solution study and by the performance of the subsequently prepared MIPs in the chromatographic mode.

INTRODUCTION

Interest in molecularly imprinted polymers (MIPs) has burgeoned in recent years [1]. The imprinting of nucleic acid bases and related compounds has attracted particular interest [2]. A survey of this literature shows that much MIP research has focused on the use of commercially available functional monomers, e.g. methacrylic acid, to create the binding sites in such non-covalent MIPs [3]. Among the exceptions is the use of 2,6-bis(acrylamido)pyridine (5) as a functional monomer for the imprinting of alloxan, where the selectivity of the MIP over the non-imprinted polymer (NIP) with respect to the recognition of thymine was also assessed [4]. Here, the ability of the monomer to form multiple hydrogen-bond interactions with substrate molecules was stressed. The same group has also recently reported the use of (5) as functional monomer in the imprinting of 5-fluorouracil [5].

We now wish to report the preparation of the novel monomers 9-(3/4-vinylbenzyl) adenine (3) and 2,6-diamino-9-(3/4-vinylbenzyl)purine (4) and their ability to form hydrogen-bonded complexes with uracils. As a comparison, the previously reported functional monomer (5) has also been studied. Adenine is, of course, the base-pair partner of thymine in nucleic acids and so (3) could be expected to participate in hydrogen-bonding interactions with uracil molecules. The additional amino- function in (4) should lead to stronger association with uracils (1) and (2) by virtue of the potential extra hydrogen-bond interaction. The association of uracils with (5) has been studied to explore the difference between the amido- and amino-functionalities.
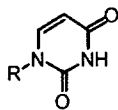
(1) R = cyclohexyl
(2) R = benzyl
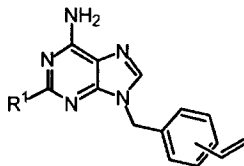
(3) R^1 = H
(4) R^1 = NH_2
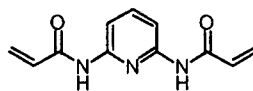
(5)

EXPERIMENTAL

(1) was purchased from Sigma, while **(2)** and 1,3-(dibenzyl)uracil were prepared *via* a published procedure [6]. Uracil and thymine were purchased from Acros, while AZT was purchased from Sigma.

Novel monomer **(3)** was synthesised in 45% yield *via* the reaction of adenine and vinylbenzyl chloride (mixture of *meta-* and *para-* isomers) in the presence of potassium carbonate in dimethylformamide. Novel monomer **(4)** was obtained in 50% yield by modification of a published procedure for the synthesis of 9-benzyl-2,4-diaminopurine [7]. **(5)** was synthesised according to the method of Oikawa *et al.* [8].

^{1}H NMR titrations were performed by adding increasing amounts of monomer (0.5-10mM in $CDCl_3$) to solutions of either **(1)** or **(2)** (1mM in $CDCl_3$) and the spectra were recorded using a Bruker Advance DRX 400 spectrometer. The complex induced shift (CIS) of the imide proton of **(1)** or **(2)** was followed. Apparent association constants were extracted from the raw data by fitting to a 1:1 binding isotherm [9], using Microcal^{TM} Origin.

Molecularly imprinted polymers ($P_M(x)$) were prepared by dissolving the template **(2)** (0.05mmol), the functional monomer (x) (0.1mmol), ethyleneglycol dimethacrylate (20mmol) and polymerisation initiator (ABDV) (1%w/w total monomer) in chloroform (5.6cm^3) in glass tubes, degassing the solutions with N_2 for 10 minutes, sealing the tubes and polymerising thermally at 40°C for 24 hours. The glass tubes were then broken and the polymers extracted with chloroform in a Soxhlet apparatus for 24 hours. The polymers were then crushed and sieved to obtain particles in the size range 25-50μm. After repeated sedimentation (methanol/water : 80/20) to remove fine particles, the polymers were slurry- packed (methanol/water : 80/20) into HPLC columns (125mm x 5mm, i.d.). Control, non-imprinted polymers ($P_N(x)$) were prepared in the same manner, but with the omission of **(2)**.

HPLC analyses were performed using an HP1050 system equipped with a DAD-UV detector. The mobile phase was acetonitrile (HPLC grade), the flow-rate 1ml/min, analyte injection volume was 20μl and the analyte concentrations were 0.01-0.5mM. Analyte detection was performed at 260nm. Analyte retentions are quoted as their capacity factors, k' = $(t-t_o)/t_o$, where t is the retention time for the analyte and t_o is the retention time of the void volume marker (acetone).

Table 1. Apparent association constants (K_{app}) for the interaction of (1) and (2) with the respective functional monomers.

Monomer	K_{app} (M^{-1}) with (1)	K_{app} (M^{-1}) with (2)
(3)	63 ± 7	57 ± 8
(4)	282 ± 10	320 ± 16
(5)	567 ± 28	757 ± 28

DISCUSSION

^{1}H NMR Titrations

The extent of the association between the (1) and (2) and each of the functional monomers was followed *via* NMR titration by examining the change in chemical shift of the imide-proton of the respective uracil with varying concentrations of the respective functional monomers. A large downfield shift was observed in all three cases. The maximum observed $\Delta\delta$ (ppm) with (1)/(2) as guest (at the concentrations detailed in the Experimental section) were, for (3) = 2.23/2.24, for (4) = 3.95/4.33 and for (5) = 4.41/4.42. This is indicative of hydrogen-bonding interactions between the uracils and the monomers. The apparent association constants (K_{app}) extracted from the raw data, as described in the previous section, for the three monomers with each uracil are shown in Table 1.

The results of these experiments demonstrate the effects of using monomers capable of two-point and three-point binding, respectively. Gratifyingly, in keeping with our assumptions in the design of the monomers, (4) exhibited a much higher association constant with (1) and (2) than did (3), thus demonstrating the effect of the "extra" hydrogen-bonding interaction. While there is also the possibility that (3) might self-associate, which would also reduce its effectiveness in forming a complex with (1) or (2), previous studies have shown that in $CDCl_3$ such self-association may be considered negligible [10]. The use of monomer (5) illustrates the increase in association constant obtained when switching from amino- to amido- functionalities; the association constants obtained here are also consistent with previous studies [11]. Thus, of the three monomers studied, (5) exhibits the largest association constant with (1) and (2).

Polymer Preparation and Chromatographic Evaluation

To test whether the above observations would be translated into the subsequent polymers, MIPs were prepared using each of the monomers using (2) as the template molecule (polymers $P_M(3)$, $P_M(4)$ and $P_M(5)$, respectively). Control, non-imprinted polymers (NIPs) were prepared in the same manner, but with the omission of the template molecule (polymers $P_N(3)$, $P_N(4)$ and $P_N(5)$, respectively). In all cases, the crosslinking monomer was ethyleneglycol dimethacrylate (EDMA) and the porogenic solvent was chloroform.

The recognition properties of the polymers were then evaluated in the chromatographic mode. In Table 2 are shown the imprinting factors ($IF = k'_{MIP}/k'_{NIP}$) obtained for the different MIP/NIP combinations when injecting the template (2). In general agreement with the association constant data derived from the NMR titration experiments, it can be seen that $P_M(3)$ and $P_N(3)$ exhibit the same behaviour; (2) is equally weakly retained on both polymers and no

Table 2. Imprinting factors (IF) for (**2**) for polymers prepared against (**2**)with the respective functional monomers at various analyte loads.

Monomer used	IF (0.01mM)	IF (0.05mM)	IF (0.1mM)
(**3**)	0.99	0.97	0.96
(**4**)	2.02	1.80	1.68
(**5**)	4.64	3.50	3.07

imprinting effect is observed. For $P_M(4)$ and $P_N(4)$, we observe a difference in the retention behaviour of (**2**) on the respective polymers and a mild imprinting effect is seen. Finally, for the $P_M(5)$ and $P_N(5)$ polymer pair, a much larger imprinting effect is obtained, as the MIP is seen to recognise its template. We attribute this trend in the behaviour of the polymer pairs to the strength of the template-monomer complex in the pre-polymerisation solution, i.e. the stronger the association, the more complex is present and, subsequently, more and higher quality binding sites are obtained.

In Table 3 are shown the capacity factors obtained at different template concentrations and the capacity factors of molecules containing similar functionality to the template. Here we see the effect of changing either the peripheral substitution or hydrogen-bonding capabilities of the analyte.

For polymers prepared with (**3**) as the functional monomer, little or no change in the retention behaviour of the analytes is observed (on either the MIP or the NIP); this is consistent with the lack of imprinting effect observed for the template molecule (and the weak solution association exhibited by this monomer).

For polymers prepared with (**4**) as the functional monomer, little shape selectivity is observed for the template over different 1-substituted uracils or for unsubtituted uracils. However, the retention behaviour of 1,3-dibenzyl uracil, where a hydrogen-bonding site has been removed (compared to (**2**)), is markedly different.

Finally, the retention behaviour of the different analytes on the polymers prepared from (**5**) show the largest differences. Thus, we observe signs of shape selectivity on changing the

Table 3. Capacity factors (k') for different analytes on the respective imprinted and non-imprinted polymers.

Analyte (concentration)	$P_M(3)$ k'	$P_N(3)$ k'	$P_M(4)$ k'	$P_N(4)$ k'	$P_M(5)$ k'	$P_N(5)$ k'
2 (0.01mM)	0.49	0.50	1.06	0.53	3.32	0.72
2 (0.05mM)	0.48	0.49	0.95	0.53	2.42	0.69
2 (0.1mM)	0.47	0.49	0.90	0.54	2.07	0.67
2 (0.5mM)	-	-	-	-	1.16	0.46
1 (0.1mM)	0.48	0.50	0.97	0.61	1.43	0.67
1,3-dibenzyluracil (0.1mM)	0.31	0.31	0.31	0.23	0.27	0.30
Uracil (0.1mM)	0.38	0.67	0.77	0.49	0.97	0.82
Thymine (0.1mM)	0.41	0.56	0.88	0.56	1.16	0.96
AZT (0.5mM)	0.41	0.42	0.82	0.50	0.81	0.56

substituent at the 1-position of uracil ($k'_M(\mathbf{2})$ versus $k'_M(\mathbf{1})$ and $k'_M(\mathbf{AZT})$)). We also observe that removing or adding hydrogen-bonding sites to the analyte adversely affects the retention behaviour (with 1,3-dibenzyl uracil being extremely weakly retained).

CONCLUSION

We have demonstrated that the strength of the interaction between the template and functional monomer in a solution mimicking the pre-polymerisation solution is indeed translated into the subsequently prepared MIPs. Novel monomers (3) and (4) are seen to perform less well than the previously reported monomer (5) and we are currently pursuing the synthesis and evaluation of improved functional monomers as part of a continuing programme of functional monomer design for use in molecular imprinting.

ACKNOWLEDGEMENTS

REFERENCES

1. B. Sellergren (Ed.), *Molecularly Imprinted Polymers : Man-Made Mimics of Antibodies and Their Applications in Analytical Chemistry* (Elsevier Science B.V. (NL), 2001); R.A. Bartsch and M. Maeda (Eds.), *Molecular and Ionic Recognition with Imprinted Polymers* (ACS Symposium Series 703, Washington, D.C., 1998).
2. K.J. Shea, D.A. Spivak, B.Sellergren, J. Am. Chem. Soc., **115**, 3368 (1993).
3. R. Arshady and K. Mosbach, Makromol. Chem., **182**, 687 (1981); B. Sellergren, M. Lepistö, K. Mosbach, Tetrahedron Lett., **25**, 5211 (1984).
4. K. Yano, K. Tanabe, T. Takeuchi, J. Matsui, K. Ikebukuro, I. Karube, Anal. Chim. Acta, **363**, 111-117 (1998).
5. A. Kugimiya, T. Mukawa & T. Takeuchi, *The Analyst*, **126** (6), 772-774 (2001).
6. N.G. Kundu, S. Sikdar, R.P. Hertzberg, S.A. Schmitz, S.G. Khatri, J. Chem. Soc., Perkin Trans. 1, *1985*, 1295.
7. J.A. Montgomery and K. Hewson, J. Am. Chem. Soc., **82**, 463 (1960).
8. E. Oikawa, K. Motomi, T. Aoki, J. Polym. Sci. : Part A : Polym. Chem., **31**, 457-465 (1993).
9. K.A. Connors, *Binding Constants : The Measurement of Molecular Complex Stability* (J.Wiley & Sons, New York, 1987).
10. G. Lancelot, J. Am. Chem. Soc., **99**, 7037 (1977).
11. L. Yu & H.-J. Schneider, Eur. J. Org. Chem., *1999*, 1619-1625.

Characterization of MIPs Using Heterogeneous Binding Models

Ken D. Shimizu
Department of Chemistry and Biochemistry
University of South Carolina
Columbia, SC 29208, U.S.A.

ABSTRACT

New methods are presented for characterizing MIPs. These methods address the problems of quantitatively comparing the binding properties of different MIPs. Heterogeneous binding models were applied to MIPs based on an exponentially decaying distribution known as the Freundlich isotherm. The Freundlich isotherm was found to accurately model the binding isotherm of the majority of non-covalently imprinted MIPs. Using this model the experimental binding isotherm can be fit in log-log form to a linear equation from which the fitting parameters can be used to plot a quantitative affinity distribution which is a plot of the number of sites with respect to the binding constant of those sites. Comparison of MIPs using this methodology allowed for simpler and more accurate assessment of the binding properties than by previous methods such as the limiting slopes analysese of curved Scatchard plots

INTRODUCTION

Molecularly imprinted polymers (MIPs) are highly crosslinked polymers that are synthesized in the presence of a template molecule.[1,2] Upon removal of the molecular template, a binding cavity is formed with affinity and selectivity for the original template molecule. MIPs compare favorably to other synthetic materials that can be tailored with recognition properties including synthetic molecular receptors and designer antibodies. For example, MIPs have high thermal and chemical stability, are easily and inexpensively synthesized, and are easily tailored with binding properties for almost any molecule of interest.

Clearly, the binding properties of molecularly imprinted polymers (MIPs) are their most important characteristic. The comparison of the binding properties of MIPs, however, is complicated by the heterogeneity in MIPs. Unlike antibodies or enzymes that have a single type of binding site with high affinity and selectivity, MIPs contain a wide variation of binding sites that span the range in terms of binding affinity and selectivity. This binding site heterogeneity diminishes the utility of MIPs in chromatographic applications by leading to poor resolutions, highly concentration dependent selectivity, and severe peak asymmetry.[3] Heterogeneity also complicates the quantification and comparison of the binding properties of MIPs. For example, a common method to characterize MIPs is using a Scatchard plot (Figure 1). A homogenous system would yield a straight line in a Scatchard plot. MIPs, however, typically have a curved Scatchard plot due to the heterogeneity of the underlying binding sites. The heterogeneity in MIP1 can be modeled by the limiting slopes method by two straight lines to the curve, yielding two sets of binding parameters corresponding to the high- and low-affinity sites. Complications quickly arise when using this analysis to compare two polymers. For example, the high-affinity sites of a second polymer (MIP2) were measured and found to have a lower binding constant than MIP1($K_a = 5 \times 10^4$ M^{-1} versus 1.0×10^5 M^{-1}) but at the same time a greater number of binding sites ($N = 16.0$ μmol/g versus 4.0 μmol/g). From this comparison, it is unclear which is the better polymer: MIP1 or MIP2, because it is unclear which binding parameter is more important: the number of binding sites (N) or the association constant (K_a).
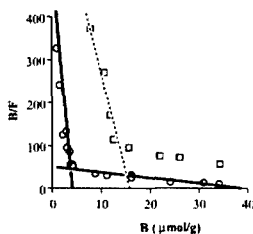
Figure 1. Scatchard plots of MIP1 (circles) and MIP2 (squares).

Table 1. Binding properties of high-affinity sites as measured by Scatchard analyses.

	MIP1	MIP2
N (μmol/g)	4.0	16.0
K (M^{-1})	1.0×10^5	5×10^4

Due to these difficulties, new methods were sought that might more clearly allow for the quantitative comparison of MIPs. First, it became clear that the number of binding sites and the association constant were not independent parameters but are dependent variables in heterogeneous systems such as MIPs. Thus, the question is not 'what is the association constant of an MIP?' Rather, the more appropriate question is 'what is the number of binding sites having a particular association constant?' This led to the use of affinity distributions that plots the number of binding sites (N) with respect to their association constants (K) to characterize MIPs. We have quantitatively measured the affinity distribution for a wide range of MIPs and found that MIPs can be well modeled by an unimodal exponentially decaying Langmuir-Freundlich distribution (Figure 2). In the case of the covalently imprinted polymer the peak of the distribution is in the analytical window and the exponentially; whereas, for the non-covalently imprinted polymer, only the exponentially decaying tail of the distribution is in the analytical window.
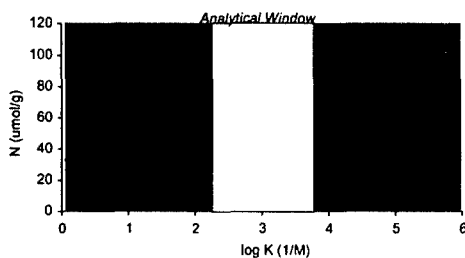
Figure 2. Affinity distributions calculated[4] for a covalently imprinted polymer[5] and non-covalently imprinted polymer.[6] The measured analytical window is shown as a gray box.

The relative positions of the distributions with respect to the analytical window appear to be fairly general as the examination of a wide range of non-covalent imprinted polymers from the literature were found to be accurately modeled by fairly simple exponentially decaying binding model, the Freundlich.[7] The appropriateness of the Freundlich isotherm in modeling the binding behavior of a MIP is easily graphically verified by plotting the binding isotherm in log bound (B) versus log free (F) format. Isotherms that conform to the Freundlich isotherm will fall on a straight line (Figure 3a). A linear regression fit of the isotherm to a log form of the Freundlich isotherm (log $B = m$ log $F +$ log a), yields two fitting parameters a and m. These can be used to generate the corresponding affinity distribution using the new derived affinity distribution expression for the Freundlich isotherm ($N = 2.3\ am\ (1-m^2)\ K^{-m}$) that relates the

number of binding sites (N) for each class of binding site having an association constant (K). The overall process is simpler than the Scatchard analyses, requiring only a single linear regression analysis, and generates an affinity distribution that more accurately characterizes the heterogeneous distribution of sites present in MIPs than the bimodal distribution of the limiting slopes Scatchard method.
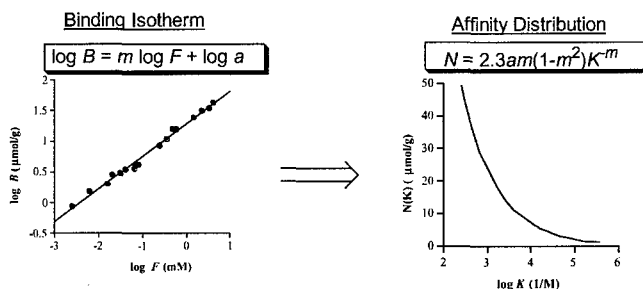
Figure 3. Binding isotherm (left) for an ethyladenine-9-acetate imprinted polymer in acetonitrile and the corresponding affinity distribution (right).

The ability to readily generate affinity distributions for MIPs, yielded the sought after method to quantitatively characterize MIPs that takes into account the heterogeneous distribution present in MIPs. In applying affinity distributions to characterize MIPs, there are a few practical limitations. First, the affinity distribution expression ($N = 2.3\ am\ (1-m^2)\ K^{-m}$) allows calculation of the distribution over the entire range of binding constants. However, in practice the accuracy of the calculated affinity distribution is limited by the concentration ranges of the binding isotherm. Typical boundaries are from $K_{min} = 1/F_{max}$ to $K_{max} = 1/F_{min}$.[8] Secondly, the application of an exponentially decaying distribution to model MIPs is only accurate with a given analytical window. The distribution cannot be globally accurate because 1) it would imply that there are an infinite number of binding sites (a physically impossiblility) and 2) at higher association (lower concentrations) it must reduce to Henry's law. Thus, in applying the Freundlich binding model to a given isotherm, it is necessary to first check if the Freundlich model actually accurately models the binding behavior over the measured concentration range. The easiest way to do this is graphically as shown in Figure 2. If the log-log plot of the binding isotherm does not fall in a straight line then the Freundlich isotherm cannot be used to model the binding behavior of the MIP over that concentration range. Either a different or more narrow concentration range can be selected or a different heterogeneous binding model must be used.[4]

The affinity distribution is commonly presented in two formats: 1) N versus log K and 2) log N versus log K. The first (N versus log K) is also known as the site energy distribution as log K is proportional to the binding energy (ΔG). In this format, the area under the distribution is the number of sites. This does not give the total number of binding sites rather the number of binding sites within a narrow range of association constants. In fact, the majority of MIPs have been measured in concentration ranges that do not allow for the accurate estimation of the total number of sites. The application of the Freundlich binding model only underscores this limitation. A second format for the affinity distribution (log N versus log K) allows for simple visual comparison of two polymers because the exponentially decaying distribution becomes straight lines. The slope (m) of the distribution, in this format, yields a measure of the ratio of

the number of high-affinity to low-affinity sites, with a flatter the slope corresponding to a higher percentage of high-affinity sites in the polymer.
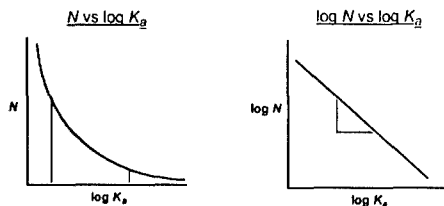
Figure 4. Representations of the two formats for the affinity distributions.

With the ability to readily characterize MIPs using affinity distributions, we were interested in the comparative distributions of imprinted and non-imprinted polymers. There are several different possibilities, shown in Figure 5. The imprinted polymer could have increased capacity and similar ratio of high- to low-affinity sites (Figure 5a), similar capacity but a more favorable ratio of high- to low-affinity sites (Figure 5b), or a combination of both (Figure 5c). A fourth possibility (not shown) is that either the imprinted or non-imprinted polymer do not conform to the exponential distribution.
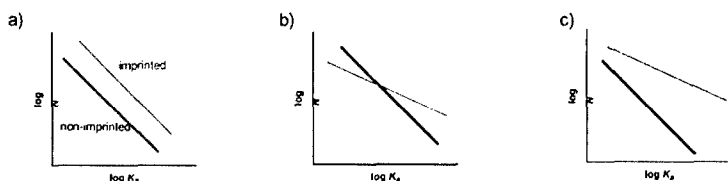
Figure 5. Representations of three different possible relative distributions for imprinted and non-imprinted polymers.

The MIP system selected for study was a well characterized non-covalently imprinted ethyl adenine-9-acetate (EA9A) selective system[4,6,7] which was based on a similar adenine selective MAA/EGDMA MIP reported by Shea *et al.*[9] The binding isotherms for the imprinted and non-imprinted polymers were measured from batch rebinding studies and all the polymers were found to be well modeled by the exponentially decaying distribution of the Freundlich isotherm. The comparison of the corresponding affinity distributions revealed that the imprinted polymers had higher capacity and ratio of high- to low-affinity sites in comparison to the non-imprinted polymer (Figure 6).

The three imprinted polymers differ in the concentration of template molecule (EA9A) in the polymerization mixture: (2.5 mM, 5.0 mM, and 12.5 mM). Both the capacity and percentage of high affinity sites improved as the concentration of template molecule was increased. In the case of the lowest concentration (2.5 mM EA9A) the molar monomer to template ratio was 120:1 and yet there was still a significant imprinting effect as seen by the much higher affinity distribution of the imprinted versus the non-imprinted polymer.
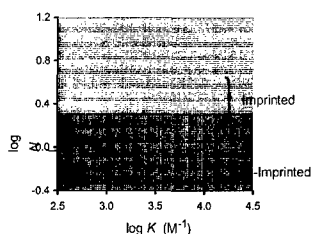
Figure 6. Measured affinity distributions for non-covalently imprinted and non-imprinted EA9A polymers. The imprinted polymers differ in the concentration of EA9A in the polymerization mixture: 2.5 mM (gray), 5.0 mM (broken), and 12.5 mM (solid lines), respectively.

Other variables in the imprinting process such as temperature (Figure 7a) and crosslinking percentage (Figure 7b) were also examined. Although these parameters have been extensively examined, the ability to quantitatively measure the breadth of the heterogeneity using affinity distribution analyses provided an opportunity to more accurately observe and understand the imprinting effect. Again, all the polymers were found to be accurately modeled by the Freundlich isotherm, yielding exponentially decaying distributions.
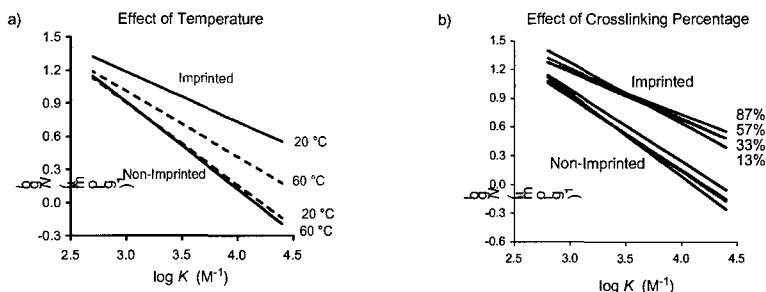
Figure 7. Overlaid affinity distributions of EA9A non-covalently imprinted and non-imprinted polymers that were synthesized under (a) differing temperatures and (b) crosslinking percentages.

Temperature had the more profound effect on the imprinting effect. The polymer imprinted under lower temperature conditions (20° C) displayed improved characteristics of higher capacity and ratio of high- to low-affinity sites in comparison the same formulation imprinted at higher temperatures (60° C). In contrast, the non-imprinted polymers synthesized at both temperatures were virtually identical in binding properties.

The effect of crosslinking percentage was examined by synthesizing polymers in which the crosslinking agent (EGDMA) has been substituted with increasing amounts of monomeric methyl methacrylate (MMA) reducing the overall crosslinking percentages without altering the concentration of functional monomer (MAA). The reduction of crosslinking percentage was expected to increase the flexibility of the matrix thereby decreasing the ability of the matrix to maintain the shape and affinity for the imprint molecules. Surprisingly, the crosslinking percentage has a relatively small effect on the affinity distributions. The polymer with 13%

21

through 87% crosslinking agent still showed a significant imprinting effect as seen by the higher affinity distributions of the imprinted versus imprinted polymers. Unlike changes in temperature and concentrations of template molecules, imprinted polymers with differing crosslinking agents all had similar numbers of binding sites. The polymers, however, were differentiated in the percentage of high-affinity sites. The affinity distribution of the 87% crosslinking agent MIP had the flattest slope and therefore the highest percentage of high-affinity sites. This study reveals some advantages of the affinity distribution analyses and helps explains some of the discrepancies in the literature on the effects of crosslinking percentage. If the polymers were compared at higher concentrations (low-affinity sites), then the 13% crosslinked polymer would be the best; whereas, if the polymers were compared at lower concentrations (high-affinity sites), then the 87% crosslinked polymer would be the best.

The heterogeneous distributions observed in non-covalent MIPs has a number of consequences on the binding properties and ultimate utility of MIPs. First, the severe heterogeneity of the exponentially decaying distributions explains the strong concentration dependence on the affinity and selectivity of MIPs. The MIPs show poor binding properties at high concentrations and excellent binding properties at low concentrations. This heterogeneous distribution is not well suited toward chromatographic applications that are operative over a wide concentration range from high to low concentrations. This distribution is compatible with applications at low-concentrations such as in sensing, where the small number of high-affinity sites would dominate the binding properties. In fact, the exponentially tailing distribution ensures that there will be a small but appreciable population of high-affinity sites. Finally, we have seen that improvements in the imprinting process increase the ratio of high- to low-affinity sites, but at the same time they also increase the heterogeneity of the polymers. The slope of the affinity distribution in the log N versus log K format also is the heterogeneity index, with a flatter slope being more heterogeneous. This helps explains results seen in the chromatographic applications, where polymers with higher affinity do yield greater separation factors but from a practical sense are worse off because of much lower resolution factors due to severe peak asymmetry and broadening.

ACKNOWLEDGEMENTS

REFERENCES

1. B. Sellergren, Molecularly imprinted polymers. Man made mimics of antibodies and their applications in analytical chemistry. (Elsevier, Amsterdam, 2001).
2. G. Wulff, *Angew. Chem., Int. Ed. Engl.* **34**, 1812-1832 (1995).
3. B. Sellergren, K. J. Shea., *J. Chromatogr. A* **690**, 29-30 (1995).
4. R. J. Umpleby, II, S. C. Baxter, Y. Chen, R. N. Shah, K. D. Shimizu, *Anal. Chem.* **73**, 4584-4591 (2001).
5. M. J. Whitcombe, M. E. Rodriguez, P. Villar, E. N. Vulfson., *J. Am. Chem. Soc.* **117**, 7105-7111 (1995).
6. R. J. Umpleby, II, M. Bode, K. D. Shimizu, *Analyst* **125**, 1261-65 (2000).
7. R. J. Umpleby, II, S. C. Baxter, M. Bode, J. K. Berch, R. N. Shah, K. D. Shimizu, *Anal. Chim. Acta* **435**, 35-42 (2001).
8. A. K. Thakur, P. J. Munson, D. L. Hunston, D. Rodbard, *Anal. Biochem.* **103**, 240-254 (1980).
9. K. J. Shea, D. A. Spivak, B. Sellergren, *J. Am. Chem. Soc.* **115**, 3368-3369 (1993).

Microfabrication and
Silica Imprinting

M2.1

Sensor Materials
- Detecting Molecules, Mixtures and Microorganisms -

Franz L. Dickert, Oliver Hayden, Peter A. Lieberzeit and Christian Palfinger
Institute of Analytical Chemistry, Vienna University
Waehringer Strasse 38, A-1090 Vienna, Austria

ABSTRACT

Sensor materials based on molecularly imprinted organic and inorganic polymers were designed and characterized according to their selectivity and sensitivity using mass-sensitive quartz crystal microbalances (QCMs). Cavities of differing shapes and sizes were created in both organic and inorganic polymers, able to selectively re-include the template species. Imprinting was performed both on the molecular and the micrometer scale. The chemical and biomimetic sensors developed allow the detection of various analytes, such as VOCs in ambient conditions, complex mixtures (automotive engine oils) and microorganisms. Thus, the extraordinary flexibility of templating methods is proved as the most versatile platform technology for advanced sensor materials.

INTRODUCTION

The design of chemical sensors is a key issue in modern analytical chemistry, as they open us the way for small, easy-to-use and economically priced analytical instruments. Sensors usually consist of a chemically sensitive layer, a transducer and an electronic data collection and processing system. The keynote is the design of materials with pronounced chemical recognition abilities. The idea is to design sensor layers with antibody-like selectivities, but without the disadvantages of biological materials, such as biodegradation, availability, costs and - most important – ruggedness against physical and chemical stress [1].

Early strategies for layer development included host-guest interactions with molecular cavities, such as crown ethers, cylcodextrins or calixarenes [2]. Although these materials have proven to be highly suitable for the specific detection of small organic molecules, major improvements in sensor layer design can be achieved by molecular imprinting methods [3,4]. In this case the later analyte or analyte-analogue species is used as template and mixed with the precursors of a highly cross-linked polymer or ceramic material. The template molecules are removed from the material after polymerization, either by evaporation or washing. The resulting cavities and diffusion pathways are corresponding to the respective analyte and hence ideally prone to re-inclusion. Some of the major advantages of chemical sensor design by molecularly imprinted layers are the following: the resulting polymer is usually chemically and mechanically stable, can be produced by well-established technological processes (on-chip polymerization or spin coating), and no costly chemicals are needed. Additionally, it could be shown that templating materials impose no limits concerning analyte size, shape and chemical composition. In the present study sensor materials for the detection and monitoring of different sizes, shapes and chemical composition were designed. Analytes surveyed include VOCs and automotive engine oils as well as microorganisms.

EXPERIMENTAL DETAILS

Sensor Layers. Sol-gel layer synthesis was accomplished by acidic hydrolysis of the respective precursor. To produce silicon sol-gel materials 50µl tetraethoxysilane 50µl diethylaminopropyltrimethoxysilane, 20mg capric acid as template were mixed with 50 µl water in 900µl ethanol. After pre-polymerizing the mixture for two hours at 70°C and three days at room temperature, the resulting sol was spun onto the gold elektrodes of a QCM.

Titanates had to be pre-hydrolysed with concentrated hydrochloric acid before carrying out the polymerization reaction. Therefore 100mg tetraethoxytitanate and 6µl concentrated hydrochloric acid were heated at 70°C for 1h and then left hydrolysing for 2 days. Then 30 mg of capric acid, 20µl of water and 1,2 ml ethanol were added and the mixture was heated again for 1 hour at 70°C. After 3 days of condensation the sols were ready for spin coating. Non imprinted materials were prepared in the similar way in the absence of capric acid.

Pre-polyaddition of the polyurethanes was performed in tetrahydrofurane (THF) with functionality ratios of isocyanato-groups : hydroxy-groups = 1:2. Reactive 4,4′-diisocyanato-diphenylmethane (30% triisocyanato monomers, technical grade) was used for the polyurethanes and bisphenol A as a donor of hydroxy-groups. The polymerisation was continued under stirring conditions at 70°C to reach gel point. For the coating process pre-polymer solutions were diluted 1:100 with THF. S. cerevisiae with a moisture content of 30% was used for the imprinting of polymeres.

Chemicals and microorganisms. The reagents were used as received from MERCK and FLUKA. We used lyophilized *E. coli*, active dry *S. diastaticus*, compressed and cultivated *S. cerevisiae*. *E. coli* strain W (ATCC9637) was a product of SIGMA. *S. cerevisiae* from ANKER was in a compressed form. Cultivation of yeast was done in universal growth medium (YPD) for 24h. The yeasts were washed from growth medium and centrifugated. Yeasts and bacteria were resuspended in a 1/15 molar KH_2PO_4/Na_2HPO_4 buffer of pH 6. Cell concentrations were determined using a Neubauer improved erythrometer. The freshly prepared cell suspensions for the measurements showed no significant agglomeration of microorganisms (controls performed with light microscopy).

Yeast stamp. The stamp was prepared by flattening compressed *S. cerevisiae* yeast between a glass slide and Teflon. Yeast cells adhered on the glass slide and could easily be lifted off from the Teflon surface.

QCM Devices. QCM microbalaces were produced by screen-printing the desired electrode structure on a quartz blank. Therefore, AT-cut blanks were used because of their favorable temperature coefficient. The thickness of the electrodes produced is about 200 to 300 nm and the surface roughness is below 10 nm.

Frequency measurements. Microbalances were driven with self-produced oscillator circuits. Frequencies were measured with a Keithley 775 A frequency counter. Computational data acquisition was done via a HP-IB bus and a self-programmed software. For gas measurements, streams of defined gas and humidity content were produced by Tylan mass flow controllers, in liquid phase self-constructed measuring cells were used.

DISCUSSION

Detection of organic solvent vapors

When preparing a chemically sensitive layer for a definite analyte, a wide variety of parameters has to be taken into account. Figure 1 shows the effect of different titanate sol-gel-layers exposed to butanol vapor. Capric acid was used in all samples as a template to produce molecular hollows. The titanate layers synthesized only differ by the precursor used - ethoxy (TBT) or butoxy group (TEOT). Both the magnitude of the sensor responses and the time constants are significantly changing. Although all layers consist of a pure Ti-O-network, only the sensor coated with the material resulting from the butyl precursor shows pronounced sensor effects. The response times increase with titanate layers in going from TBT to TEOT. The layers have exactly the same stoichiometric composition (no alkoxy groups left in the layers). The number of sites capable of re-including butanol differs due to different layer porosities. The sensitivity of non-imprinted layers is nearly negligible.

Pronounced selectivities of sensor materials can be achieved by molecular imprinting. Figure 2 shows the sensor response to octane vapors of a titanate layer from TBT imprinted with capric acid. N-octane is incorporated into the material preferably compared to the iso-octane. The capric acid as template leads to the formation of elongated, linearly shaped pores in the ceramic material. These cavities are suitable for the incorporation of the slim-shaped n-alkane, whereas
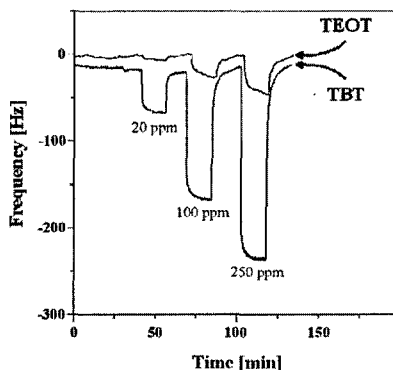
Figure 1. Sensor effects of titanate sol-gel layers synthesized from tetraethoxy-titanate (TEOT) and tetrabutoxy-titanate (TBOT) towards butanol.
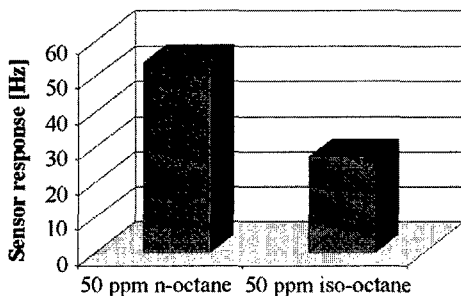
Figure 2. Sensor response of a titanate layer imprinted with capric acid towards differently branched analytes of the same molar mass.

27

the branched iso-octane is too bulky to fit efficiently into the cavities. Thus, the molecular sieve-like titanate sensor layers allow to selectively distinguish between isomeric analytes. The template directed synthesis of "porous" sol-gel layers is believed to be an economical approach to generate very stable interaction sites for analytes.

When measuring a series of different n-alkanes with the same concentration the frequency changes are following a quadratic relationship to the molecular weight. All these data can be used to model sensor effects for the system under observation. Generally, predictions of the sensor responses are not possible using solely the molecular mass of analytes, as this does not take into account the shape of a given molecule. Excellent results are obtained, however, by including sterical features into the calculations according to the so-called Wiener Index, which can be calculated as shown by the following formula:

$$w = \sum_{i=1}^{n-1} \sum_{j=i+1}^{n} b_{ij} \qquad (1)$$

Where: n   number of knots in the molecule
            b_{ij} length of the shortest distance between the knots i and j

In this way well established correlations to the boiling points of linear and branched alkanes [5] can be observed and therefore this idea should also be a suitable tool for this investigation. In Figure 3 the sensor effects obtained for different compounds are plotted against their respective Wiener Index. Once again a nearly quadratic relationship can be observed. Nonetheless there is a fundamental difference between this curve and the observation mentioned above: the data set shown in the figure also contains branched molecules, which also perfectly fit into the model curve. Therefore a topological model for the prediction of the sensor effect caused by a defined compound could be found. This is a highly advantageous tool for the assessment of observable frequency shifts.
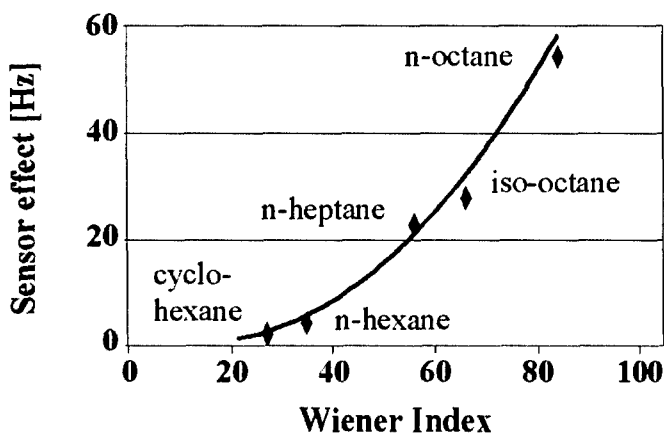
Figure 3. Correlation between the sensor effects of different organic compounds and their respective Wiener Index.

Engine oil degradation measurements

Molecular imprinting has given extraordinary flexibility to sensor layer design. This enables the chemist to develop chemically sensitive materials for analytes which before were beyond the reach of mass-sensitive detection principles. One strategy makes use of the fact that imprinting does not necessarily need an exactly defined template compound. We apply this fact to design a sensor system suitable for the monitoring of automotive engine oil degradation. Such sensor systems would be highly appreciated commercially, as the determination of the remaining useful time for a lubricant is not only of economical but also of high ecological interest. Both organic and inorganic polymers were used for imprinting, we also employed different templating strategies. First, polyurethanes were imprinted with fresh and used engine oils, respectively, the resulting layers yielded mass-effects according to their template molecule [6]. Naturally, engine oils are highly complex mixtures of a base oil and an additive package. Nonetheless molecular hollows can be generated in a polymer thus leading to a functional material capable of selective lubricant inclusion. Contrary to methods used up to now for engine oil characterization, which usually depend on a single chemical (total acid number, total base number) or physical (viscosity, conductivity) parameter, the mass sensitive sensor monitors changes in the entire chemical composition of the lubricant. This means that a totality of chemical changes is transferred into a change of frequency, or, in other words, a very complex procedure can be monitored by a comparably easy measurable quantity. To corroborate the theory of a mass-effect resulting from adapted cavities due to molecular imprinting, series of measurements were carried out with lubricants of different defined states of degradation and the resulting frequency shifts were correlated with one of the physical parameters mentioned above, the so-called Total Base Number (TBN), which is decreasing with the time of use (see Figure 4). The pure mass effects (viscosity changes are already compensated) give an excellent correlation and a good dynamic range not only with increasing oil age but also with TBN. Thus the sensor signal proves its reliability for the monitoring of degradation processes. In contrast to the classical determination
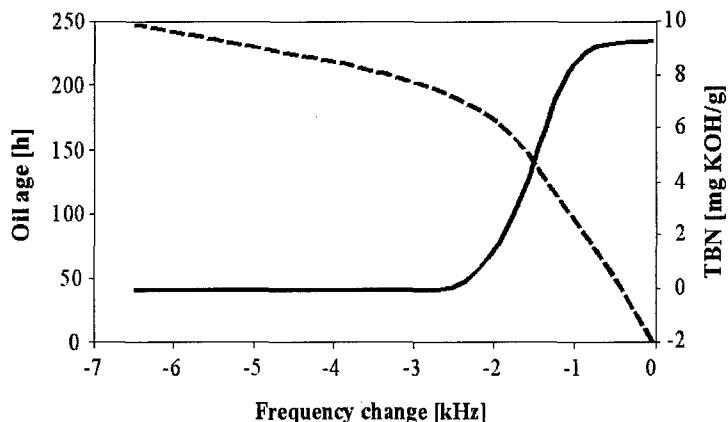
Figure 4. Correlation of the sensor responses to the oil age (- - - -) and Total Base Number (TBN) - a classical oil quality parameter.

of lead compounds, the sensor signals are influenced by the whole complex chemistry changes in the matrix rather than only by one parameter and the oil quality can be assessed directly on-line and does not need to be determined in a laboratory.

Inorganic polymers are also highly suitable for the design of chemically sensitive materials for the monitoring of engine oil degradation. Sol-gel glasses based both on silica and titanate materials have been tested for this purpose. Owing to the fact that these materials are synthesized in aqueous alcoholic (i. e. highly polar) media it is not possible to use the entire engine oil as template due to solubility problems. Hence a lead component has to be determined to fulfill the experimental needs. This can be done best by regarding the effects that occur when a lubricant is degraded: additives are worn out and base oil components get oxidized increasingly, until organic acids are formed (which in fact is measured when determining the TAN of an oil). So it was decided to use a carboxilic acid as template which combines an aliphatic residue of reasonable length with a suitable solubility. As a result of these prerequisites capric acid was chosen to produce an imprint layer for used oil. Additionally, diethyl-aminopropyl-trimethoxy-silane was added to the precursor mixture to achieve not only sterically fitting cavities but also to make use of chemical interactions between these basic groups in the material and acidic components in the oil. Figure 5 shows the mass effects of such a layer on the change from a fresh oil to a lubricant worn for 248 hours in a test stand (which, of course, can be regarded as being
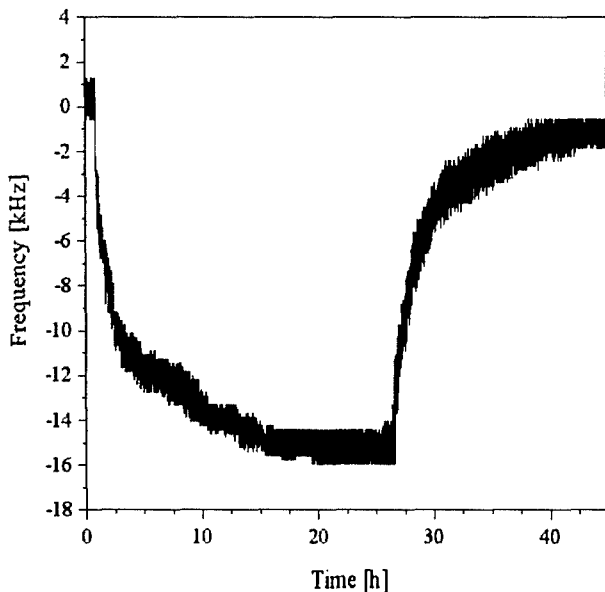
Figure 5. Mass effect of a capric acid imprinted sol-gel layer consisting of tetraethoxysilane and diethylamino-propyl-triethoxysilane (sensor in fresh oil, at 0 h change to waste oil, at 27 h change to fresh oil – proving reversibility)

completely exhausted) and back. The signal was obtained by a differential measurement between an electrode coated with an imprinted layer and a reference electrode and does therefore not contain any influence of changing viscosity. It is obvious that the material incorporates used engine oil preferably to the corresponding fresh lubricant thus yielding a reliable method for oil analysis. The resulting mass effect of 16 kHz is very high and has about the same magnitude than the corresponding frequency shift caused by the change in viscosity. This proportion is much higher than the previously observed ones. It also proves the preferential incorporation of used oil into the sensing layer and this technique proposed might be suitable for the purpose desired.

The next step in the design of mechanically, chemically and thermally stable sensor materials for engine oils is the development of purely inorganic recognition films, i.e. polymers, which do not have any organic substituents left in the sequence. In this case the materials investigated were not restricted to silicon-containing sol-gel glasses, but also other elements show favorable properties. In commercial sol-gel-methods especially alkoxides of transition metals such as aluminum and titanium are widely used (e.g. for the production of soft contact lenses). We prepared titanium glasses imprinted with capric acid, which also showed pronounced re-inclusion effects towards used engine oil. Although layer synthesis requires more experience and time, these materials show some highly favorable qualities: most of all, it is comparably easy to produce homogeneous layers on the respective device, but also the resulting layers are very stable and hard and therefore highly suitable for the rugged environment of a car engine.

The quartz crystal microbalance is highly suitable for engine oil deterioration measurements directly in the liquid phase. Additionally, gas phase would also be an interesting task, as no viscous interaction should occur between the surrounding medium and the device. Of course, some facts have to be taken care of: in order to avoid splash of small droplets to the
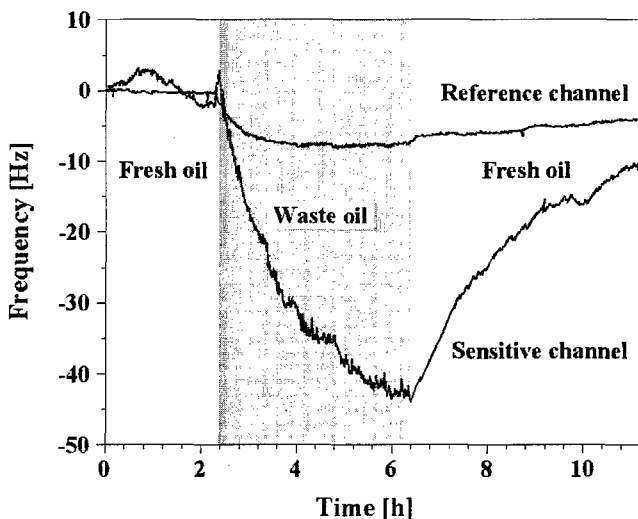
Figure 6. Sensor effects obtained with heatable QCM and an imprinted titanate layer in the gas phase.

sensor surface, which would add a major viscosity contribution to the mass effects observed, the entire device had to be encapsulated somehow. Furthermore, it has to be taken care that no oil vapors condense on the quartz surfaces and thus a heated device was used. Figure 6 shows the sensor response of both the coated and the uncoated channel of a QCM. While the uncoated channel scarcely shows any response the resonance frequency of the imprinted QCM decreases. Again, this observation can be traced back to the incorporation of waste oil components into the sensitive layer.

Microorganism detection

Diffusion limitations occur for the enrichment of the analyte in the bulk of the sensor layer, when going from small organic molecules to biopolymers or even whole cells. Surface imprinting strategies are a favorable way to overcome the limitations in the bulk. However, the number of imprinted cavities in the bulk outnumbers the imprinted pits on the surface by far. Dense receptor sites on the layer surface are needed to obtain a good sensitivity comparable to the results with "bulky" MIP sensor layers.

We are particularly interested in forming sensor layers on-chip, to demonstrate industrial production capability of our sensor design [7]. We therefore developed an elegant technique to form packed receptor sites on dual microbalances coated with a polymer surface using a stamping procedure as depicted in Figure 7. Polymer or sol-gel solutions in a pre-polymerized stage are spin cast onto the transducer surface. A stamp with a cell layer is pressed on the coated device and will embed the cells partially, depending on the layer thickness and the viscosity of the pre-polymer. Receptor sites are built during the curing process due to the self-organization process of oligomeric components around the cell surface. During this polymerization step primarily crosslinking and densification of the pre-polymerized layer will occur. Best imprinting results were gathered with constant force applied on the stamp during the polymerization of

Stamping on pre-polymerized layer

Polymer curing and template removal
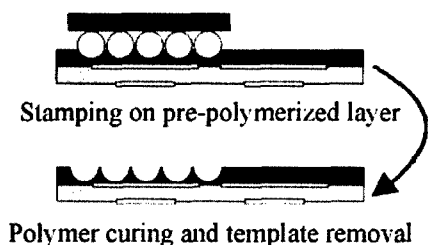
Figure 7. Schematic figure of the surface imprinting process using a stamp with a cell lawn.
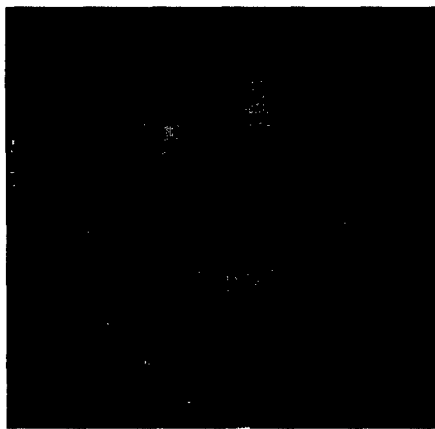
Figure 8. Yeast imprints on a polyurethane layer.

polymers. In the case of the sol-gel layers, the best results were achieved pressing the stamp on the coated microbalance for a short time. However, QCMs coated with yeast imprinted polymers (yeast-IPs) from sol-gels are much less sensitive than MIPs from polyurethane. The imprinted pits are densely packed and form a honeycomb-like structure on the polymer surface. The imprints do not have uniform diameters but a size distribution corresponding to the cell population used for the stamp. In Figure 8 the fingerprint of templating yeast cells on polyurethane is shown.

The residual moisture of the cell is a critical parameter for surface imprinting. A water content too high inhibits proper polymerization around the cell and only flattish imprinted sites are molded. On the other hand, too low moisture contents will result in molds with smaller diameters than needed for the average cell size. In the case of yeasts, we chose compressed yeast as template, which has a moisture content of around 30% or freshly cultivated yeasts which have been washed and centrifuged on filter membranes. With these templates the average mold diameter is sufficient to have a large geometrical fit between sensor layer and adhered cells.

The templating cells are removed with hot water after curing. Imprinted polyurethane layers e.g. are highly adhesive to the sensor devices and hot water creeps in-between the stamp and the sensor layer. The cells are resuspended and the stamp is lifted-off. A short washing step in an ultrasonic bath for some seconds usually removes even deeply embedded cells from the polymer layer. We have not been observing problems concerning the destruction of the surface MIPs due to the removal of the stamp. The yeast-IPs of polyurethane have pits with a usual depth of up to 1 µm. Therefore, the sensor layers have to be thicker than 1 µm to get a complete fingerprint of the cells – our layers were around 2 µm.
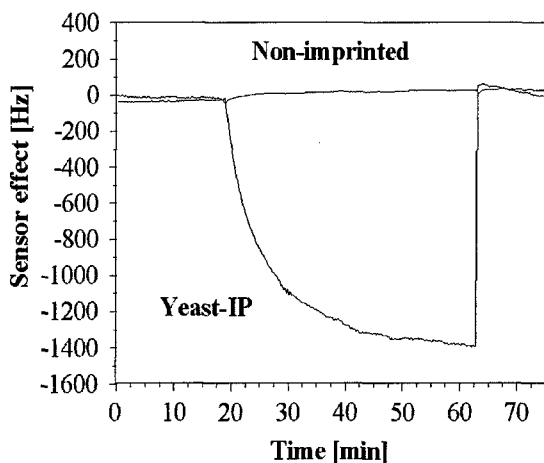
Figure 9. Polyurethane coated dual QCM. Sensor effects due to a buffered suspension (pH 6, 5 ml/min, 20°C) of 1 mg/ml *S. diastaticus* on a yeast-IP (sensitive channel) and non-imprinted polymer layer (reference channel).

We applied the layers on dual QCMs with an imprinted channel and a non-imprinted reference electrode [8]. Figure 9 shows a typical sensor response on the sensitive and reference channels. With this approach we are able to study specific and unspecific adhesion online. We also can perform excellent compensation measurements on dual QCMs. The compensation of QCM measurements in aqueous phase is done favorably on a single quartz disc. In this way, the same temperature dependence characteristics are guaranteed and the close distance of both electrodes is ideal for compensating viscosity and pressure fluctuations during online measurements. No sensor effect is observed on the non-imprinted polymer (reference channel).

To apply layers with a micrometer sized "roughness" to QCMs is unusual. These conditions could lead to a non-Sauerbrey behavior, since the adhered yeast cells are comparable to a viscoelastic layer. However, we could show that the sensor is highly sensitive to yeast with a performance equal to natural antibodies applied to QCMs observing typical gravimetric responses. The sensor effects are totally reversed by simply increasing the flow rate to 100 ml/min pulses. The extensively increased shear forces drag the cells out of the pits. However, flow rates in the range of 1-10 ml/min for example do not effect the sensitivity (liquid cell volume is around 100 μl). Interestingly, in streaming conditions no sensor effect occurs in presence of smaller microorganism, such as "sticky" E.coli, which can adhere in the larger pits. Using light microscopy we could see that the yeast cells with typical diameters of ~5 μm roll over the sensor surface and adhere from time to time in appropriate cell-fingerprints

CONLUSION

The extraordinary variety of sensing applications of molecularly imprinted polymers could be tested and proven. Potential application can take place in gaseous as well as in liquid phase, the dimension of analytes can reach from uniform molecules such as organic solvent vapors over complex mixtures (e.g. engine oils) to microorganisms with a size up to a few micrometers. An elegant technique for bioimprinting of sensor layers was described. This new type of robust cell sensor is capable of being used for biomass control in bioreactors, since the polymer is autoclavable. The surface imprinting concept is supposed to be an effective platform technique for the imprinting of microorganisms, viruses and enzymes.

REFERENCES

1. F. L. Dickert, K. Halikias, O. Hayden, L. Piu, R. Sikorsky, *Sens. Actuators B* **76**, 295 (2001).
2. F. L. Dickert, R. Sikorski, *Mater. Sci. Eng. C*, **10**, 39-46 (1999)
3. K. Mosbach, *Trends Biochem. Sci.*, **19**, 9 (1994).
4. G. Wulff, *Angew. Chem. Int. Ed. Engl.*, **34**, 1812 (1995).
5. H. Wiener, *J. Am. Chem. Soc.*, **69**, 2636 (1947)
6. F. L. Dickert, P. Forth, P. A. Lieberzeit, *Fresenius J. Anal. Chem.*, **366**, 802 (2000)
7. F. L. Dickert, O. Hayden, K. P. Halikias, *Analyst*, **126**, 766 (2001).
8. O. Hayden and F. L. Dickert, *Adv. Mater.* **13**, 1480 (2001).

Micromolding in Capillaries for the Generation of Molecularly Imprinted Polymer Filaments and Microstructures

Mingdi Yan
Department of Chemistry, Portland State University
PO Box 751, Portland, OR 97201-0751

ABSTRACT

The technique of micromolding in capillary has been employed to prepare molecularly imprinted polymer microfilaments, and to pattern MIP structures on silicon wafers. The approach relies on crosslinked poly(dimethylsiloxane) that contains relief structures as a mold to define the shape and size of the imprinted polymers. This article describes the processes leading to the fabrication of free-standing MIP micromonoliths and covalently immobilized MIP microstructures on silicon wafers. The limitations of the technique are also discussed.

The development of miniaturized systems for chemical, analytical and diagnostic applications has attracted great interest recently.[1,2,3] Significant advantages in speed, efficiency and control can be gained through the application of such miniature systems in laboratory testing. Micro devices have been fabricated to perform a variety of chemical and enzymatic reactions and in chip capillary electrophoresis separation. Much effort has also been devoted to shrinking analytical instruments such as high performance liquid chromatography,[4] combinatorial library screening system,[5] and biosensors.[6,7]

Molecular recognition and interactions play central roles in these applications. Molecular imprinting, a technique for the synthesis of polymeric materials with analyte-specific recognition properties, is an attractive alternative to natural recognition systems such as antibodies and receptors.[8,9,10] The ability to generate molecularly imprinted polymer (MIP) microstructures on devices should open new possibilities towards the development of miniaturized systems for chemical, analytical and diagnostic applications. The added advantages of long-term stability and chemical resistivity of MIPs may make these "intelligent chips" attractive for instrument and device fabrication.

We have employed a soft lithography[11,12] technique, micromolding in capillaries (MIMIC),[13,14] to fabricate MIP microstructures on silicon wafers. In MIMIC, an elastomeric stamp is placed in an intimate contact with the solid substrate. The recessed microchannels on the stamp form a network of empty capillaries. When a low-viscosity fluid precursor is placed in close contact at one end, it spontaneously fills the channels by capillary actions. Curing of the fluid leaves patterned microstructures on the substrate surface (Figure 1). An attractive feature of this technique is that the size and shape of the MIPs can be easily controlled and altered by those on the PDMS stamps. In addition, the process can be carried out conveniently in a chemical laboratory. Once the master mold is made, many elastomeric stamps can be cast and used repeatedly.

Figure 1. Schematic illustration for the fabrication of polymer microstructures using the technique of micromolding in capillaries.

Poly(dimethyl siloxane) (PDMS) has been widely used as the stamp material. PDMS can be released easily from patterned structures and substrates due to its high elasticity and low surface energy. It is also transparency to UV light, down to 300 nm, and is therefore compatible with the photochemical polymerization procedures employed in MIP synthesis. Alternative materials such as polyimide,[15] polyurethane and Novolac (phenol-formaldehyde) resin[16] have also been used to make stamps.

PDMS stamps are fabricated by casting a mixture of a PDMS prepolymer (Sylgard 184, Dow Corning) and the corresponding curing agent on a master mold. The master mold contains the inverse features of the stamp, and is made by conventional photolithography. In our studies that thick features (20-100 μm) were needed, SU-8 negative photoresists (MicroChem Corp.) were used to make master molds. The surface of the master mold was treated with a fluorinated silane, for example $C_6F_{13}CH_2CH_2SiCl_3$, to ensure facile release of the PDMS stamps.

A major limitation of this technique is that the crosslinked PDMS stamp tends to swell in many organic solvents that include chloroform, methylene chloride, toluene and tetrahydrofuran. These solvents have been widely used as the porogen in the synthesis of molecularly imprinted polymers, with chloroform and toluene especially popular in non-covalent imprinting systems where it is critical for the solvents not to interfere with the hydrogen bonding/ionic interactions between monomers and template molecules. We found that PDMS stamps swelled dramatically in these solvents and subsequently lost the conformal contact with the substrate. We have successfully fabricated MIP microstructures with dimethylformamide (DMF) as the solvent in both an acrylic acid-based[17] and a polyurethane-based[18] imprinting system. On the other hand, solvents that do not swell PDMS stamps include alcohols and water. Alcohols have low surface tension and wet the surface of PDMS and the wafer substrate. They are most useful in MIMIC and should therefore be very appropriate for imprinting systems that employ alcohols as the solvent. Water is another solvent that does not cause swelling of the PDMS stamps. However, water has a high surface tension and it does not wet hydrophobic surfaces. A small amount of alcohol (~5%) can be added to the aqueous solution to promote the liquid flow through the channels,

The swelling of PDMS stamps by solvents was studied using DMF and acetonitrile. The effect of swelling was evaluated by measuring the width of the PDMS ridges and the microchannels after polymerization. The imprinting solution contained 4-vinylpyridine (4-VP, monomer), ethylene glycol dimethacrylate (EGDMA, crosslinker), 2,4-dichlorophenoxyacetic acid (2,4-D, template molecule), 2,2'-azobisisobutyronitrile (AIBN, initiator), and the solvent. The solution was photopolymerized inside the microchannels with a 450 W medium pressure Hg lamp at 0 °C for 2 h. Optical images were taken on the area of stamps before the imprinting solution was introduced and after the imprinted polymers were formed inside the microchannels (Figure 2). It was found that after polymerization, the width of the PDMS ridges increased whereas the width of the channels decreased. This indicated that as the PDMS was swollen by the solution, it expanded thus reducing the size of the channels. This swelling effect was more

pronounced for acetonitrile as compared to DMF. With acetonitrile as the solvent, the width of the PDMS ridges increased by 12% and that of the channels containing the polymers decreased by 14%. For DMF, the expansion and shrinkage were 5% and 7%, respectively. Note that besides the solvent, the organic monomers also contribute to the swelling of the PDMS stamps. 4-Vinylpyridine was especially problematic.
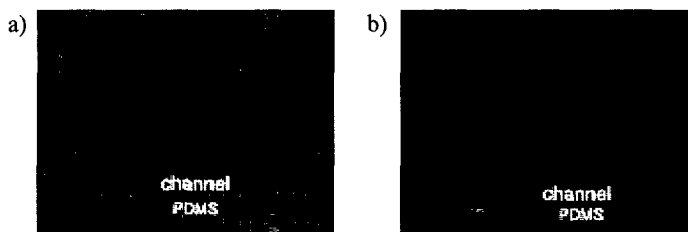
Figure 2. Optical micrographs of a) section of a PDMS stamp placed on a silicon wafer; b) the same area after the imprinted polymers were formed inside the channels. Acetonitrile was used as the solvent. The width of the PDMS ridges and the channels was measured using a free imaging software (Scion Corporation). About 6-8 measurements were taken and averaged. The PDMS stamps were fabricated from a master mold that contains features with a 20 μm x 20 μm cross-sectional dimension.

The polymers synthesized inside the channels can be isolated from the assembly as freestanding microfilaments. When the PDMS stamp was placed directly on the silicon wafer, the polymers formed would partially adhere to the substrate or the PDMS, and they were difficult to remove even after treating with HF. To avoid this problem, a PDMS thin layer was spin cast and cured on the wafer before the PDMS stamp was placed on the substrate. Therefore, the polymers were sandwiched between two PDMS, and could be released after the PDMS was removed. Two approaches were employed to facilitate the release of the MIP microfilaments: to dissolve PDMS with tetrabutylammonium fluoride in THF,[17] or to swell PDMS with a solvent such as toluene.[18] In the later case, the polymers were released from the PDMS after the PDMS were physically deformed. The imprinted polymers could then be centrifuged and extracted with solvents to remove template molecules for subsequent analysis.

In order to make MIP microfilaments of good quality, the amount of solvent used in the free radical polymerization was reduced dramatically. This was probably because the solvent was difficult to escape from the confined microchannels. As a result, the pore size, pore volume, and distribution of the MIPs will be affected. In addition, these MIP microfilaments may have different surface morphology as compared to MIPs prepared by the conventional method due to the surface property and the large surface areas provided by the PDMS microchannels. Studies are underway to characterize these MIP microfilaments.

Compared with MIPs prepared by bulk polymerization in large test tubes, this technique produces a much smaller quantity of materials. With a cross-sectional dimension of 20 μm x 20 μm and the spacing of 20 μm between channels, a PDMS stamp of 1 cm x 1 cm in size produces a maximum of 1.5 mg of MIP, assuming the density of the MIP to be ~1 g/cm^3. To prepare a

larger amount of materials is time consuming. One approach is to use several PDMS stamps simultaneously on a substrate.

The technique could be modified for the synthesis of MIP membranes. In this case, a drop of the imprinting solution was applied on the PDMS film that was spin cast on a wafer or glass surface. A flat PDMS block was then placed on the solution and the assembly was allowed to photopolymerize. The thickness of the MIP membrane was controlled by the amount of imprinting solution applied. We have successfully synthesized MIP membranes using the imprinting system described above (4-VP, EGDMA, 2,4-D, AIBN, acetonitrile). However, these membranes were quite fragile. After solvent extraction, they frequently fractured into small fragments.

We have employed the technique of MIMIC to fabricate MIP microstructures on silicon wafers for the construction of a MIP-based waveguide sensor. A polyurethane-based imprinting system was adapted and the details of the studies are described in a separate publication in this Proceeding.[18] In this type of application, it is desirable that the polymers be covalently attached to the substrates so that the device can withstand subsequent processing conditions. To achieve this, the wafers were treated with aminopropyltrimethoxysilane. The amino groups copolymerized with the isocyanate groups in the monomer feeds, thus forming covalent bonds between the polymer and the wafer. For acrylate-based MIPs, reagent such as (meth)acryloxypropyltrimethoxysilane can be used to treat the surface of the wafer.

MIMIC has been employed by others for the fabrication of functional microelectronic devices such as transistors and diodes.[11] A limitation of the technique is that it relies on the *interconnected* capillary channels in order for the fluid to flow through. For non-interconnected patterns, one solution was to create access holes through the PDMS stamp.[19] When the liquid was fed through the access holes, it was forced into the closed capillary patterns by the evaporation of solvent from the filled capillaries. However, if the device contains a large amount of non-interconnected patterns, the process can be extremely slow and inefficient.

In summary, MIMIC has been selected as the fabrication technique for the generation of MIP microstructures. Although the technique has a number of limitations, its simplicity, flexibility, and ease of use proved to be advantageous over other microfabrication methods. Using this approach, we have synthesized free-standing MIP microfilaments and created patterned MIP microstructures on silicon wafers. The integration of MIPs with microfabrication may lead to new types of functional devices with potential applications in separation, sensing and diagnostics.

ACKNOWLEDGEMENTS

REFERENCES

1. H. Zhu, M. Bilgin, R. Bangham, D. Hall, A. Casamayor, P. Bertone, N. Lan, R. Jansen, S. Bidlingmaier, T. Houfek, T. Mitchell, P. Miller, R. A. Dean, M. Gerstein, and M. Snyder, Science **293**, 2101-2105 (2001).
2. T. Chen, S. C. Barton, G. Binyamin, Z. Gao, Y. Zhang, H-H Kim, and A. Heller, J. Am. Chem. Soc. **123**, 8630-8631 (2001).
3. C. Hagleitner, A. Hierlemann, D. Lange, A. Kummer, N. Kerness, O. Brand, and H. Baltes, Nature **414**, 293-296 (2001).
4. M. Aiello and R. McLaren, Anal. Chem. **73**, 1387-1392 (2001).
5. T. A. T. Andrew Taton, C. A. Mirkin, and R. L. Letsinger, Science **289**, 1757-1760 (2000).
6. F. Favier, E. C. Walter, M. P. Zach, T. Benter, and R. M. Penner, Science **293**, 2227-2231 (2001).
7. Wang.J. and X. Zhang, Anal. Chem. **73**, 844-847 (2001).
8. *Man-Made Mimics of Antibodies and their Application in Analytical Chemistry*, ed. B. Sellegren (Elsevier Science, New York, 2000).
9. G. Wulff, Chem. Rev. **102**, 1-28 (2002).
10. K. Haupt and K. Mosbach, Chem. Rev. **100**, 2495-2504 (2000).
11. Y. Xia and G. M. Whitesides, Angew. Chem. Int. Ed. **37**, 550-575 (1998).
12. X.-M. Zhao, Y. Xia, and G. M. Whitesides, J. Mater. Chem. **7**, 106901074 (1997).
13. E. Kim, Y. Xia, and G. M. Whitesides, J. Am. Chem. Soc. **118**, 5722-5731 (1996).
14. E. Kim, Y. Xia, and G. M. Whitesides, Nature **376**, 581-584 (1995).
15. J. A. Bride, S. Baskaran, N. Taylor, J. W. Halloran, W. H. Juan, S. W. Pang, and M. O'Donnell, Appl. Phys. Lett. **63**, 3379-3381 (1993).
16. A. Kumar and G. M. Whitesides, Appl Phys. Lett. **63**, 2002-2004 (1993).
17. a) M. Yan and A. Kapua, Anal. Chim. Acta **435**, 163-167. (2001). b) M. Yan and A. Kapua, Polym. Preprint **41,** 264-265 (2000).
18. J. Brazier and M. Yan, Mater. Res. Soc. Symp. Proc., submitted (2002).
19. Z. Bao, J. A. Rogers, and H. E. Katz, J. Mater. Chem. **9,** 1895-1904 (1999).

On Route to the Chiral Imprinting of Bulk Silica

Santiago Ini, Jessica L. Defreese, Nicholas Parra-Vasquez and Alexander Katz
Department of Chemical Engineering, University of California at Berkeley
Berkeley, CA 94720-1462, U.S.A.

ABSTRACT

Shape-selective pores have been synthesized in bulk silica via imprinting. The synthetic approach relies on a sol-gel process to immobilize the imprint within a hybrid organic/inorganic material. Cleavage of the carbamate linkage from this material generates a primary amine within a microporous binding site. Characterization studies, including potentiometric titration and solid-state nuclear magnetic resonance spectroscopy, indicate that most imprinted amine sites are accessible during binding with small molecule probes. However, larger probes are unable to adsorb to the same material, indicating significant shape-selectivity in binding. Additionally, an investigation of framework pore size effects in a catalytic system shows that shape-selectivity can be solely a result of the imprinted active site and not the framework structure.

INTRODUCTION

Shape-selective catalysis originating from specific imprinted pockets has been observed in a variety of imprinted systems [1]. Previous studies of silica imprinting have largely focused on surface imprinting, utilizing both covalent [2,3] and non-covalent [4,5] strategies to prepare selective sites for adsorption and catalysis by functional group organization. Covalent imprinting in silica has recently been extended to three dimensions, and the control of local functional group density was demonstrated by organizing up to three primary amines within a microporous cavity [6]. Importantly, the porosity generated during the imprinting process was quantified with argon physisorption. The material demonstrated shape-selective catalysis in the Knoevenagel condensation of isophthalaldehyde and malononitrile, by inhibiting a second addition of malononitrile to the aldehyde, whereas an amorphous aminopropyl-functionalized silica gel catalyzed both additions [6]. The present study investigates the role of imprinted as well as framework porosity in achieving shape-selectivity in this catalytic system. Shape-selective binding in a silica synthesized from an asymmetric imprint is also described.

EXPERIMENTAL DETAILS

Imprint molecules were prepared by the reaction of a parent alcohol with 3-aminopropyltriethoxysilane and 1,1'-carbonyldiimidazole in the presence of a catalytic amount of sodium ethoxide. A chiral imprint was synthesized from (R)-(+)-sec-phenethyl alcohol (Figure 1), and a non-chiral imprint was synthesized from benzyl alcohol.
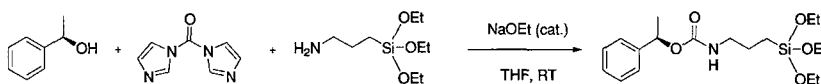
Figure 1. Synthesis of the chiral imprint molecule.

Microporous bulk silicas were prepared by co-condensing the appropriate imprint with 50 equivalents of tetraethylorthosilicate (TEOS) in an acid-catalyzed sol-gel process (Figure 2). The resulting optically clear glasses were Soxhlet extracted with acetonitrile over calcium hydride, and the internal silanols were capped with an equimolar mixture of hexamethyldisilazane and trimethylsilylchloride. The imprints were removed by reaction with trimethylsilyliodide in acetonitrile for 24 hours at 40 °C, followed by treatment with triethylamine in methanol for 24 hours at room temperature. The final materials were Soxhlet extracted with benzene over *p*-toluenesulfonic acid to remove the remaining triethylamine. The mesoporous imprinted silica was synthesized from TEOS and the benzyl carbamate imprint via a base-catalyzed condensation route. The remaining processing steps were carried out as with the microporous materials.

The presence of amine sites in each of the materials was quantified by a non-aqueous titration with perchloric acid in glacial acetic acid. Condensations of aldehydes with the imprinted amines were performed in toluene with continuous water removal and 1,3,5-trimethoxybenzene as an internal standard. Reactions of carboxylic acids with the imprinted amines were performed in chloroform also using 1,3,5-trimethoxybenzene as an internal standard. Gas chromatography (GC) was performed on an Agilent 6890 equipped with a Cyclosil-B column for aldehyde analysis and an Innowax column for analysis of acids. The
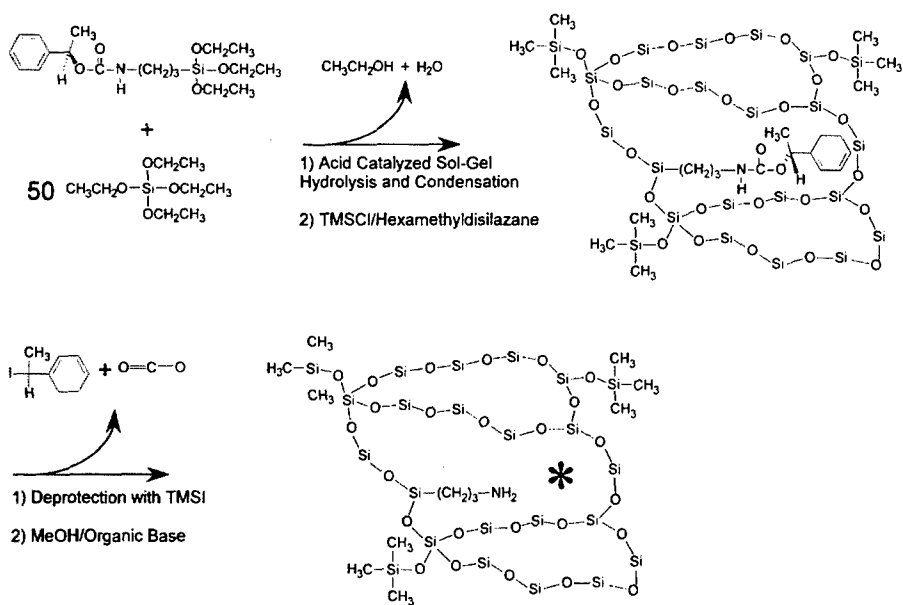
Figure 2. Schematic illustration of microporous bulk silica imprinting synthesis.

catalytic Knoevenagel reactions were performed at 60 °C and 80 °C with 0.75 mmol of isophthalaldehyde, 0.75 mmol of hexamethylbenzene (internal standard), 1.5 mmol of malononitrile, and 0.22 mol% of catalyst in 50 mL of acetonitrile. Solid-state NMR spectroscopy was performed on Bruker AM-300 spectrometer equipped with solids accessories. Nitrogen physisorptions were carried out on a Quantachrome Autosorb 1. Solid-state UV-Vis spectra were obtained on a Cary 400 Bio equipped with solids accessories.

DISCUSSION

Material Characterization

Solid-state NMR spectroscopy was performed to investigate the state of the imprint during material synthesis. As seen from the ^{13}C CP/MAS spectra in Figure 3a, the protected material shows high-field signals from the carbamate functionality. After deprotection (Figure 3b), the high-field signals are eliminated while the propyl tether signals remain. This result indicates near quantitative removal of the imprint. Variable contact time experiments were consistent with a lack of rotation about carbons labeled 4 and 5 in the protected material. The result for a typical potentiometric titration of the material is presented in Figure 4 and shows the presence of approximately 0.17 mmol primary amine sites per gram of silica.
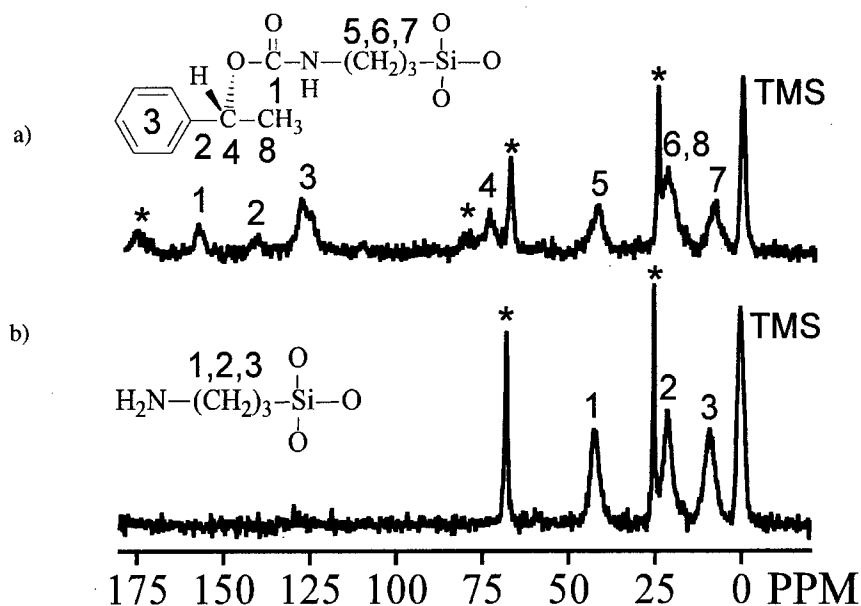
Figure 3. ^{13}C CP/MAS solid-state NMR spectra of a protected (a) and deprotected (b) bulk imprinted silicate. Asterisk (*) denotes either a spinning sideband or solvent (THF) resonance.
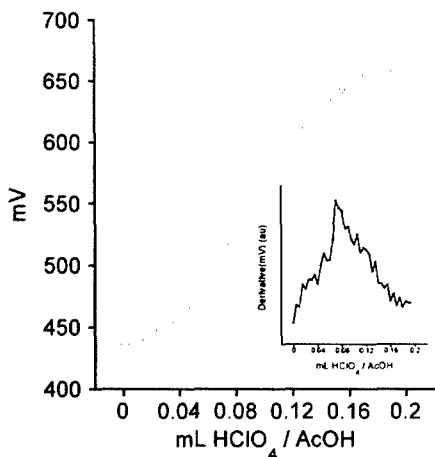
Figure 4. Potentiometric titration of imprinted amine sites in deprotected material.

Probe Molecule Binding

The shape-selectivity of the chiral imprinted system was investigated via covalent and non-covalent probe molecule binding. Salicylaldehyde was bound into the imprinted material by stirring with two equivalents of the aldehyde in refluxing toluene for 5 days. As assessed by GC, almost all (95%) of the imprinted sites were accessed via formation of the hydrogen bond-stabilized imine. A solid-state diffuse reflectance UV-Vis spectrum of the material before and after salicylaldehyde treatment (Figure 5) shows a strong band at 390 nm associated with the Schiff base.

Non-covalent binding into the material was explored via carboxylic acids. Benzoic acid bound to 51% of the imprinted sites at room temperature and 42% at 50 °C, while the larger acids 3-phenylbutyric acid and α-methylhydrocinnamic acid bound to less than 5% of the sites under the same conditions. This shape-selectivity in acid binding was especially significant considering the accessibility of almost all sites to salicylaldehyde. As an additional control experiment, the isostructural aldehyde 3-phenylbutyraldehyde of 3-phenylbutyric acid was successfully bound, as evidenced by solid-state NMR and GC. In summary, imprinted sites in microporous silica were accessible to salicylaldehyde, benzoic acid, and 3-phenylbutyraldehyde; however, the larger probes comprising 3-phenylbutyric acid and α-methylhydrocinnamic acid were unable to bind under identical conditions.
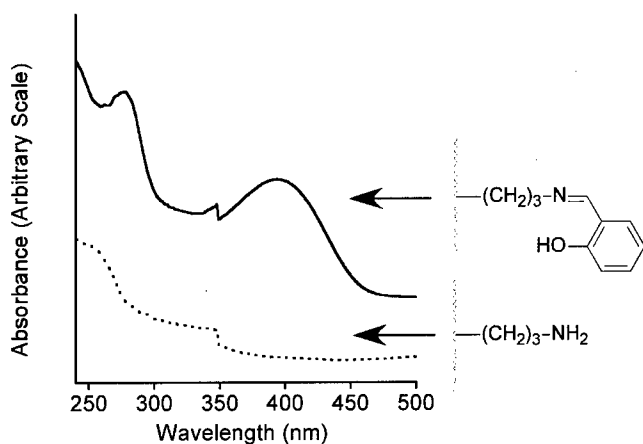
Figure 5. Diffuse reflectance UV spectra of salicylaldehyde-bound material (top) and control material (bottom).

Knoevenagel Catalysis

A mesoporous imprinted silica was synthesized to separate the role of the imprinted pore from the framework porosity in performing shape-selective molecular recognition. The nitrogen physisorption isotherm of this material exhibited the presence of microporosity from the imprinted sites and mesoporosity from the framework (Figure 6). Possible effects of the framework pore size were studied by running a catalytic Knoevenagel condensation of isophthalaldehyde with malononitrile in the presence of both microporous and mesoporous imprinted silicas, as well as a post-synthetically functionalized amorphous control silica (aminopropyl-functionalized mesoporous silica). Figure 7 shows the product distribution for each of these materials. Both imprinted systems suppressed the formation of the double-addition product C, suggesting shape-selectivity arising from the imprinted sites. In other words, the imprinted systems were able to selectively catalyze the synthesis of the mono-addition product B from isophthalaldehyde A, whereas the surface-functionalized material non-selectively catalyzed the synthesis of A to the double-addition product C. Given the stark contrast in framework pore sizes between the microporous and mesoporous imprinted materials, the catalytic selectivity must be due to the imprinted active site characteristics rather than an effect of the bulk framework porosity.

45
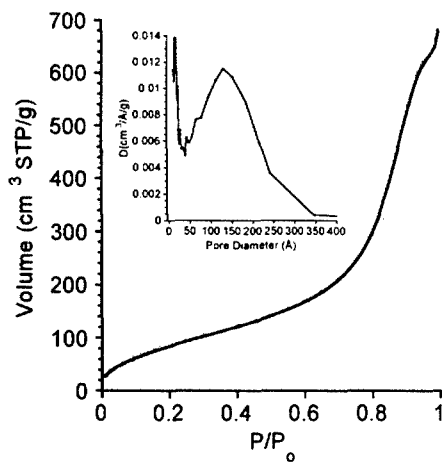
Figure 6. Nitrogen physisorption isotherm of imprinted mesoporous silica. Inset: Barrett-Joyner-Halenda (BJH) size distribution [7] showing bimodal microporosity (imprinted) and mesoporosity (framework).
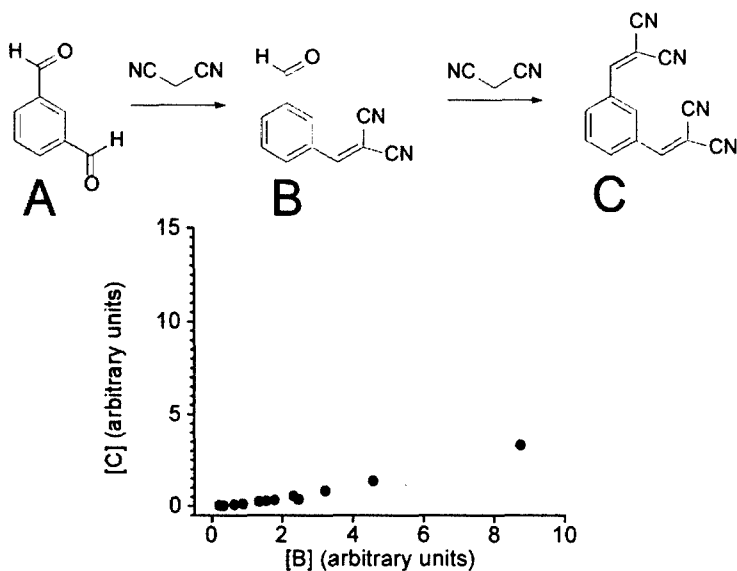
Figure 7. Relative concentration of di-addition product, C, versus mono-addition product, B, for surface-functionalized (hollow circles), mesoporous imprinted (solid circles) and microporous imprinted (crosses) silicates.

46

CONCLUSIONS

Shape-selectivity in bulk imprinted silica was studied using probe molecule adsorption experiments and Knoevenagel catalysis. Results indicate that imprinted silica can perform shape-selective molecular recognition in binding carboxylic acids. Comparison of shape-selective catalysis observed in a microporous versus mesoporous bulk imprinted silica suggests that shape-selectivity arises due to the effect of the active site rather than the bulk framework structure. These results point to the promise of an imprinting-based approach in bulk silicates for selective catalysis and adsorption, including enantioselective recognition.

ACKNOWLEDGMENTS

REFERENCES

1. G. Wulff, Chem. Rev. **102**, 1 (2002).
2. G. Wulff, B. Heide and G. Helfmeier, J. Am. Chem. Soc. **108**, 1089 (1986).
3. K.-O. Hwang, Y. Yakura, F. S. Ohuchi and T. Sasaki, Mater. Sci. Eng., C. **3**, 137 (1995).
4. S. Dai, M. C. Burleigh, Y. Shin, C. C. Morrow, C. E. Barnes and Z. L. Xue, Angew. Chem., Int. Ed. Engl. **38**, 1235 (1999).
5. D. Y. Sasaki and T. M. Alam, Chem. Mater. **12**, 1400 (2000).
6. A. Katz and M. E. Davis, Nature **403**, 286 (2000).
7. E. P. Barret, L. G. Joyner and P. P. Halenda, J. Am. Chem. Soc. **73**, 373 (1951).

Membranes and Nanoparticles

Molecularly Imprinted Materials: Towards the Next Generation

Lei Ye and Klaus Mosbach*
Center for Molecular Imprinting, Pure and Applied Biochemistry
Chemical Center, Lund University
Box 124, 221 00 Lund, Sweden
Email: klausmosbach@compuserve.com

ABSTRACT

This brief overview summarizes some recent developments from our Center for Molecular Imprinting related to the topic of this symposium. After a short presentation of the principle of molecular imprinting and recognition, the use of different materials including hybrids for the formation of the host will be discussed, followed by examples given of different formats used such as small polymer beads. In closing, potential directions for the next generation of molecular imprinting technology will be discussed.

INTRODUCTION

In the materials science area, defined structures in both organic and inorganic materials can be created using various structural templates to direct the fabrication process. As an example, polystyrene latex spheres have been used as template for the synthesis of highly ordered macroporous inorganic oxides [1]. Similarly, colloidal silica spheres were used to template a cross-linked polymer with ordered mesopores [2]. Following template removal, well-organized pore networks are formed in these materials, which have great potential uses in catalysis, separation technology, and biomaterials sciences. Not surprisingly, the same concept of template-assisted fabrication of defined structures has long been utilized in the research of molecular imprinting, aiming to generate molecular footprints in synthetic materials.

The molecular imprinting technique has attracted enormous research interests over the past decade. Commercialization of molecularly imprinted materials is now one of the major goals among the imprinting community, and indeed we have seen several startup companies utilizing molecular imprinting as a platform technology to be established. Compared to the supramolecular chemical approach [3], molecular imprinting is straightforward in producing tailor-made recognition materials, which display binding characteristics similar to biological antibodies, but with much more pronounced physical and chemical robustness. Uses of molecularly imprinted materials for separation, catalysis, polymer-assisted synthesis and biomimetic sensors have been demonstrated over the past years.

In general, molecular imprinting can be defined as a process of target directed synthesis of molecular hosts. For historical reasons, it has been largely related to the preparation of cross-linked synthetic polymers using a target molecule as a template. The complex formed between a template and appropriate functional monomers is fixed by co-polymerization with excess of a cross-linking monomer. After polymerization, the template is removed from the polymer matrix, which leaves binding sites specific for the original template, as well as its closely related structural analogues. Binding specificity of these sites is conferred by their well-defined shape and functionalities, which are complementary to those of the original template (Figure 1).
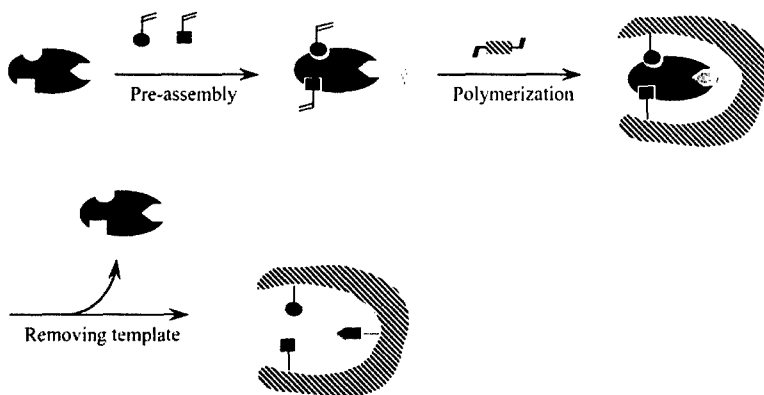
Figure 1. Schematic representation of a molecular imprinting process. Pre-assembly of functional monomers is driven by their complementary interactions with the template (in red). Co-polymerization with a cross-linker "freezes" binding groups to form a template-defined "cavity". Removal of the template by solvent extraction or chemical cleavage affords binding sites specific to the original template.

MOLECULAR IMPRINTING APPROACHES

Depending on the interactions between a template and functional monomers involved in the imprinting and rebinding steps, two distinct approaches have been followed to assemble molecularly imprinted polymers (MIPs). In the covalent approach pioneered by Wulff and co-workers, reversible chemical bonds are maintained between the template and the functional monomers during the polymerization and rebinding. In principle, this approach should lead to homogeneous binding sites, given the fact that the template-functional monomer complex is kept intact during the polymerization reaction. However, removal of the chemically bonded template from highly cross-linked polymer matrix is not a trivial task, and the re-binding process is normally much slower due to the necessary formation of the covalent bonds between the target compound and the MIP. Finally, this method requires prior derivatization of the template, and is often difficult to carry out except for those who are experienced in organic synthesis.

In the non-covalent approach invented by Mosbach and co-workers, various non-covalent molecular interactions such as hydrogen bond, ionic interactions and hydrophobic interactions are utilized. Due to the relatively weak interactions involved, often excess of functional monomers are added to stabilize the template-functional monomer complex during the polymerization, which often results in a heterogeneous distribution of binding sites. However, the large varieties of readily available functional monomers and the ease of preparation of MIPs have attracted the widely accepted use following this approach. Furthermore, the recent development of more potent functional monomers, e.g. use of metal coordinating interactions for specific amino acid sequences [4], should generate more homogeneous binding sites. In addition to the above-mentioned covalent and non-covalent approaches, attempts have been made to combine the advantages of both the covalent and non-covalent methods, whereby imprinting is carried out using polymerization of functional monomer being covalently coupled to a template, and selective rebinding by carefully designed non-covalent interactions [5].

52

MOLECULARLY IMPRINTED POLYMER BEADS

The most common format of molecularly imprinted materials is the cross-linked macroporous monolith, which is often ground and sieved to result in mostly irregularly shaped particles of different sizes. The grinding and sieving processes are labor intensive and waste useful polymers. When used as chromatographic stationary phases, the irregular particle shape also reduces column efficiency. For these reasons imprinted polymer beads are preferable. Although the well-established suspension and dispersion polymerization methods can be used to produce polymer beads, they are however not compatible with most non-covalent imprinting systems, since the aqueous continuous phase used interferes with the molecular interactions between template and functional monomers. In addition, hydrophilic functional monomers, such as the commonly used methacrylic acid, tend to partition into the water phase during the imprinting polymerization, which prevents their incorporation into the binding cavities. To solve all these problems, we have developed a suspension polymerization technique suitable for molecular imprinting in general [6]. This was achieved by using a liquid perfluorocarbon as the dispersing phase. The liquid perfluorocarbon is largely immiscible with most organic compounds and hence form an appropriate inert dispersing phase. A specially designed perfluorinated polymer surfactant was used to maintain stable emulsion droplets containing functional monomers, cross-linker, template and porogenic solvent during the polymerization. Using this technique we could obtain imprinted polymer beads ranging from 5 to 50 μm by varying the amount of the polymer surfactant. When used as a stationary phase in column chromatography, our imprinted polymer beads displayed a chiral resolution of amino acid derivatives similar to those achieved with the traditional ground and sieved MIP particles, however with low back pressure and at high flow rates.

To further simplify MIP preparation, we have recently introduced a precipitation polymerization method for the preparation of imprinted polymer microspheres [7,8]. In comparison with previous imprinting compositions, we started imprinting polymerization from a highly diluted solution of template, functional monomer, cross-linker and initiator. Uniform polymer microspheres ranging form 100 nm to 5 μm can be readily obtained, with favorable binding characteristics for different target compounds. Our polymerization condition is compatible with both covalent and non-covalent imprinting, because there is no interfering surfactant or stabilizer present in the reaction mixture. The small MIP microspheres can be easily suspended in assay solvents and dispensed, and yet readily collected by simple centrifugation. These characteristics are ideal for binding assays using MIPs instead of antibodies. Figure 2 shows the molecularly imprinted microspheres specific for the steroid hormone 17β-estradiol. As demonstrated by a competitive binding analysis, the MIP microspheres had very low cross-reactivity towards a compound that is only slightly different from the template, 17α-estradiol. The small particle size of imprinted microspheres also allows them to be used in microanalysis systems where fluidic apparatus has highly limited dimensions. In a later demonstration, similar molecularly imprinted microspheres were used as chiral selectors in capillary electrophoresis for enantiomer separations [9].

An attractive feature of imprinted microspheres is the fact that their binding sites are more accessible to bulky molecules such as a template labeled with an enzyme probe. In this way, the MIP bound not only the template itself, but also the template-enzyme conjugate in the same specific manner [10]. Thus we have successfully used imprinted microspheres in an enzyme-linked immunosorbent assay (ELISA) for determination of the herbicide, 2,4-

dichlorophenoxyacetic acid. The enzyme label tobacco peroxidase was used to catalyze both colorimetric and chemiluminescent reactions. The same assay was later improved to give much lower detection limit [11] along with potential high sample throughput [12].

It should be mentioned that similar cross-linking polymerization in dilute monomer solution was used to prepare molecularly imprinted microgels [13]. By adjusting monomer concentration and solvent composition, the cross-linking polymerization produced mainly intramolecularly cross-linked microgels. The model system utilized covalent bonds between a sugar derivative and a boronic acid monomer in the imprinting and rebinding reactions. Although binding selectivity of the obtained polymers was only modest, the obtainable nanometer-sized microgels were attractive for many potential applications.
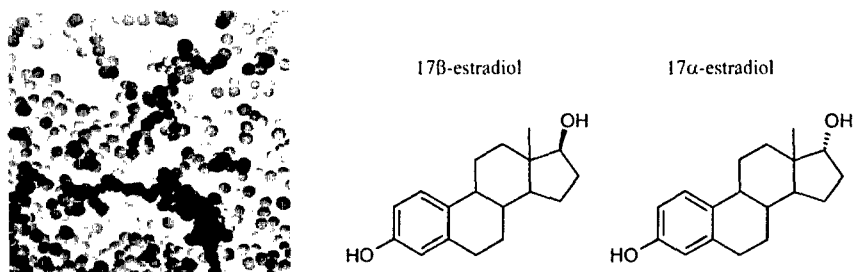
Figure 2. Molecularly imprinted microspheres against 17β-estradiol.

MOLECULARLY IMPRINTED HYBRID MATERIALS

Composite materials can combine desirable features of individual components. In many cases one component provides a stable structural framework to support other functional materials. In other cases it gives the final composite favorable physicochemical characteristics, for example magnetic susceptibility, that can be used to facilitate isolation of the hybrid materials.

As to the first aspect, molecularly imprinted composite polymers were prepared using preformed poly(trimethylolpropane trimethacrylate) beads as the supporting material [14]. The residual double bonds in the supporting beads were used to graft up to 64 mol% of molecularly imprinted cross-linked polymethacrylate. The resulting composite polymer beads were used as chiral stationary phase, which gave an enantioselectivity for the template molecule, Boc-L-Phe equivalent to the purely imprinted polymer, but with improved column efficiency. Instead of a polymer support, silica particles were also used as support and derivatized with vinyl monomers, followed by an imprinting polymerization with a metal coordinating monomer, N-(4-vinyl)-benzyliminodiacetic acid, using the enzyme ribonuclease A as template [15]. The imprinted composite material, when used as a stationary phase, demonstrated specific retention of the template protein due to the metal coordinated interactions between the adsorbent and the target protein. This protein-imprinted composite material represented one of the few early successes in imprinting against biomacromolecules.

By incorporating magnetic iron oxide, we have prepared superparamagnetic molecularly imprinted polymer beads using a suspension polymerisation methodology with a perfluorocarbon liquid as the dispersing phase. The imprinted polymers can be easily withdrawn from solution by

application of a magnetic field, which greatly simplified the separation and washing steps that are routinely used in binding assays [16].

IMPRINTING USING IMMOBILIZED TEMPLATE

For imprinting against small target molecules, the templates are commonly allowed to form complexes with functional monomers free in solution. An alternative route demonstrated by our group and others was to use a template immobilized on a solid support [17]. Following imprinting polymerization, the template and the carrier support were removed by chemical dissolution, which leaves surface imprinted sites on the obtained MIP. In this manner we could control not only the orientation of the binding cavities, but also the pore size distribution of the resulting MIPs, using for example silica beads with different porous structures as the carrier. Compared with imprinting against the free standing template, the surface imprinted binding sites resulting from immobilized template are much more accessible to large analyte-protein conjugates, or to analytes labeled with other bulky reporter entities such as gold colloids. It should be noted that our approach of using an analyte-carrier as template is analogous to the generation of biological antibodies using hapten-protein conjugates. In both cases specific binding sites for small target molecules are generated.

To demonstrate the concept of imprinting against immobilized template, we have chosen in one case theophylline as a model template compound. The template was immobilized by coupling 8-carboxypropyltheophylline to amino-functionalized porous silica beads. The pore volume was filled with a mixture containing the functional monomer, trifluoromethacrylic acid, divinylbenzene and a polymerization initiator. After polymerization, the silica gel was removed by treatment with aqueous HF, which resulted in macroporous organic polymer beads having surface-exposed binding sites (Figure 3). In addition to generating a surface imprinted polymer, the use of the silica framework as a pore-forming template gave well-controlled pore size distribution for the resulting organic polymer beads. When used in radioligand binding analysis using tritium-labeled theophylline as a probe, the imprinted organic polymer beads displayed binding characteristics similar to that obtained with the traditionally imprinted bulk polymers.
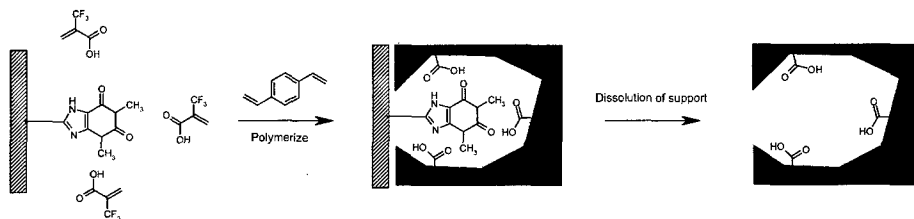
Figure 3. Molecular imprinting using immobilized template.

In a recent report, methacrylate-based mesoporous beads were imprinted against adenine and triaminopyrimidine analogues pre-immobilized on porous silica particles. Dissolution of the silica also resulted in surface confined binding sites specific for adenine and triaminopyrimidine [18].

IMPRINTED SCINTILLATION POLYMERS: A NEW SENSOR CONCEPT

Although molecularly imprinted polymers (MIPs) often display high binding affinity and specificity mimicking natural antibodies [19], there are only few examples of imprinted polymers capable of effective signal generation. For certain types of template molecules, it is possible to design special fluorescent functional monomers that are responsive to template binding, these monomers however can rarely be used when a different analyte is targeted. To circumvent the synthetic difficulties, we have proposed a concept of combining molecular imprinting with proximity resonance energy transfer for chemical sensing [20], where a universal reporter molecule is incorporated into close proximity of the imprinted binding sites. As a proof of principle, we developed a polymerizable organic scintillator and incorporated it into molecularly imprinted microspheres. The imprinted microspheres were prepared by the same precipitation polymerization method as discussed above. Due to the small size of the polymer beads, the organic scintillator was confined in close proximity to the imprinted binding sites that were created by the template, (S)-propranolol (Figure 4). When a tritium-labeled template binds to the MIP, the radioactive decay triggers the scintillator to generate a fluorescent light. The radioactive template free in solution is simply too far away from the scintillator to provide efficient energy transfer, therefore no fluorescence light can be observed. In this way our imprinted polymer can be looked at as a true biomimetic sensor - it directly reports the event of target binding with high selectivity. Following this concept, we have developed a competitive scintillation proximity assay using a radiolabeled template as the probe. The imprinted scintillation polymers could be used in both organic and aqueous solvents [21].
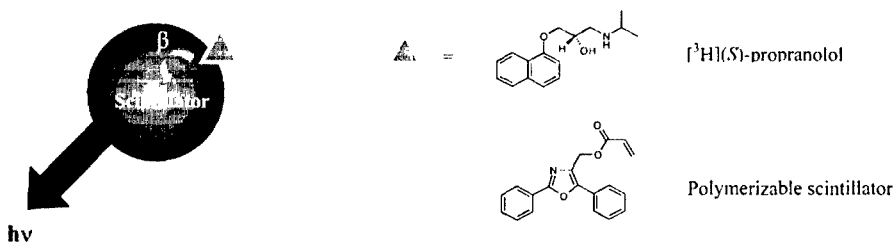
Figure 4. Molecularly imprinted scintillation polymer specific for (S)-propranolol.

"ANTI-IDIOTYPIC IMPRINTING" AND "DIRECT MOLDING": THE NEXT GENERATION

Until now, most research activities have focused on generating imprinted materials recognizing different target entities ranging from small molecules to proteins [22,23], and, even to whole cells [24]. Although in a limited number of examples, imprinted sites have been used to control chemical transformations [25,26], few attempts have been made to explore the utility of molecularly imprinted sites per se as a template to generate new chemical entities.
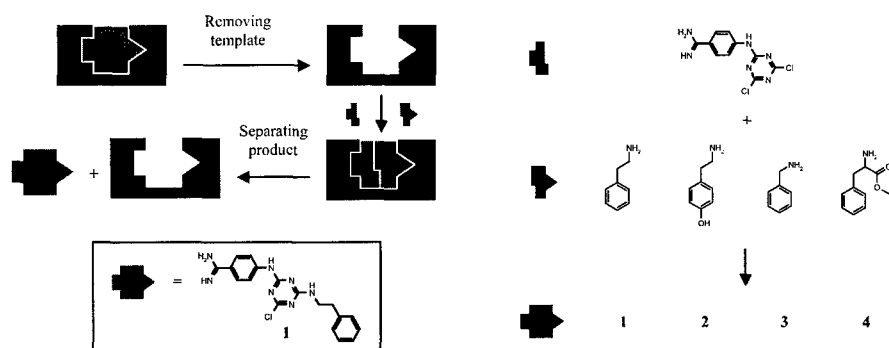
Figure 5. Anti-idiotypic imprinting for generating bioactive molecules.
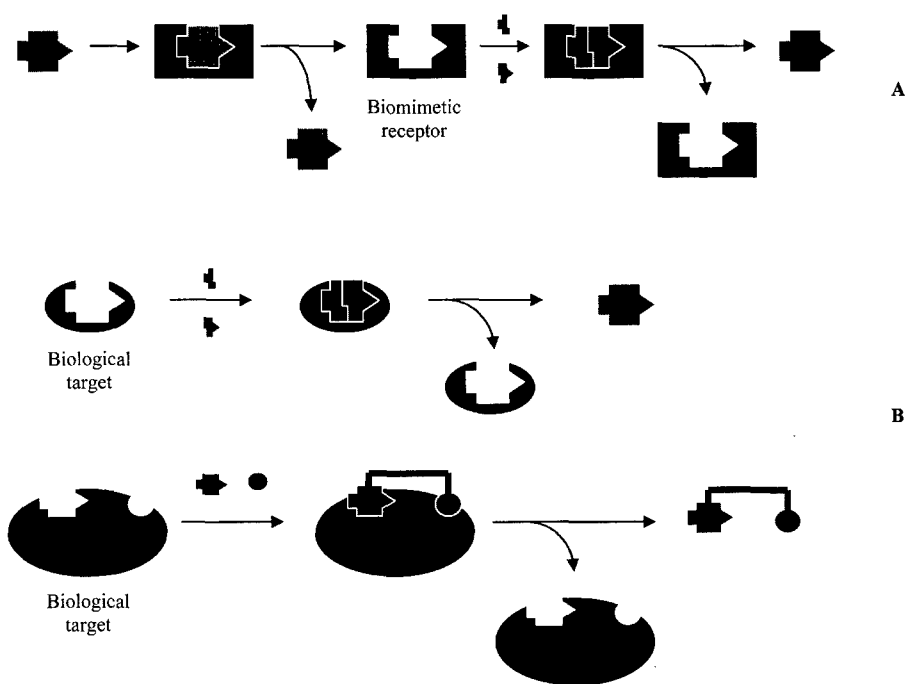
Figure 6. Schematic representation of the "anti-idiotypic" and "direct molding" methodologies. (A) The "anti-idiotypic imprinting" leads to new compounds mimicking the original template. (B) "Direct molding" assembles ligands by polymerization within or between sites of a biological target.

To address this issue, we have recently used pre-imprinted binding sites to generate bioactive compounds mimicking the original template, which was chosen from a known enzyme inhibitor [27]. This "double imprinting" is analogous to the formation of anti-idiotypic antibodies in the immune response system, where the combining site of the secondary antibody is an "internal image" of the original antigen. We envision that our synthetic anti-idiotypic imprinting approach should be useful for finding new drug candidates, especially when the three-dimensional structure of a biological target, a prerequisite for the rational drug design, is unresolved.

In our model anti-idiotypic imprinting we have chosen the medicinally interesting proteinase kallikrein as a model system. In the first step, a previously identified inhibitor (1) was used as the original template to prepare an imprinted polymer. The polymer contains specific binding "cavities" mimicking the enzyme's active site. These "cavities" were then used in a second round of imprinting to synthesize the original template, as well as that of new inhibitors using a small library of building blocks (Figure 5). In addition to the original template, we have identified a new enzyme inhibitor using this approach. In principle, our concept of using MIPs to screen building blocks instead of product libraries should greatly simplify the drug discovery process by saving enormous synthetic operations, since only the hit reactions need to be scaled up for further investigation.

The above approach can also be more schematically depicted as shown in Figure 6. Alternatively, a biological target can be used directly as a template to direct polymerization reactions [28] to give synthetic molecules affecting biological recognition process.

CONCLUDING REMARKS

Starting from relatively simple building blocks, molecular imprinting can be used to prepare synthetic materials mimicking biological antibodies and enzymes. Due to their physicochemical robustness, MIPs are favorable in many practical applications to replace biologically generated binding materials. It can be envisioned that MIPs will find potential applications in almost all aspects where natural antibodies have been utilized to provide selective target binding. Recent achievements in molecular imprinting on micro- and nano-spheres, molecularly imprinted "hierarchical structures" generated by using immobilized templates and simultaneous use of multiple templates at different dimensional scales are among the new breakthroughs. We foresee that the merger with novel preparation techniques in materials science will certainly open up new opportunities for molecular imprinting. As examples, microfabricated molecularly imprinted materials may be used in micro fluidic devices [29], and arrays of MIPs addressing different sample markers may lead to more intelligent artificial noses and tongues. In closing this discussion, we would like to point out that the borderline between regular molecular imprinting and the next generation leading to new bioactive molecules, using either the "anti-idiotypic imprinting" or the "direct molding" methodologies, is now being erased.

REFERENCES

1. B. T. Holland, C. F. Blanford, T. Do, A. Stein, *Chem. Mater.* **11**, 795 (1999).
2. S. A. Johnson, P. J. Ollivier, T. E. Mallouk, *Science* **283**, 963 (1999).
3. J. –M. Lehn, *Angew. Chem., Int. Ed. Engl.* **27**, 89 (1988).

4. B. R. Hart, K. J. Shea, *J. Am. Chem. Soc.* **117**, 7105 (1995).
5. M. J. Whitcombe, M. E. Rodriguez, P. Villar, E. N. Vulfson, *J. Am. Chem. Soc.* **123**, 2072 (2001).
6. A. G. Mayes, K. Mosbach, *Anal. Chem.* **68**, 3769 (1996).
7. L. Ye, P. A. G. Cormack, K. Mosbach, *Anal. Commun.* **36**, 35 (1999).
8. L. Ye, R. Weiss, K. Mosbach, *Macromolecules* **33**, 8239 (2000).
9. L. Schweitz, P. Spegel, S. Nilsson, *Analyst* **125**, 1899 (2000).
10. I. Surugiu, L. Ye, E. Yilmaz, A. Dzgoev, B. Danielsson, K. Mosbach, K. Haupt, *Analyst* **125**, 13 (2000).
11. I. Surugiu, J. Svitel, L. Ye, K. Haupt, B. Danielsson, *Anal. Chem.* **73**, 4388 (2001).
12. I. Surugiu, B. Danielsson, L. Ye, K. Mosbach, K. Haupt, *Anal. Chem.* **73**, 487 (2001).
13. A. Biffis, N. B. Graham, G. Siedlaczek, S. Stalberg, G. Wulff, *Macromol. Chem. Phy.* **202**, 163 (2001).
14. M. Glad, P. Reinholdsson, K. Mosbach, *React. Polym.* **25**, 47 (1995).
15. M. Kempe, M. Glad, K. Mosbach, *J. Mol. Recogn.* **8**, 35 (1995).
16. R. J. Ansell, K. Mosbach, *Analyst* **123**, 1611 (1998).
17. E. Yilmaz, K. Haupt, K. Mosbach, *Angew. Chem., Int. Ed. Engl.* **39**, 2115 (2000).
18. M. M. Titirici, A. J. Hall, B. Sellergren, *Chem. Mater.* **14**, 21 (2002).
19. G. Vlatakis, L. I. Andersson, R. Müller, K. Mosbach, *Nature* **361**, 645 (1993).
20. L. Ye, K. Mosbach, *J. Am. Chem. Soc.* **123**, 2901 (2001).
21. L. Ye, I. Surugiu, K. Haupt, *Anal. Chem.* **74**, 959 (2002).
22. J. –L. Liao, Y. Wang, S. Hjertén, *Chromatographia* **42**, 259 (1996).
23. H. Shi, W. –B. Tsai, M. D. Garrison, S. Ferrari, B. D. Ratner, *Nature* **398**, 593 (1999).
24. A. Aherne, C. Alexander, M. J. Payne, N. Perez, E. N. Vulfson, *J. Am. Chem. Soc.* **118**, 8771 (1996).
25. S. E. Byström, A. Borje, B. Akermark, *J. Am. Chem. Soc.* **115**, 2081 (1993).
26. C. Alexander, C. R. Smith, M. J. Whitcombe, E. N. Vulfson, *J. Am. Chem. Soc.* **121**, 6640 (1999).
27. K. Mosbach, Y. Yu, J. Andersch, L. Ye, *J. Am. Chem. Soc.* **123**, 12420 (2001).
28. K. Mosbach, *Anal. Chim. Acta* **435**, 3 (2001).
29. M. Yan, A. Kapua, *Anal. Chim. Acta* **435**, 163 (2001).

M3.2

MOLECULAR IMPRINTING OF POLYMERIC CORE-SHELL NANOPARTICLES

Natalia Pérez Moral and Andrew G. Mayes
School of Chemical Sciences, University of East Anglia, Norwich, NR4 7TJ, U.K.

ABSTRACT

In order to evaluate the compatibility of structured nanoparticles produced by aqueous emulsion polymerisation with the non-covalent imprinting procedure, a number of imprinted polymeric nanoparticles have been synthesised by seeded emulsion polymerisation in the presence and absence of a porogenic solvent. Propranolol was chosen as the template molecule using methacrylic acid (MAA) and ethylene glycol dimethacrylate (EDMA) as functional monomer and crosslinker respectively. The influence of the porogen and the amount of template added was studied by measuring the capacity of the polymeric particles to rebind template both in organic and aqueous buffers by radioligand binding assay. By increasing the amount of template from 0.5 to 6% (mol/mol with respect to monomers) the specific rebinding was increased from 2% to 24% in aqueous buffer and to 31% in a toluene based assay. The influence of the porosity was also established when the rebinding was performed in an organic solvent.

INTRODUCTION

Molecularly imprinted polymers (MIPs) address the need for robust, simple, fast and efficient methods to detect and separate specific molecules of interest such as drugs and pesticides. They are prepared easily and rapidly, and can be used in pre-concentration techniques, analysis, extraction, catalysis or separation. The imprinting technology consists basically of the synthesis of a highly crosslinked polymer in the presence of a template molecule. After removal of the template, the polymer is left with imprinted sites "fixed" in its structure that are complementary in shape, size and functionality to the targeted molecule, and therefore will selectively distinguish and bind such molecules when present in the medium to be processed or analysed.

Specific recognition in the imprinted polymer depends on the type of interaction established between the template and the monomer(s) prior to polymerisation, which could be covalent, non-covalent or a combination of the two. Covalent interactions are strong and more selective but there are few types sufficiently labile to be made and broken under the mild conditions required for dynamic rebinding, limiting this approach to only a few specific functional groups. The use of a combination of covalent interactions in the creation of the imprinted step and non-covalent interactions in the rebinding of the ligand has also proved to be useful in some cases, but its use is restricted by the synthetic steps required to modify the template molecule prior to polymerisation. There are numerous examples of imprinted polymers based on non-covalent interactions, a more adaptable methodology that can be used with a large number of template molecules and allows fast kinetics in the rebinding of ligands. So far, molecules have been successfully imprinted based on hydrogen bonds, electrostatic and hydrophobic interactions, albeit with some limitations encountered as a consequence of the heterogeneity of binding sites and limitations in the use of certain solvents.

An important factor in the performance of the MIP is the morphology of the polymer. Most imprinted polymers are synthesised by bulk polymerisation because of its simplicity and convenience, despite the irregularity of the particles produced, the waste of polymer and the lack

of control in the process. New methods of MIP synthesis giving control of the morphology of the polymer offer the possibility of applying MIP to new fields and conditions. For these reasons, imprinted polymers in the form of particles have been developed. The production of polymers directly in the particle format avoids the necessity of grinding them, and also allows the creation of polymers with high surface areas where diffusion of the ligands should be facilitated. Some of the new methodologies developed in recent years for imprinting of polymeric particles in organic media using non-covalent interactions are the synthesis of imprinted microsized particles in a fluorocarbonated solvent by suspension polymerisation [1] or the synthesis of nanoparticles by precipitation polymerisation [2]. In aqueous environments imprinted particles of 2-50 micron have also been described using a 2-step swelling method [3]. Emulsion polymerisation has also been used to create imprinted nanoparticles in an aqueous environment using the combination of covalent-non covalent interaction or directed imprinting at the surface of particles based on hydrophobic interactions [4,5]. To date, it has not been combined with the classical non-covalent approach. In particular, a two-stage emulsion polymerisation procedure would provide many attractive opportunities if it could be combined with non-covalent imprinting, since core-shell structures can be produced by this well-established methodology. Core-Shell methodology provides an efficient way to control and predict the final number and size, and therefore surface area, of imprinted monodisperse particles, as well as the opportunity to introduce specific properties such as fluorescence or magnetism into the cores. The binding sites should be restricted to the thin particle shells where they would have good accessibility and exchange kinetics for ligand binding.

In this paper, in order to evaluate the compatibility of core-shell nanoparticles produced by a 2-stage emulsion polymerisation system and imprinting with the versatile non-covalent imprinting procedure, we have synthesised a series of polymeric nanoparticles using a seeded emulsion polymerisation procedure. Imprinted shells have been made both in the presence and absence of a porogenic solvent. The influence of the porogen and the amount of template added were studied together with the capacity of the polymeric particles to rebind template both from organic and aqueous buffers by radioligand binding assay. Propranolol was selected as the template to be imprinted in the shell of the nanoparticles because it has been previously non-covalently imprinted by other polymerisation methods and its rebinding analysed in aqueous buffers and organic solvents.

EXPERIMENTAL SECTION

To remove the inhibitor prior to polymerisation, methacrylic acid (MAA) was distilled under vacuum, while methyl methacrylate (MMA) and ethylene glycol dimethacrylate (EDMA) were washed with 1M aqueous sodium hydroxide, dried over $MgSO_4$ and stored with molecular sieves at 4 °C until required. Sodium dodecyl sulfate (SDS), ammonium peroxodisulfate (APS) and other solvents and reagents were used as received. ^{3}H-propranolol (specific activity 29Ci/mmol, 1μCi/ μL in ethanol) was obtained from Sigma. Scintillation counting was performed in a Wallac 1409 DSA β-radiation counter. Scintillation cocktail Ecoscint A (National Diagnostics) was used for aqueous samples. Organic samples were counted in toluene containing 2,5 diphenyloxazol (PPO - 3g/l) and 1,4-bis (5phenyloxazol- 2-yl)-benzene (POPOP - 0.2g/l), both obtained from Aldrich. Particles were characterised by T.E.M. using a Jeol JEM 200E X Transmission Electron Microscope. Samples were prepared by drying a drop of a solution of particles in water with SDS over a grid coated by a carbon film.

Synthesis of particles

The seeds were prepared using a standard batch emulsion polymerisation in a 1 litre three-necked jacketed reactor connected to a water bath to control the temperature. The system was equipped with a condenser, a mechanical stirrer and a gas inlet to maintain an inert argon atmosphere. A solution of $NaHCO_3$ (0.95 gr.; 11.3 mmol) in distilled water (520 gr.) with SDS (0.913gr.; 3.16 mmol) was added into the reactor and purged with argon to remove oxygen under gentle stirring, while increasing the temperature to 90 °C. Once the temperature was reached, the monomer mixture was added and the stirring speed increased to 600 rpm. After 1 minute, the initiator APS was added dissolved in 1 ml of water to initiate the polymerisation. The temperature was maintained at 90 °C for 24 hours to ensure total decomposition of the initiator. The final latex was filtered through a fine nylon mesh and its solid content calculated before being used in the next step.

Core-shell particles were synthesised using a 500-ml reactor similar to that described above. In a typical reaction, firstly, a solution containing water (88.5 gr.) and SDS (0.5gr.; 1.73 mmol) was added into the reactor and purged with argon under gentle stirring while the temperature was raised to 70 °C. A solution containing a mixture of monomers (EDMA 10.1gr; 50.9 mmol; MAA 1.1 gr.; 12.7 mmol), porogen (10.6 ml toluene), template and seed (51.4 gr.) that had been previously mixed for 20 minutes, was also charged into the reactor followed by an aqueous solution of 0.112 gr (0.84 mmol) of APS. The stirring speed was increased to 200 rpm and the reaction allowed to proceed for 6 hours before cooling to room temperature.

The resultant polymer particles were ultrafiltered to remove any surfactant adsorbed on the particles, and then the template was removed by washes with ammonium acetate 1M dissolved in a mixture of ethanol (40) / acetic acid (25) / water (35), followed by washes in acetic acid/ ethanol 1:3 and methanol [7].

Radioligand Binding Assay

0.25mg of particles were mixed with 1ml of a solution of ^{3}H-propranolol (0.07 μl H^3-propranolol ml^{-1}) in the solvent mixture (toluene with 0.5% acetic acid or aqueous solution of sodium citrate 25 mM with 0.5% acetic acid and 2% ethanol) and incubated overnight at room temperature. The solution was then centrifuged at 12000 rpm for 5 minutes, and 0.5 ml of the supernatant mixed with 3 ml of scintillation liquid. The radioactivity was measured by liquid scintillation counting.

RESULTS AND DISCUSSION

Synthesis of core-shell particles

Polymer particles made in a 2-stage emulsion polymerisation system can produce structured particles with a core-shell arrangement if conditions are chosen appropriately. A latex obtained by a standard batch emulsion polymerisation was used as a seed to polymerise a crosslinked shell polymer over it in a second stage. By assigning the amount of seed polymer, and as long as secondary nucleation is restricted, the final number, size and size distribution of particles can be controlled.

Core-shell particles are not always produced, however, when polymer particles are synthesised in two successive stages. Various alternative outcomes, such as nucleation of new

particles or different distributions of the components ("raspberry-like", "acorn like") can also occur [6]. The final particle structure is determined by the influence of thermodynamic and kinetic stability forces between the components of the polymer. In order to find a good system to promote the creation of core-shell particles, two different seeds were synthesised and their ability to generate imprinted shells were assessed (see table I).

Table I. Synthesis of core particles. Polymerisation conditions: 90 °C for 24 hours, initiatior= ammonium persulfate; S.C.= solid content, Dp= particle diameter.

	Monomer(s) (mol %)	SDS/M (mol %)	S.C. (%)	Dp (nm)	Nature of latex
1	MMA: EDMA 95/5	0.84	7.8%	53	monodisperse
2	MMA 100	0.84	7%	55	monodisperse

Both of the resultant polymers were assessed by TEM, which showed that the latices were monodisperse in size, with diameters in the order of 55nm when the core was made 100% of MMA and 53 nm when the core was 5% crosslinked with EDMA.

After being characterised, each of these latices was used as a seed in a second stage of the polymerisation to create a highly crosslinked shell around it. Attempts to create a core-shell structure over the MMA core under the chosen conditions were not successful, resulting in high viscosity and low conversion of monomers to polymers. On the other hand, the core-shell arrangement was kinetically favoured when a small level of crosslinker was incorporated into the core, yielding a high conversion latex. Consequently, core 1 was selected as the seed for the imprinting of shells in the second stage.

The influence of porogen (toluene) and template was studied by preparing different core-shell particles varying the amount of propranolol added in the second stage of polymerisation from 0.5% to 6%, with and without porogen (Table II). Control particles were also synthesised in the absence of propranolol.

Table II. Synthesis of core-shell particles using core 1 as seed.
(prop = propranolol, M = MAA+EDMA, porogen = toluene, porogen/monomer ratio = 1/1 (vol/vol), Dp = particle diameter).

Composition of polymer		Dp (nm)	
% prop/M (mol)	MAA/prop (mol)	with porogen	without porogen
----	----	70	60
6	3.4 / 1	72	
3.9	5 / 1	66	60
2	10 / 1	70	52
1	20 / 1	55	59
0.5	40 / 1	37	60

In general, the particle sizes (measured from the TEM images) were as expected based on the seed size and monomer charge during shell synthesis. In a few cases, however, notably in porous polymer imprinted with 0.5% of propranolol and to a certain extent in non-porous

polymer imprinted with 2% propranolol (visible in figure 1e), secondary nucleation occurred giving a population of smaller particles which reduced the average Dp below that expected.

Particles synthesised in the presence of a porogenic solvent are expected to have a porous shell with higher surface area than the particles synthesised in its absence. In general terms, porous particles present a slightly wider polydispersity in size. Some electron micrographs of the particles are shown in Figure 1.
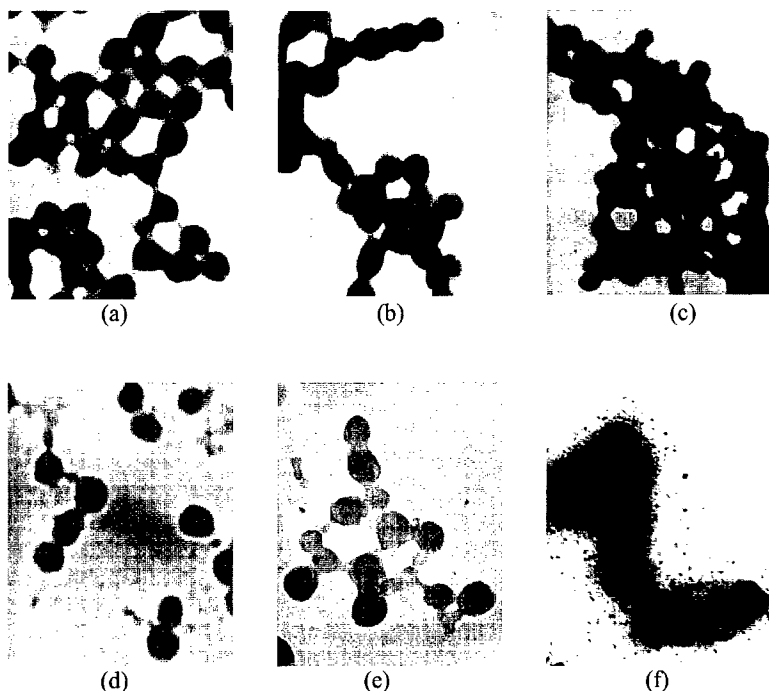
Figure 1. TEM photographs of (a) seed 1; (b) non-imprinted porous core-shell; (c) 3.9% imprinted porous core-shell; (d) non-imprinted non-porous core-shell; (e) 2% imprinted non-porous core-shell and (f) 3.9% imprinted non-porous core-shell.

The capacity of the imprinted polymers to rebind propranolol from organic and aqueous solutions was analysed by radioligand binding assay. Results are presented in table III. As expected, it was found that the rebinding of propranolol to MIP increases with the amount of template incorporated into the shell. When the imprinted sites are made more accessible to the ligands by incorporating porosity into the shell, this effect is more significant. The specific rebinding of propranolol (defined as the amount of ligand rebound to the imprinted polymer after subtraction of the amount rebound non-specifically to non-imprinted particles) in toluene containing 0.5% acetic acid was higher than when the analysis was performed in an aqueous buffer, but in both cases the imprinting effect was significant.

The particles that contain a porous shell showed a higher uptake of propranolol than the "compact" non-porous imprinted shells. Presumably, the latter particles have the imprinted sites situated at or very near the surface, but they still bind significant levels of propranolol compared to control particles. More detailed studies are underway to determine the effect of shell porosity on site accessibility, exchange kinetics and the balance of forces involved in the binding interactions.

Table III. Specific rebinding of propranolol ((rebinding to imprinted particles) – (rebinding to non-imprinted particles)) to 0.25 mg.of polymer, buffer = Na citrate 25mM + 0.5% acetic acid + 2% ethanol pH = 4.2, toluene* = toluene + 0.5% acetic acid ; values are means of 4 replicates.

Polymer	% Specific rebinding in buffer		% Specific rebinding in toluene*	
% prop/M	particles with porogen	particles without porogen	particles with porogen	particles without porogen
(----)	(16)	(11)	C(2)	(16)
6	24		31	
3.9	19	14	27	8
2	18	10	15	8
1	15	6	9	9
0.5	2	3	2	3

CONCLUSIONS

It has been demonstrated that non-covalent imprinting of templates is possible in the shells of core-shell nanoparticles, despite the fact that they are synthesised in the presence of an aqueous continuous phase and the organic imprinting phase must be saturated with water. The binding capacity is somewhat lower than that usually measured for bulk imprinting of propranolol, but this can no doubt be increased by careful optimisation of the many system variables such as template concentration and continuous phase pH. Including a porogenic solvent during shell synthesis increased the binding capacity of the particles, but significant rebinding was also shown by the non-porous shells. Further studies are under way to characterise the effect of the porogen in greater detail, and to measure its effect on binding site accessibility, selectivity and exchange kinetics.

REFERENCES

1. A. G. Mayes and K. Mosbach, *Anal. Chem.* **68**, 3769-3774 (1996).
2. L. Ye, P. A. G. Cormack and K. Mosback, *Anal. Commun.* **36**, 35-38 (1999).
3. K. Hosoya, K. Yoshizako, N. Tanaka, K. Kimata, T. Araki and J. Haginaka, *Chemistry. Letters*, 1437-1438 (1994).
4. N. Perez, M. J. Whitcombe and E. N. Vulfson, *J. Appl. Polym. Sci.* **77**, 1851-1859 (2000).
5. N. Perez, M. J. Whitcombe and E. N. Vulfson, *Macromolecules* **34**, 830-836 (2001).
6. S. Lee and A. Rudin in *Polymer Latexes*, edited by E. S. Daniels, E. D. Sudol and M. S. El-Aaser, (ACS Symposium series 492, 1992) pp 234-254.
7. L. I Andersson, *Anal. Chem.* **68**, 111-117 (1996).

M3.3

Molecularly Imprinted Ionomers

George M. Murray and Glen E. Southard
Johns Hopkins University Applied Physics Laboratory,
Laurel, MD 20723-6099

ABSTRACT

Ionomers have been defined as copolymers that have a certain proportion of ionic groups. The ionic groups have a significant effect on the mechanical properties of the copolymers. This is generally due to aggregation of ions in a low dielectric medium. The primary result is to restrict chain motion and raise the glass transition temperature. These attributes have relevance to molecular imprinting, since restricted chain motion should help preserve the integrity of the binding site. The connection between ionomers and molecular imprinting has come from the production of metal ion imprinted resins. Metal ions are used in the production of molecularly imprinted polymer ion exchange resins and ionically permeable membranes. The polymers have applications as separations media, sequestering media and as ion selective sensors. Metal ions are also being used to form imprinted polymers based on metal mediated imprint binding. We have prepared ion exchange resins, selectively permeable polymer membranes, ion selective electrodes and ion selective optical sensors using a modified version of the molecular imprinting technique. The modification is a reduction in the amount of covalent crosslinking used to form the polymers. This reduction may be justified by the presence of residual metal ion crosslinking in the immediate region of the imprinted binding site. The effects of metal ions on the thermal and mechanical properties of the polymers, as well their impact on binding selectivity are critical variables.

INTRODUCTION

The production of selective metal ion sequestering and separation materials is a growing field with broad application and critical importance. Industry requires vast quantities of metals and generates tons of metal wastes. Nuclear energy production and past weapons production facilities have created unique challenges in the area of metal ions separation. Ultimately, technology must reach a point where all metal containing waste streams are treated as recoverable metal resources. Metal ion selective molecularly imprinted materials may be the means to realize this goal. An additional application of metal ion imprinted polymers is as sensors. The ability to detect a specific metal ion in a complex matrix is keenly appreciated.

Several issues need to be addressed in the design of molecularly imprinted ion complexing. Of primary concern is to make a rebinding site with good affinity. The binding selectivity afforded by metal ions is starting to be appreciated [1]. The large literature database of tabulated metal to ligand affinities forms a useful guide to the selection of the correct metal for a specific target [2]. Another useful aspect of metal ions in site production is the tendency of metal ions to exhibit directional bonding. The stereo-regularity of metal coordination geometries can be exploited to form a favorable geometry for secondary interactions. Many organic compounds have functional groups that are amenable to metal ion tethers. The selection of a metal ion with useful spectroscopic properties allows the imprinted polymer to be used as an optical sensor [3]. Metal ions can be spectroscopically useful by forming metal-analyte complexes that absorb specific wavelengths of light. Metal ions can be chosen that will not

exhibit color unless coordinated by a target ligand. A metal can be chosen that forms a fluorescent complex, such as Zn^{2+} with benzoin. When the imprinted site is to sense a heavy metal ion, a fluorescent ligand may be induced to phosphoresce, via the external heavy atom effect, yielding an emission band that is Stokes shifted and longer lived than with the unbound molecule [4]. To prepare an anion sensing polymer, it is useful to choose a luminescent metal ion as a component of the binding site to acquire both a high thermodynamic binding affinity and a highly sensitive reporter [3].

Perhaps the greatest general utility in the use of metal ions to form imprinted polymers is the change in structural properties. The inclusion of cations into polymer acids to form polymer salts drastically changes the structural relaxation and other physical properties due to strong coulombic interchain interactions [5]. The effect is to raise the glass transition temperature and impede structural relaxation. When trying to produce a stable rebinding site in a polymer it is important to maintain site integrity. By using ionic crosslinks through metal ions the polymer chains become rigid and should maintain site integrity. Since metal ion crosslinking can have a greater effect on polymer properties than does covalent crosslinking, less total crosslinking can be used and some of the recoil effect described earlier may be avoided. This hypothesis is being examined in this work.

As stated previously, the chemical recognition element must be stable and reusable. A potential problem with MIPs as chemical recognition elements would be a gradual loss of specificity. The problem has not been directly addressed in the chemical literature but efforts to understand temperature effects on imprinted polymers have shown that selectivity can be destroyed by exposure to an elevated temperature for short periods. This sort of temperature study is analogous to the techniques used to artificially age materials. Chen et al. [6] showed a loss in selectivity with increasing time and temperature. Essentially, the selectivity was annealed away. These studies were performed on the usual highly covalently cross-linked polymers. No such studies have been performed on polymers with relatively low levels of covalent crosslinking or polymers, with low levels of covalent crosslinking supplemented by metal ion crosslinks or materials with only metal ion crosslinks.

EXPERIMENTAL DETAILS

The synthetic procedures involved in producing the polymers under investigation have been published previously [7-10]. The steps involved in acquiring the capacity data are shown in Figure 1. The data thus acquired are used in the equations that follow the Figure to calculate the metal ion capacity and selectivity parameters. In addition to the cation used to prepare the polymer, other cations with differing charges, sizes, coordination numbers, and/or coordination geometries are used in these selectivity quotient measurements to verify specificity. Measurements are also made using the polymers prepared with no metal cation (H^+ or NH_4^+). Measurements required for these studies are made using a pH meter for $[H^+]_a$ and elemental analysis (electro-thermal atomization atomic absorption, ETA-AAS or inductively coupled plasma mass spectrometry, ICP-MS) for $[M^{n+}]_a$.
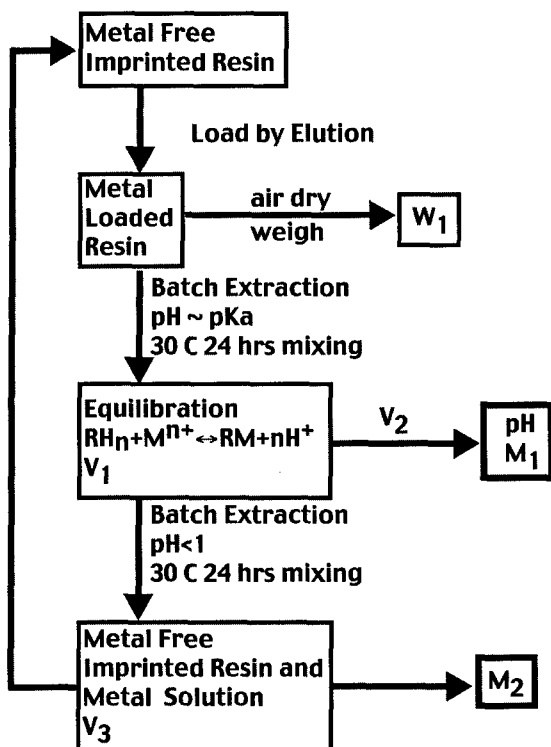
Figure 1. Steps involved in ascertaining resin capacity.

$$capacity = \frac{[M^{n+}]_1 V_2 + [M^{n+}]_2 V_3}{W_1} \tag{1}$$

$$K = \frac{[H^+]^n \left(capacity - [M^{n+}]_1 V_1 / W_1 \right)}{[M^{n+}]_1 \left(n[M^{n+}]_1 V_1 / W_1 \right)^n} \tag{2}$$

$$\alpha_{M_1, M_2} \, (selectivity) = \frac{capacity \, M_1}{capacity \, M_2} \tag{3}$$

The capacity of an imprinted polymer is affected by the amount of crosslinking. Polymers we have prepared with a fairly low level of crosslinking result in a maximum capacity at a certain level of crosslinking. Table I shows the effects of divinylbenezene (DVB) crosslinking on the capacities of lead imprinted styrenic resins and an unimprinted styrenic control resin. Although the unimprinted control (P-0) has double the amount of ligand (4-vinylbenzoic acid or VBA) as the imprinted resins, the Pb^{2+} capacities of all the imprinted resins are larger than the non-imprinted control resin. The capacity optimum of 2 % crosslinking suggests that a balance of site rigidity and accessibility can be obtained. In the case of Pb^{2+}, high levels of covalent crosslinking (>5 mole %) resulted in resins with no selectivity. In the case of styrenic Fe^{3+} resins, high levels of covalent crosslinking (85 mole %) gave reduced selectivity, but higher capacity, due to greater porosity (Figure 2).

Table I. The effect of cross-linking on lead ion capacity

polymer ID	mole % complex (mole % ligand)	mole % DVB	capacity (μmole/g)
P-0	(4)	1	0.112
P-1	1	1	0.179
P-2	1	2	0.231
P-3	1	4	0.127

In order to be certain as to the selectivity of the resins, experiments were performed to verify selectivity by the simultaneous loading of two or more metal ions. The results of one study are presented in Table II. As expected the Pb^{2+} imprinted polymer had better selectivity for Pb^{2+} ion.

Table II. Capacity and capacitive selectivity of unimprinted and Pb imprinted resins toward Pb, Cu and Cd in multiple exposure experiments

polymer ID	Pb capacity (μmole/g)	Cd capacity (μmole/g)	selectivity $\alpha_{Pb, Cd}$	Cu capacity (μmole/g)	selectivity $\alpha_{Pb, Cu}$
P-0	0.162	0.00463	35		
P-1	0.119	0.00220	54		
P-6	0.107	0.00120	90	0.00931	12

Further characterization included the determination of the acidity constants of some of the resins. The titration of a resin allows the determination of the number of ionogenic sites that have, during swelling and cleaning, become accessible to H^+ ion. This "capacity" is indicative of the relative amount of metal ion complex that has been incorporated in the copolymerization reaction. A calculation of the expected load of lead vinyl benzoate complex in a polymer containing 5.00 mole percent complex (with 1.00 percent crosslinking) is 416 μmole/gram. A titration of this copolymer yields a value of 20.2 μmole/gram for H^+ or just 10.1 μmole/gram of lead ion. This corresponds to only 2.50 percent of the metal ion complex being exchangeable into the copolymer. The remaining metal ion is locked in place and, for the reasons stated above, may contribute to the binding site rigidity.
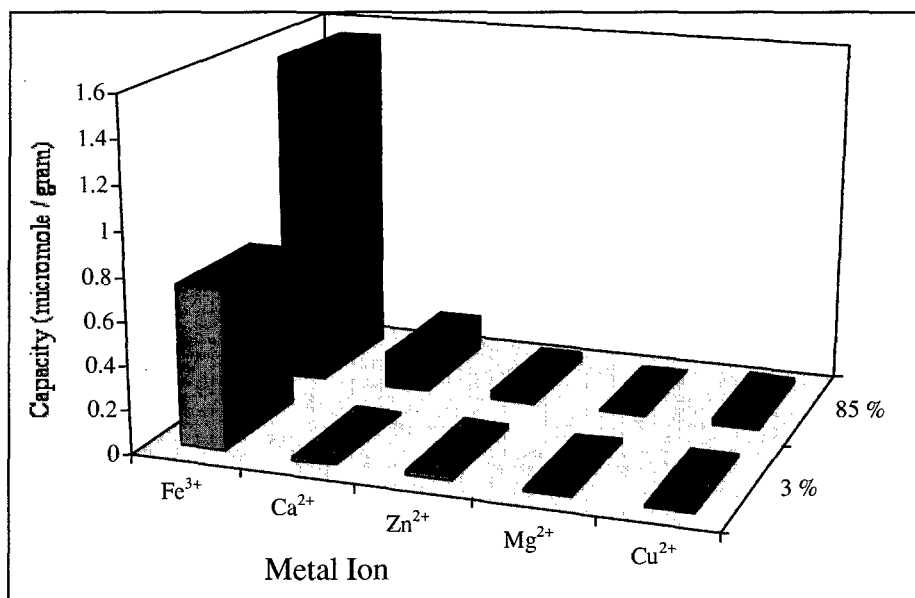
Figure 2. Ion loading capacity for Fe^{3+} imprinted polymers showing higher capacity but lower selectivity with high degrees of covalent crosslinking (% refers to divinyl benzene).

Blank resins, that are prepared without a template metal ion, exhibit a degree of selectivity based upon thermodynamic affinity. Thus, a comparison of the selectivity (α) values of the imprinted resins with those of the blank resins provides an estimate of the overall effect of imprinting on selectivity. Thus, a comparison of the selectivity (α) values of the imprinted resins with those of the blank resins provides an estimate of the overall effect of imprinting on selectivity. Thus the relative selectivity is:

$$\alpha' = \frac{\text{Selectivity of the imprinted Polymer}}{\text{Selectivity of the unimprinted Polymer}} \tag{4}$$

where the unimprinted polymer is prepared without a metal ion template. The effect of imprinting is dramatic in the case of uranyl ion imprinted resins using VBA as the template ligand. In this case the selectivity of the blank polymers are favorable to first row transition metals. Thus, imprinting the resins results in selectivity values of 10 or greater for uranyl against ions tested; Cd^{2+}, Cu^{2+}, Ni^{2+}, Zn^{2+} and Fe^{3+} as compared to the 1 to 3 fold selectivity against exhibited by a blank polymer.

Table III. Effect of imprinting (α') of the uranyl templated 4-vinylbenzoate resins.[*]

Polymer Resin	$\alpha'\ UO_2^{2+}, Cd^{2+}$	$\alpha'\ UO_2^{2+}, Cu^{2+}$	$\alpha'\ UO_2^{2+}, Ni^{2+}$
P12	19.1 ± 0.4	10.1 ± 0.2	24.5 ± 0.4
P22	21.4 ± 0.5	15.6 ± 0.4	29.5 ± 0.3
P32	33.0 ± 0.9	21.4 ± 0.3	33.5 ± 0.9
P42	37.2 ± 1.3	23.2 ± 0.5	36.2 ± 1.4

[*] The identity code for these polymers is as follows: the first digit is the mole % complex and the second digit is the mole % divinylbenzene.

The studies outlined above show that imprinted ion exchange resins made with small amounts of covalent crosslinking generally have much better selectivity but lower capacity than resins made by the conventional approach using large amounts of covalent crosslinking. This observation has been made by other practitioners. Harkins and Schweitzer, [11] first observed this phenomenon for Ni^{2+} and Cu^{2+} imprinted ion exchange resins. Lemaire, et al. observed this trend in their work with imprinting chelating resins for lanthanides [12]. We have observed this trend for Pb^{2+}, Fe^{3+} and UO_2^{2+} and intend to explore the implications of this observation and its ramifications to the field of molecular imprinting.

•CurveFit line
Tg =101.75 +4.0647 (mol %DVB)
r= 0.995931
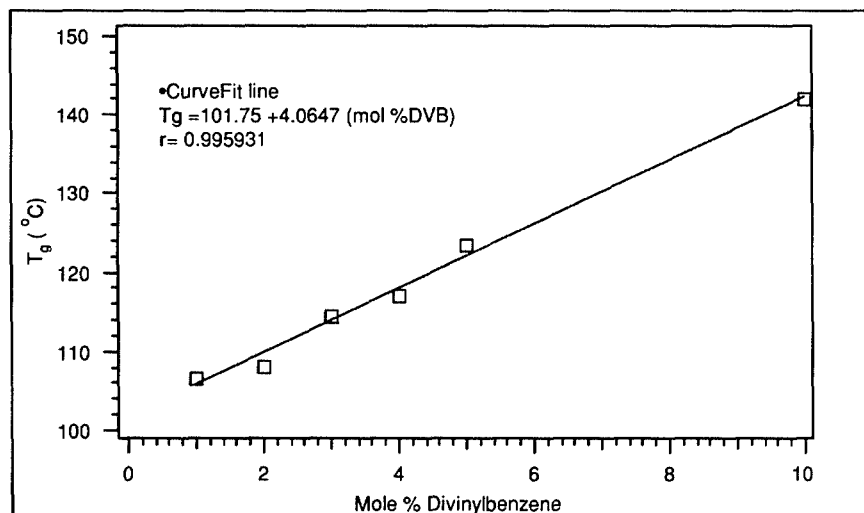
Figure 3. The glass transition temperatures of a series of polymers containing 1 mole % Pb(VBA)$_2$, equivalent to 0.41 mole % Pb, with increasing amounts of covalent crosslinking, as mole % DVB.

Differential scanning calorimetry (DSC) is a popular technique since it is capable of determining both thermodynamic properties and kinetic characteristics of thermal processes. The ability to define thermal transients in polymer relaxation, especially the glass transition temperature (Tg) and relaxation events that occur at temperatures other than Tg is of importance to this study. The relaxational transitions that occur at temperatures below the bulk Tg are referred to using Greek letters beginning with β, α being reserved for Tg. These lower temperature relaxational transitions may be important to the understanding of the stability and selectivity of the imprinted sites since they may represent motion at the site of the imprint. Figure 3 shows the effect that covalent crosslinking has on the Tg of a Pb^{2+} ion imprinted polymer.

A sufficient amount of metal ion crosslinking produces an additional transition at temperatures that are higher than the bulk, or "matrix" Tg. This higher temperature transition has been observed in certain cases by using DSC. It is much more readily apparent when using dynamic mechanical analysis (DMA). Thus, the high temperature transition induced by metal aggregation has a much greater effect on the mechanical properties than on the heat capacity of the bulk material. DMA can provide more information but requires a solid chunk of material as opposed to powders. This requirement makes it unsuitable to ascertain the differences in loaded and unloaded imprinted polymers. In the case of styrenic polymers similar to those we have produced, metal ion concentrations reach a threshold and the two glass transitions observed by DMA are seen as a single intermediate glass transition when measured by DSC. A plot of the DSC Tg values versus the amount of metal in a polymer gives an "s" shaped curve with the deviation from linearity being attributed to ion clustering (Figure 4). The bend of the "s" seems to occur when aggregation forms a new "cluster" Tg. This means that most of the investigation can be performed using the logistically simpler DSC with an occasional verification by DMA (Figure 5).
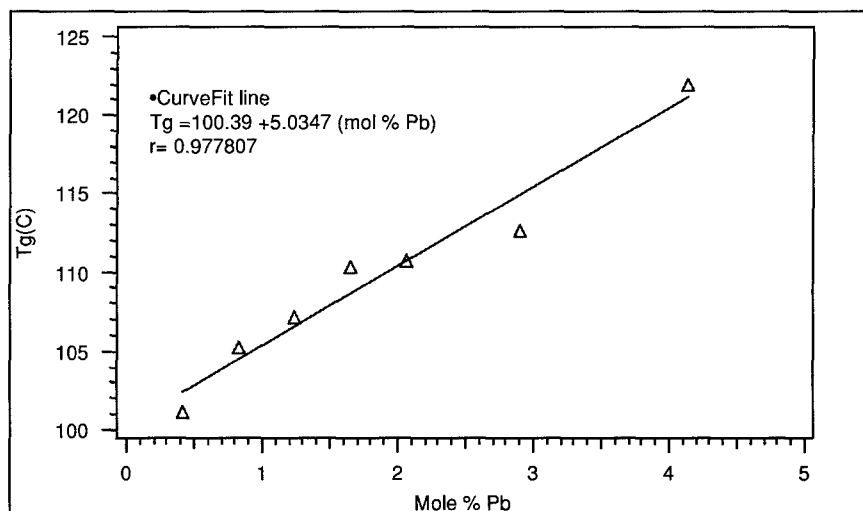
Figure 4. Graph of a series of polymers containing 1 mole % DVB with increasing amounts of ionic crosslinking, as $Pb(VBA)_2$.

The most recent development in scanning calorimetry is modulated DSC (MDSC). MDSC has advantages over conventional DSC that are of particular utility in the present investigation. Conventional DSC measures the sum of all the thermal events in the sample. This can be confusing when events overlap or are affected by fabrication. MDSC helps discriminate thermodynamic properties from thermal history and each of these from the other. For example, the glass transition is an enthalpic relaxation that can be affected by thermal history and in some instances may appear as a melting transition. Use of MDSC provides a means to discriminate against such artifacts. MDSC also has advantages in sensitivity and resolution, both critical in evaluating higher order transitions. We have begun to look at MDSC traces of Pb^{2+} and UO_2^{2+} imprinted polymers (Table IV). The data for uranyl imprinted ion exchange resins shows the expected increase in Tg with the increase in the amount of metal ion crosslinking. The abrupt jump at 5 mole % of the complex indicates that at this level complex aggregation has occurred. The thermal behavior has been examined in greater detail for the Pb^{2+} containing polymers.
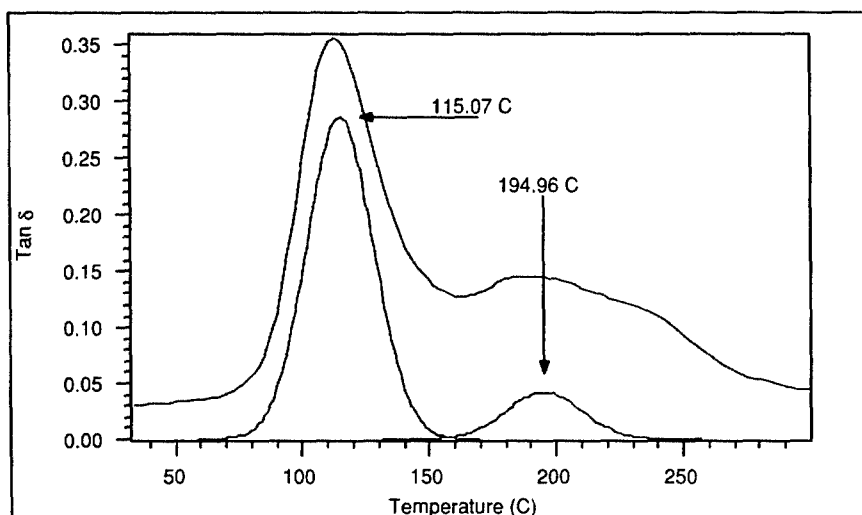
Figure 5. Dynamic Mechanical Analysis of the 4.1 mole % $Pb(VBA)_2$ containing polymer showing two glass transitions (upper trace smoothed data, lower trace Gaussian fit).

Table IV. Glass transition temperatures of uranyl vinylbenzoate imprinted polymers

Polymer ID	Tg by MDSC (°C)
polystyrene	102.56
P12	111
P22	112.24
P32	113.25
P42	113.89
P52	121.89

* For these polymers the identity code is: the first digit is the mole % complex and the second digit is the mole % divinylbenzene.

DISCUSSION

The discovery of the influence of metal ion crosslinking on molecular imprinting is a natural consequence of using the process to make ion exchange resins. The theory regarding the allowable reduction in the amount of covalent crosslinking was based on the expectation that in a highly crosslinked polymer matrix, the removal of the imprinting species will result in a recoil of the ligating atoms. The recoil occurs due to the relaxation of the polymer chains when the imprinting crosslink is broken. A highly crosslinked polymer is under a considerable amount of internal stress created during fabrication. The removal of the imprinting crosslink can relieve that stress by relaxation. A larger amount of covalent crosslinking restricts chain motion and a greater the amount of flexure stress is placed on the polymer chains during their growth. This theory predicts that higher levels of covalent crosslinking results in a larger amount of recoil and a greater loss in selectivity. The substitution of a small amount of ionic crosslinking has been shown to have dramatic effects on polymer properties. The benefits of ionic crosslinking on molecular imprinting are two-fold. First, ionic crosslinks have a greater effect on the localized rigidity of the binding sites through aggregation. Second, the crosslinks formed by a metal ion are by electrostatic attraction and may allow some rotational flexure at the crosslink, necessitating less adjustment in the region of the imprint and resulting in less selectivity loss when the imprint species is removed.

The properties of metal ion containing polymers have been studied from the materials science perspective for many years. Much of the work has appeared in a recent monograph by Eisenberg and Kim, entitled ,"Introduction to Ionomers" [13]. Of interest to this work is the characterization of the sodium salt of a copolymer of styrene and methacrylic acid. Several models for the structure of this copolymer have been developed. Central to these models is the concept of the aggregation of the ion pairs. Aggregation creates regions of reduced chain mobility in the manner of multiple crosslinks. When the amount of ion content is increased clusters of the aggregates cause regions of the polymer to behave differently and a second, higher glass transition temperature can be observed indicative of the effect of the clusters. As metal content continues to increase, the regions of restricted motion begin to overlap and a single, high glass transition temperature is observed. The metal ion aggregation is a result of dielectric constant and is similar to the processes involved in the production of reverse micelles.

Thus, the regions of greatest chain restriction are near the metal ion aggregates. The optimal placement of binding sites for imprinted polymers should also be near the metal ion aggregates. In the event that an ion exchange resin is being fabricated with low levels of covalent crosslinking, both of these criteria will be met, since some of the imprinting ions are left in the polymer after the ion exchange sites are liberated. We believe we have encountered this phenomenon in regard to Pb^{2+}, Fe^{3+} and UO_2^{2+}resins [7-10]

CONCLUSIONS

Metal ion imprinted polymers have yet to be characterized in sufficient detail. This lack of characterization is starting to be remedied. The associated field of ionomers gives clues toward the direction some of these new efforts should take. This is especially relevant since characterization of metal ion imprinted polymers has revealed that some of the metal ions are trapped in inaccessible locations or are bound too strongly to be released. This is especially true of resins formed with a non-complexing matrix monomer. Such resins possess residual metal ion crosslinks that may have a dramatic effect on the polymer properties. The effects of metal ion crosslinks on molecular imprinting are not well understood. The effects may help to explain why selectivity of some metal ion imprinted polymers is increased when the amount of covalent crosslinking is decreased.

ACKNOWLEDGEMENTS

REFERENCES

1. J. Matsui, I. A. Nicholls, T. Takeuchi, K. Mosbach, and I. Karube, *Anal. Chim. Acta*, *335*, 71 (1996).
2. L. Gmelin and R. Meyer, Leipzig-Berlin, 1995.
3. A. L. Jenkins, O. M. Uy, and G. M. Murray, *Anal. Chem.*, *71*, 373 (1999).
4. G. M. Murray, A. L. Jenkins, A. Bzhelyansky, and O. M. Uy, *JHUAPL Tech. Digest*, *18*, 432 (1997).
5. V. A. Bershtein and V. M. Egorov, *Differential Scanning Calorimetry of Polymers*, Ellis Horwood, New York, 1994.
6. Y. Chen, M. Kele, P. Sajonz, B. Sellergren, and G. Guiochon, *Anal. Chem.*, *71*, 928 (1999).
7. S. Y. Bae, X. Zeng, and G. M. Murray, *J. of Anal. At. Spec.*, *10*, 1177 (1998).
8. S. Y. Bae, G. E. Southard, and G. M. Murray, *Anal. Chim. Acta*, *397*, 173 (1999).
9. X. Zeng and G. M. Murray, *Sep. Sci. & Technol.*, *31*, 2403 (1996).
10. A. Kimaro, L. A. Kelly, and G. M. Murray, *Chem. Comm.*, 1282 (2001).
11. D. A. Harkins and G. K. Schweitzer, *Sep. Sci. & Technol.*, *26*, 345 (1991).
12. O. Vigneau, C. Pinel, and M. Lemaire, *Anal. Chim. Acta*, *435*, 75 (2001).
13. A. Eisenberg and J. Kim, *Introduction to Ionomers*, John Wiley & Sons, New York, 1998.

Poster Session

Computational Fluid Dynamics Models of Molecularly Imprinted Materials in Microfluidic Channels

Cindy K. Webber and M. Joseph Roberts
Polymer Science and Engineering Branch, Code 4T4220D, NAVAIR, NAWCWD, China Lake, CA 93555, USA

ABSTRACT

Current research will lead to rapid-prototyping of chemical sensors that utilize microfabricated molecularly imprinted (MI) materials. CFD/CAD software may be used to model flow and chemical binding properties of MI materials in microfluidic channels. Use of this type of software expedites results when changes in properties are made. The surface concentration of bound analyte on a monolithic molecularly imprinted polymer (MIP) within microfluidic channels can be modeled using its experimental binding kinetics. The time necessary to reach a detection limit is calculated and optimized as a function of flow parameters. In this report, we discuss the unique issues associated with the modeling of chemical sensors that utilize MI materials.

INTRODUCTION

In the broadest sense, device engineering is a multi-step process that includes 1) design concept, 2) computer aided design (CAD) and computer aided modeling (CAM), and 3) prototype fabrication. The utilization of CAD/CAM allows the engineer to iteratively optimize a device design before prototype fabrication. Thus, CAD/CAM adds to the efficiency of the device engineering process. Presently, this paradigm has entered into the device engineering sub-discipline of microfluidic devices, often called 'lab-on-a-chip'. CAD/CAM software under development by several research groups and companies offer the capabilities to model fluid flow in micrometer-scale channels using computational fluid dynamics (CFD). Added capabilities include simultaneous modeling of fluid flow, chemical reactions, and analyte binding to surfaces. Our project is concerned with the incorporation of molecularly imprinted materials into this device engineering paradigm. We seek to determine the properties of MI materials which are most relevant to the ultimate performance of devices and thus to the device engineer. In this paper, we will focus on the CAD/CAM issues. We report our initial experience adapting available software along with a simple example that illustrates present design and modeling capabilities, and provide a list of properties that are necessary for designing with MI materials. Ultimately, this work points the way to the generation of a database of MI material properties incorporated into software for the engineer to use in new device designs. We hope our list will encourage the reporting of these properties as new MI materials are developed and optimized.
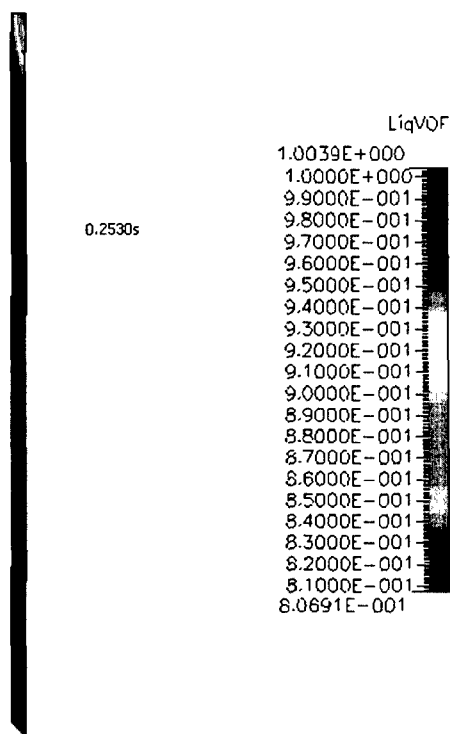
Figure 1: Flow model in a microfluidic channel.

COMPUTATION DETAILS

Materials properties of a recently reported MI polymer were used in the model we report here.[1]

The software used in the project was obtained from CFD Research Corporation, 215 Wynn Dr., Huntsville, AL 35805. This software contains 3 components: CFD-Geom where the geometric models can be drawn and gridded; CFD-ACE where analysis is done; and CFD-View to view by 2 and 3 dimensions and animation.

The CFD ACE+ software was used to demonstrate flow and binding in a microfluidic channel 100 microns in diameter.

A typical design drawing begins with wire frame models drawn in 2 or 3 dimensions. These are then gridded for finite element analysis.[2] We chose to start with a simple straight 2D microfluidic channel 100 microns wide. The volume is separated into three sections, to allow different properties in the center 'patch'. Flow is modeled first with the channel initially filled with water, then at t=0, flow begins with the analyte solution. This first model shows the channel nearly full of the analyte fluid at a t= 0.25 seconds at an initial velocity of 0.02 m/s (12µl/min), 0 pressure, and T=300K (Figure 1.).
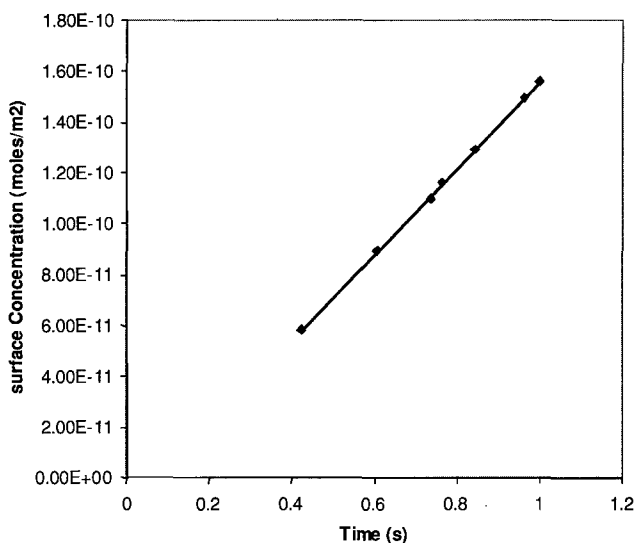
Figure 2. Time vs. Surface Concentration at an analyte concentration of 1×10^{-5}M.

The next step introduces the values for binding kinetics (determined by experiment), and other variables. For instance:

Density of receptors= maximum possible surface concentration = 5×10^{-8} mole/m^2
Association rate constant = 41.2 M^{-1}s^{-1}
Disassociation rate constant = 3.21×10^{-4} s^{-1}

To show the changes in histamine binding on the surface over time, an analyte concentration of 4.5×10^{-8}M was chosen and the surface concentration determined at 1.0, 4.9, 7.5, and 10.0 seconds. The results show that less than 4.9 seconds are needed to reach a steady state surface concentration of 10^{-13}M

To show velocity effects, all variables are kept the same except the inlet velocity. The inlet velocity was varied between 0.001m/s and 0.002 m/s to look at changes in the concentrations at the surface. Effects of changing the analyte concentration from 1M to 1×10^{-5}M were also investigated.

The flow models show some time constraints of velocity changes. For instance, if the channel needed to fill in one second, a velocity greater than 0.02 m/s is required.

Using data from different times at the same analyte concentration it can be determine that it would take 5.1 seconds to have a detectable surface concentration based on a Mach-Zehnder interferometer (Figure 2).
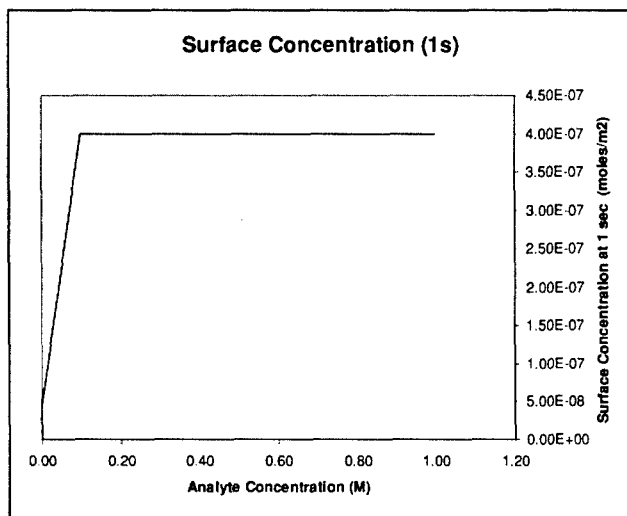
Figure 3. Analyte concentration vs. surface concentration at 1 second.

Investigating the surface concentration as the analyte concentration is changed, the limit of binding can be determined. This is based on the density of receptors possible $(5 \times 10^{-8} \text{mole/m}^2)$. At an analyte concentration of 1M, the maximum binding is reached at 1 second (Figure 3).

CONCLUSION

Computer modeling expedites the device engineering process when chemical and geometric changes are made. The simple example presented above demonstrates that fluid and MI material properties are critical for a complete and accurate design (Table 1). Furthermore, as new MI materials are developed, monomer formulation properties that may be needed by device fabrication methods should be considered also.[3] For example, low viscosity monomer formulations may be required for certain well-known techniques.[4] In another example, a materials' optical properties might dictate to the engineer the choice of an optical detector to use with a highly transparent imprinted acrylate. In conclusion, we hope that this paper will encourage dialog between the MI materials synthesis and the engineering communities during the early stages of MI material development for more efficient production of new devices that utilize MI materials.

Table 1. List of Important Kinetic and Materials Properties for CFD/CAM

Fluid	MI Material
viscosity	association rate constant
density	dissociation rate constant
velocity	irreversible rate constant
surface tension	diffusivity
analyte concentration	receptor density
elasticity	surface roughness

ACKNOWLEDGMENTS

REFERENCES

1. Hart, B. R.; Shea, K. J. *J. Am. Chem. Soc.* **123**, 2072 (2001).
2. J. Welty, C. Wicks, and R. Wilson, *Fundamentals of Momentum, Heat, and Mass Transfer*, (John Wiley & Sons, Inc., 1984).
3. Yan, M.; Kapua, A. "Fabrication of Molecularly Imprinted Polymer Microstructures," *Anal. Chim. Acta*, **435**, 163-167 (2001).
4. Zhang, X., X. Jiang, and Sun, C., " Micro-stereolithography for polymeric and ceramic micro parts," *Sensors and Actuators, A*, **77(2),** 149-156 (1999).

Oligonucleotide Imprinting in Aqueous Environment

Dolly Batra and Kenneth J. Shea*
Department of Chemistry
University of California, Irvine
Irvine, CA 92697

INTRODUCTION

The development of synthetic receptors that recognize nucleotide bases and their derivatives is an important area of research [1-3]. Applications are envisioned in separation science, biosensors, drug therapy and genetic engineering. Previously in this laboratory, we have developed a molecularly imprinted synthetic receptor for 9-ethyladenine (9-EA). The network polymer has an affinity for adenine and its derivatives with an average association constant (K_a) of 75,000 M^{-1} in CHCl$_3$ [4]. When a 9-EA imprinted polymer was used as the chromatographic support, adenine eluted at 27 minutes using 92.5/5.0/2.5 CH$_3$CN/H$_2$O/CH$_3$CO$_2$H as the mobile phase, while cytosine, guanine and thymine derivatives all eluted close to the void volume (2.0 min). In addition, imprinted polymers have been made with complementary binding sites for cytosine and guanine [5], as well as other nucleotide base analogues [6].

The extension of these results to construct robust receptors for *oligonucleotides* requires fundamental changes in imprinting strategies. Most importantly, since oligonucleotides are water soluble, strategies that employ EGDMA/MAA formulations in organic solvents will need to be replaced with those that do not compromise the interactions between template (the oligo) and functional monomer.

Initially, the imprinting of a 2'-deoxyadenosine dimer (1) was attempted. Due to the hydrophilicity of a DNA oligomer, it was difficult to find a suitable organic solvent that would solubilize the oligomers without disrupting the template's interaction with the polymer matrix [7]. To combat the solubility problems and to insure the homogeniety of the polymerization solution, we examined various polymer formulations with organic and/or aqueous-based solvents that would dissolve the template without disrupting these key interactions.

EXPERIMENTAL DETAILS

Synthesis of Template

The first phase of this research involved synthesis of an adenine dimer **1**. Since imprinting involves milligram quantities of template molecules, it was decided to synthesize these quantities using a solution phase technique. The synthesis utilized phosphoramidite methodology (Scheme 1) [8]. The coupling of individually protected nucleotides using a phosphoramidite linkage yields phosphite **2**. This linkage is later oxidized to the phosphate group, and, following deprotection with TFA, treatment with concentrated NH$_4$OH leads to the desired oligonucleotide (**3**).

1
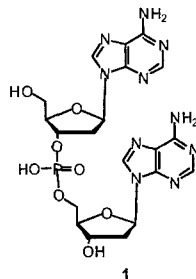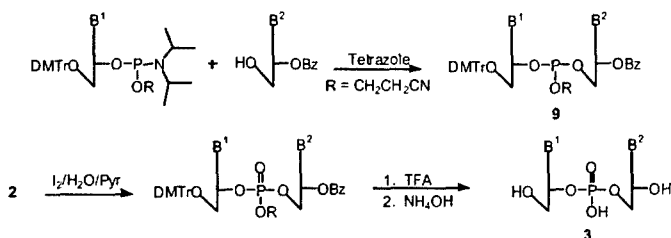
Scheme 1

Protected nucleoside **6** was synthesized from 2'-deoxyadenosine (**4**, Scheme 2). Selective protection of the primary 5'-alcohol with dimethoxytrityl chloride (DMTrCl), followed by protection of the secondary 3'-alcohol with benzoyl chloride provided fully protected nucleotide **5**. Deprotection of the DMTr group with TFA furnished alcohol **6** [9].

Scheme 2
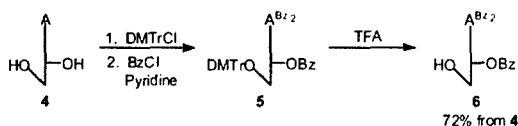
Protected 2'-deoxyadenosine **6** was then coupled with the commercially available phosphoramidite **7** using standard coupling conditions to provide 2'-deoxyadenosine dimer **8** (Scheme 6) [10].

Scheme 3
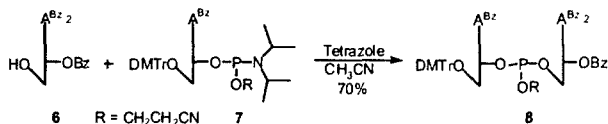
Phosphite **8** was then oxidized using I_2 to yield phosphate **9** [10]. The fully protected dimer **9** was treated with NH_4OH and AcOH deprotection, and following reverse-phase HPLC purification gave adenine dimer **1**.

Scheme 4
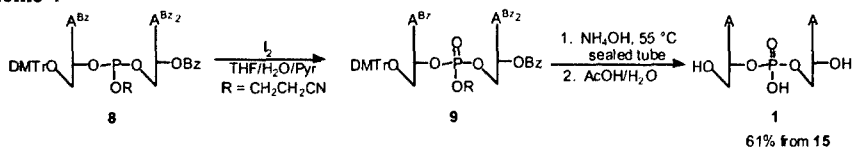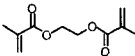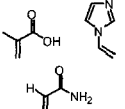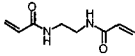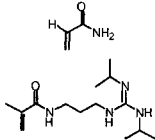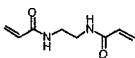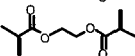
Polymerization Reactions

The 2'-deoxyadenosine dimer **1** was used as the imprint molecule for various organic and aqueous polymerization formulations (Table 1). The polymer formulations were selected on the basis of earlier work from our and other laboratories (**P1** and **P4**) or were newly developed (**P2** and **P3**). Buchardt and Mathew developed a molecularly imprinted polymer for adenine in an organic/aqueous medium similar to **P1** [11]. **P4** was synthesized using a polymerization

formulation similar to that used for 9-EA imprinting [4, 7]. A quaternary ammonium surfactant, which has been shown to be stable under the polymerization conditions used for 9-EA, was used to solubilize the oligonucleotide in an organic solvent [7].

An aqueous formulation, **P2**, was based on the known interaction of a guanidine group with a phosphate salt [5]. Ethylene bisacrylamide[12] was used as the crosslinking monomer for its solubility in H_2O and its compatibility to co-polymerize with acrylamide, which was added for its interaction with the adenine base. A similar formulation, **P3**, was made without the guanidine functional monomer. Non-imprinted polymers **P1₀** - **P4₀**, were also synthesized as controls to test for non-specific interactions (Table 1).

Table 1. Polymer formulations used to imprint adenosine dimer **1**. Molecularly imprinted polymer (MIP) using 1% dimer **1** as template (MIP) were made together with polymers made in the absence of template (Blank Polymer).

MIP	Blank Polymer	Crosslinking Monomer	Functional Monomer(s)	Solvent	Splitting Yields
P1	P1₀	(structure)	(structures)	95/5 MeOH/H_2O	73 %
P2	P2₀	(structure)	(structures)	95/5 H_2O/MeOH	40 %
P3	P3₀	(structure)	(structure)	95/5 MeOH/H_2O	60 %
P4*	P4₀*	(structure)	(structure)	CHCl₃	90 %

*A quarternary ammonium surfactant (*N,N,N,N*-Bis(octadecyl)dimethylammonium bromide) was used to solubilize the oligonucleotide in an organic solvent.

Polymers **P1** – **P4** were prepared by thermal polymerization of degassed solutions of the above formulations for 24 h at 65 °C using AIBN (1 %) as initiator. The resulting polymers were coarsely crushed and Soxhlet extracted using MeOH. After the polymers were ground to 25 – 125 μm particles, rebinding studies with the dimer **1** were carried out in water, by studying the uptake of the dimer over a concentration range of 0.2 – 3 mM. The pH of the uptake solutions was ~3.5 and did not change significantly over time.

Rebinding Studies with Dimer 1

P1 and **P4**, along with their non-imprinted counterparts **P1₀** and **P4₀**, were found to rebind poorly with the dimer **1**. **P2** and **P2₀** bound the dimer equally well, with non-specific interactions drowning any specific interactions. MIP **P3**, however, showed imprinting effects as its uptake of dimer **1** was significantly better than the non-imprinted polymer **P3₀** (Figure 1, below).
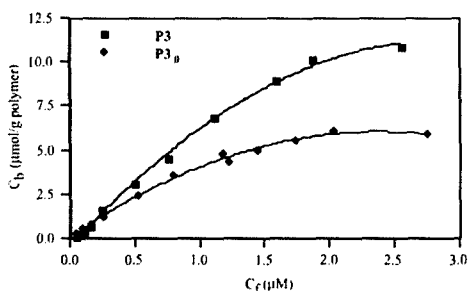
Figure 1. The rebinding of dimer **1** to MIP **P3** is compared to its rebinding with non-imprinted polymer **P3$_0$**. C_b is the amount of dimer rebound to the polymer. C_f is the remaining concentration of the dimer in solution.

Rebinding studies were also performed in a buffer solution of 10mM K_3PO_4 buffer, but polymers showed a decrease in uptake of analyte in both imprinted and non-imprinted polymers. Previous results in this laboratory have shown that increased ionic strength due to buffers has an adverse affect on analyte uptake [13] . This phenomenon has been attributed to the sensitivity of dissolved salt on the solution conformation of high molecular weight polyacrylamides, with the salts causing contraction or collapse of polymer chains [14]. These changes in the polymer structure may cause changes in the microenvironment of a binding site giving decreased uptake of the analyte. Because of problems with using buffer solutions, further rebinding studies were performed in water alone.

To establish if an equilibrium is achieved at higher concentrations, the binding of polymer **P3** was evaluated as a function of concentration. As seen in Figure 2 below, instead of reaching an equilibrium, the bound dimer concentration reaches a maximum around 2.5 mM and then falls off. One possibility why this fall-off in binding occurs may be due to some self-association of the analyte at higher concentrations which may decrease the binding of the analytes to the polymers. Another possibility maybe that at the higher concentrations, the increased ionic strength due to the increased concentration of the ionic analyte **1** causes the same fall off in binding as observed in binding of the analytes with buffers (*vide supra*).

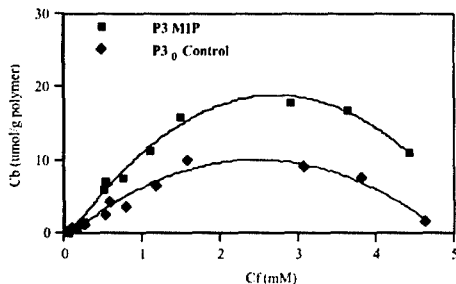**Figure 2.** The rebinding of dimer **1** to MIP **P3** is compared to its rebinding with non-imprinted polymer **P3$_0$**. C_b is the amount of dimer rebound to the polymer. C_f is the remaining concentration of the dimer in solution.

Rebinding Experiments with dAMP as analyte

Dimer imprinted polymer **P3** and the control polymer **P3₀** were then compared for the uptake of 2'-deoxyadenosine-5'-monophosphoric acid (dAMP, **11**) and 2'-deoxyguanosine-5'-monophosphate (dGMP, **12**).
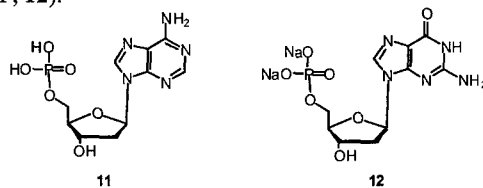
P3 showed selective uptake of dAMP, but not dGMP (Figures 3 and 4, below).
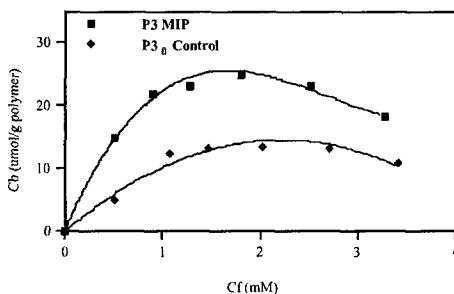
Figure 3. The rebinding of dAMP **11** to MIP **P3** is compared to its rebinding with non-imprinted polymer **P3₀**. (**P3** was imprinted for adenosine dimer **1**).
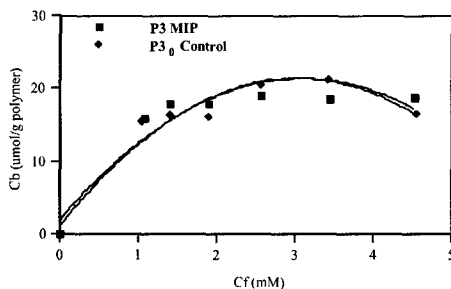
Figure 4. The rebinding of dGMP **12** to MIP **P3** is compared to its rebinding with non-imprinted polymer **P3₀**. (**P3** was imprinted for adenosine dimer **1**).

Rebinding Experiments with dAMP as Template

To optimize the MIP formulation disodium salt of 2'-deoxyadenonsine monophosphate (dAMP disodium salt, **13**) was used as the imprint molecule in various formulations (Table 2). (The disodium salt of dAMP **13** was used because of the sodium salt's greater solubility in MeOH, which is used as the polymerization solvent for some of the formulations).

89
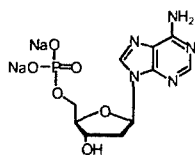
13

Polymer **P5** was based on the successful **P3** formulation, but H_2O, instead of MeOH was employed as porogen (Table 2). **P6** and **P7** formulations were similar to the formulation **P2**, except the guanidinum functional monomer concentration was reduced to 1% (from 14% in **P2**). Finally, **P8** was based on the successful imprinting formulation for the dimer, but dAMP **13** was used as template instead of the dimer. Non-imprinted polymers **P5₀** – **P8₀**, were also synthesized as controls to test for non-specific interactions (Table 2)

Table 2. Polymer formulations used to imprint dAMP **13**. Molecularly imprinted polymers (MIP) using 1% dAMP **13** as template (MIP) were made together with blank polymers prepared in the absence of template.

MIP	Blank Polymer	Crosslinking Monomer	Functional Monomer(s)	Solvent	Splitting Yields
P5	P5₀			H_2O	85 %
P6	P6₀			H_2O	32 %
P7	P7₀			MeOH	32 %
P8	P8₀			MeOH	60 %

As in the previous polymerizations using template **1**, polymers **P5** – **P8** were prepared by thermal polymerization of degassed solutions of the above formulations for 24 h at 65 °C using AIBN (1 %) as initiator. The resulting solid polymers were coarsely crushed and Soxhlet extracted using MeOH. The extracted polymers were ground to 25 – 125 μm, and rebinding studies with various analytes were carried out in water (pH = 3.5, unadjusted).

It was found that when water was employed as the porogen as for polymers **P5** and **P5₀**, the materials exhibited equal uptake of the dAMP template **13**. With a reduced amount of the guanidinium functional group in **P6**, it was anticipated that non-specific binding would be reduced during the rebinding studies. Uptake studies comparing **P6** and **P6₀**, unfortunately, showed better uptake in the non-imprinted polymer **P6₀** than the MIP **P6**. This was perhaps due to the low splitting yield observed for the polymer (~30%); the guanidinium functional group in the MIP may be occupied by the remaining template molecule.

Since the **P7** formulation was very similar to **P6** except for the use of methanol in place of water as solvent, the results were very similar. Once again due to the low splitting yield (25%), the control polymer **P7₀** seemed to adsorb more template molecule than the corresponding imprinted polymer **P7**.

For **P8**, rebinding studies using dAMP **13** (pH of uptake solutions = 8.0) was not as successful as the uptake of the adenosine dimer **1** by MIP **P3** (Figure 1); in this case, both control and imprinted polymer adsorbed the template dAMP **13** equally well (Figure 5). This was surprising, as dAMP **13** was excepted to behave similar to its dimer counterpart **1**.
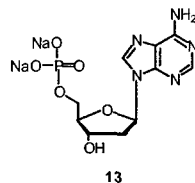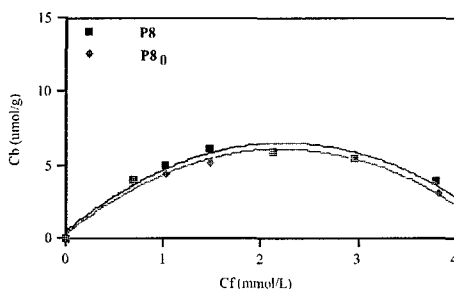
Figure 5. The rebinding of dAMP **13** to MIP **P8** is compared to its rebinding with non-imprinted polymer **P8₀**. (**P8** was imprinted for dAMP **13**).

Adjusting the pH of the uptake solution with HCl to 3.5 did not make a significant difference in the uptake of the template in either the control (**P8**) or imprinted (**P8₀**) polymers (Graphs not shown). Finally, uptake with the free acid form of dAMP **11** (pH = 3.5) gave a differential uptake in the imprinted polymer **P8** and the non-imprinted control polymer **P8₀** (Figure 6).
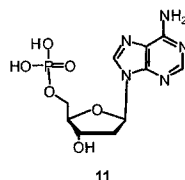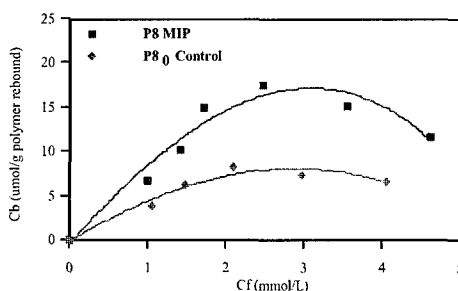
Figure 6. The rebinding of dAMP **11** to MIP **P8** is compared to its rebinding with non-imprinted polymer **P8₀**. (**P8** was imprinted for dAMP **13**).

This uptake study was compared to the uptake of free acid of dGMP (**14**) on the same polymer (Figure 7). As seen in the graph below, dGMP **14** showed greater scatter in the binding data but still bound to the polymer less selectively than dAMP.
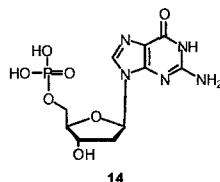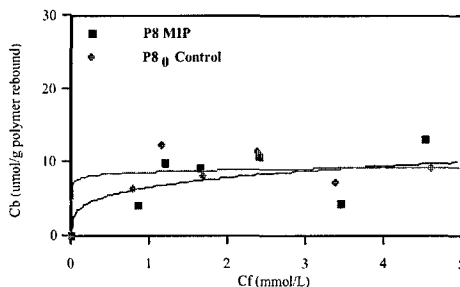
Figure 7. The rebinding of dGMP **5** to MIP **P8** is compared to its rebinding with non-imprinted polymer **P8₀**. (**P8** was imprinted for dAMP **4**).

CONCLUSIONS

We have found that imprinting of a single nucleotide base could be extended to the imprinting of a short DNA fragment. Several polymer formulations were examined to develop adenine receptors. Of these, one polymer formulation (P3), was found to have a higher capacity for 2'-deoxyadenosine dimer (1) than the corresponding non-imprinted polymer in water. The MIP also showed greater selectivity for the adenine base than guanine, when the free acid of the monophosphate salts were used for uptake experiment.

In addition, this polymer (P3) is composed of hydrophilic monomers enabling binding studies to be performed in aqueous solution. Binding studies done in 10mM K_3PO_4 buffer solutions showed decreased binding of the analyte to the polymers most likely due to a change in the solvation and conformation of the polymer and hence the microenvironment of the binding sites in a MIP.

Optimizations of the P3 formulation using dAMP 13 established that the phosphate group of the analyte must be in the free acid form to observe a differential binding between the imprinted and control polymers, during uptake studies. The origin of this observation may be due to difference in the pH of the solutions. Using the sodium salt of dAMP (13), the pH of the solution is ~8; however, using the free acid of dAMP (11), the pH of the solution is ~3.5. Better rebinding is observed using the free acid; however, adjusting the pH of dAMP 13 to 3.5 does not improve rebinding. These results once again indicate that the pH and/or the ionic strength [15] of the uptake solutions in the rebinding studies has a significant effect on the binding of the analyte to the polymer, and the uptake studies are best performed in water alone.

REFERENCES

1. J. L. Sessler, H. Furuta, V. Kral, *Supramol. Chem.* 1, 209-20 (1993).
2. W. L. Jorgensen, *Chemtracts: Org. Chem.* 2, 53-5 (1989).
3. J. Rebek, Jr., *Chemtracts: Org. Chem.* 1, 59-60 (1988).
4. D. A. Spivak, M. A. Gilmore, K. J. Shea, *J. Am. Chem. Soc.* 119, 4388-93 (1997).
5. D. A. Spivak, K. J. Shea, *Macromolecules* 31, 2160-5 (1998).
6. K. Yano, K. Tanabe, T. Takeuchi, J. Matsui, K. Ikebukuro, I. Karube, *Anal. Chim. Acta* 363, 111-7 (1998).
7. D. A. Spivak, Ph.D. Thesis. University of California, Irvine, Irvine, CA, (1995).
8. S. L. Beaucage, R. P. Iyer, *Tetrahedron* 48, 2223-311 (1992).
9. S. Shuto, M. Kanazaki, S. Ichikawa, N. Minakawa, A. Matsuda, *J. Org. Chem.* 63, 746-54 (1998).
10. J. A. Ellman, D. Mendel, S. Anthony-Cahill, C. J. Noren, P. G. Schultz, *Methods Ensymol.* 202, 301-37. (1991).
11. J. Mathew, O. Buchardt, *Bioconj. Chem.* 6, 524-8 (1995).
12. K. J. Shea, G. J. Stoddard, D. M. Shavelle, F. Wakui, R. M. Choate, *Macromolecules* 23, 4497-507 (1990).
13. B. R. Hart, Ph. D. Thesis. University of California, Irvine, Irvine, CA, (2001).
14. M. B. Hocking, K. A. Klimchuk, S. Lowen, *J. Polym. Sci., Part A: Polym. Chem.* 38, 3128-45 (2000).
15. B. Sellergren, K. J. Shea, *J. Chromatogr. A* 690, 29-39 (1995).

Studies on the Process of Formation, Nature and Stability of Binding Sites in Molecularly Imprinted Polymers

F.Lanza*, M.Rüther[1], A .J. Hall, C. Dauwe, B. Sellergren
Institut für Anorganische Chemie und Analytische Chemie, Johannes Gutenberg Universität Mainz, Duesbergweg 10-14, 55099 Mainz, Germany (e-mail: france@ak-unger.chemie.uni-mainz.de)
[1]Polymer Research Unit, Material Ireland, Trinity College Dublin, Ireland

ABSTRACT

In Molecular Imprinting the nature of the templated binding sites and the mechanism of their formation are still poorly understood. For this reason our groups are carrying out fundamental studies concerning known imprinting protocols, with the primary aim of shedding light on the role of the template in the different steps of the polymerisation, from the formation of primary chains to the build-up of the porous structure. In this paper we report our initial results concerning copolymers of methacrylic acid (MAA) and ethyleneglycol dimethacrylate (EDMA) and their formation in presence or absence of the templates 9-ethyladenine, ametryn or terbutylazine. Monitoring the monomer disappearance by ^{1}H-NMR showed that the presence of templates such as 9-ethyladenine significantly retarded the polymerisation but otherwise had minor influence on the relative reactivity of the monomers. The latter appeared in most cases to be stoichiometrically incorporated into the polymer. The signals arising from the template experienced little or no shift in the early stage of the polymerisation, although pronounced broadening was observed. By delaying the addition of the template, it was observed that binding sites with high selectivity could be induced more than one hour after the gel point of the system had been passed. Finally, the results of post-polymerisation curing on the dry and swollen state porosities and the recognition properties of terbutylazine imprinted polymers are reported. This treatment when performed at temperatures between 100-120°C, slightly enhanced the selectivity of the polymers, whereas at higher temperatures the polymers lost their molecular recognition properties. Swollen state porosity derived from inverse size exclusion chromatography (ISEC) revealed an interesting sharpening of the pore size distribution for the imprinted compared to the non-imprinted polymers.

INTRODUCTION

Although molecularly imprinted polymers are nowadays well known and increasingly employed in various fields as compound- or group- selective materials,[1] only little effort has been devoted to fundamental characterisation of these materials[2-13]

Molecularly imprinted polymers (MIPs) are typically prepared by polymerisation of commodity monomers (such as methacrylic acid and ethylenglycol dimethacrylate) in the presence of a template.(Figure 1) This results in the formation of binding sites which are complementary in shape and size to the template itself and are able to rebind it selectively in the presence of structurally related analogues. The functional group arrangement is the key to the affinity and selectivity of the templated sites[2, 14] whereas their accessibility and stability affects the performance of the MIPs in dynamic applications such as in chromatography, membrane separation or in chemical sensors.

In non-covalent molecular imprinting this arrangement requires the formation of stable complexes between the template and functional monomers in the pre-polymerisation mixture.[5] These complexes are incorporated in the network during the polymerisation giving rise to imprinted sites differently embedded in the polymer matrix. In addition non-complexed monomer gives rise to non-imprinted sites, thus diluting the selective binding occuring in the templated sites. Previous reports have suggested that the solution structure of the monomer-template complex is preserved during polymerisation and thus reflects the structure of the templated sites.[8, 15, 16] However, apart from indirect structure binding and thermodynamic studies[15, 16] on the finished polymer, there is no direct evidence in support of such a mechanism. Furthermore, it is unclear at what critical monomer conversion or crosslinking density these sites are irreversibly formed and how the template additionally affects the morphology of the materials. Finally, a better understanding of the process of formation of the sites could suggest new techniques to increase site accessibility, eventually leading to materials with improved kinetic properties. On these grounds, our groups decided to carry out a series of fundamental studies concerning known imprinting protocols with the primary aim of investigating the role of the template in the different steps of the polymerisation process, from the formation of the primary chains to the build-up of the porous structure. Ametryn, 9-ethyladenine and terbutylazine (figure 1) were chosen as model templates on account of their strong interactions with methacrylic acid, which have been shown to result in highly selective MIPs.[17, 18]
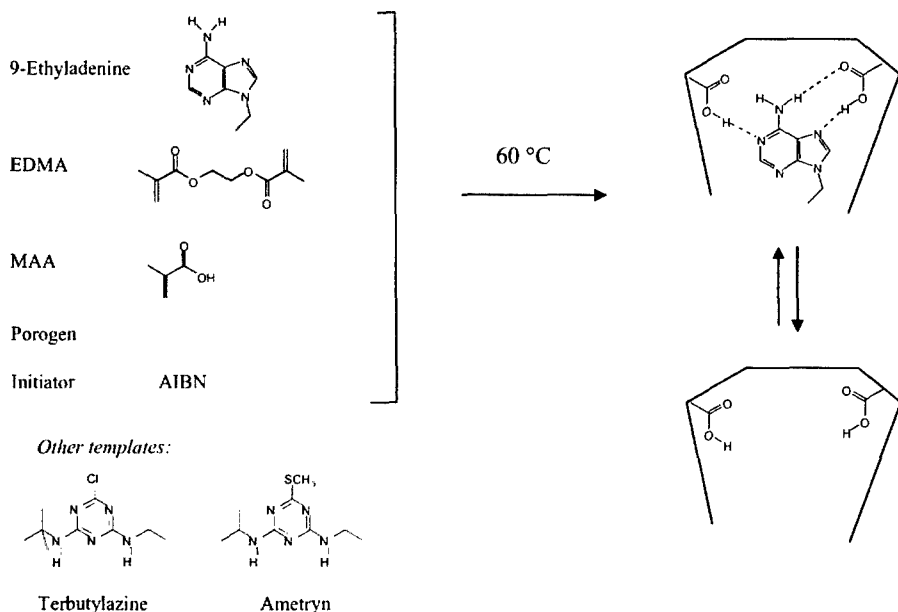
Figure 1. Molecular imprinting of poly(methacrylic acid-*co*-ethyleneglycol dimethacrylate) with the model templates used in the study

EXPERIMENTAL DETAILS

General procedures

All monomers and solvents used for the polymerisation were purified before use. MAA and EDMA were obtained from Sigma-Aldrich Chemie. EDMA was purified by extraction with 10% sodium hydroxide, washing with brine and water, drying over magnesium sulfate followed by distillation. MAA was purified by drying over anhydrous magnesium sulphate followed by distillation under reduced pressure. The porogens (CH_2Cl_2 and $CHCl_3$) were purchased by Sigma-Aldrich Chemie and Acros Chemicals and they were all distilled under a positive nitrogen atmosphere prior to use. AIBN was purchased from Acros Chemicals and recrystallised from methanol before use.

Reagents and solvents used for the *in-situ* NMR experiments were dried beforehand and when mixed they were deoxygenated by purging with oxygen free nitrogen. Polymerisation inhibitors were here removed by elution onto neutral alumina.

The UV lamp used for the photopolymerisations was a high pressure mercury vapour lamp (Philips, HPK 125 W). All chromatographic evaluations were performed using an Agilent 1100 instrument equipped with a binary pump, an autosampler, a variable wavelength detector and a work station. The ^{1}H-NMR spectra were run at Material Research Ireland, Dublin.

The inverse size exclusion measurements were performed at PSS Polymer Standard Services GmbH, Mainz, Germany.

In situ ^{1}H-NMR experiments

All proton nuclear magnetic resonance spectra were recorded on a Bruker DPX-400 (400 MHz) spectrometer. The chemical shifts are reported on the δ scale in parts per million downfield from TMS (0.00 ppm) or with deuterated chloroform as internal reference ($CDCl_3$, 7.26 ppm). Spectra were recorded at 30°C ± 1°C for the characterisation of the individual monomers, template and polymerisation mixtures. For the in-situ monitoring of the polymerisation, MAA (5 mmol) and EDMA (5 mmol) were mixed in an NMR tube and an equal volume of $CDCl_3$ (1.36 ml) was added. The initiator, AIBN, was added (1 % w/w based on the total amount of monomer) and the polymerisation monitored at 60°C for 4 to 7 hours in presence or absence of the template 9-ethyladenine (86.6 mg). At the end of this period the sample appeared solid and no further NMR signal could be detected. The peak areas of the vinyl peaks of MAA and EDMA (figure 2) were used for the calculation of the curing profiles reported in Figure 3. The cure profiles were obtained by plotting the curing time in minutes against the component integral peak area in percent. The signals of the protons in position 2 and 8 of the 9-ethyladenine were also monitored during the polymerisation as shown in Figure 2(A).

Late addition of the template

The preparation of MIPs and NIPs (Non Imprinted Polymers) on a small scale (500 mg of raw polymer) and their *in-situ* testing by batch rebinding experiments was performed as described elsewhere.[19] 20 ml scintillation vials were used as polymerisation reactors. A mother solution was prepared by mixing 11.4 ml EDMA (12 mmol), 1,02 ml MAA(12 mmol) 18 mg ABDV and 12 ml $CHCl_3$. A template solution was prepared by dissolving 1.42 g ametryn in 10 ml $CHCl_3$. 1 ml of the mother solution was dispensed into each vial; the vials were purged with nitrogen for 5 min and then placed in a thermostatted bath at 40°C. Pairs of vials were

removed at different times after the start of the polymerisation and cooled down on ice for 5 minutes. To one of these, pure solvent was added (so that a NIP was obtained upon polymerisation) while to the other the concentrated template solution was added (200µl in both cases). After addition they were manually shaken and left on ice for an additional 10 minutes. Thereafter the vials were returned in the thermostat bath and further polymerised for additional 24 hours.

After the polymerisation the polymers were subjected to different solutions to study the release and rebinding of the template.[19] The porogen chloroform was used for the release tests, $CH_3OH/CH_3COOH/H_2O$ 60/30/10 (v/v/v) to wash the polymers and a solution of ametryn in the porogen (0.5 mM in $CHCl_3$) was used for the rebinding tests. The concentration of the free template in solution was determined after 48 hours by reversed phase HPLC-UV (Luna ODS column by Phenomenex, CH_3CN/NH_4OAc 40 mM 75/25 as mobile phase, 1 ml/min flow rate, wavelength of detection 254 nm). The amount of template bound to MIPs and NIPs was calculated assuming a 500 mg weight of polymer in each vial.

Curing experiments

Terbutylazine-imprinted polymers were prepared according to a previously reported procedure.[19] EDMA (20 mmol, 3.8 ml), MAA (4 mmol, 0.34 ml) terbutylazine (1mmol), AIBN (0.24 mmol, 40 mg) were dissolved in 5.6 ml of dichloromethane and the solution was then transferred to a glass tube (14 mm i.d.). The polymerisation mixture was degassed with nitrogen for 5 min while cooled on ice and then the tubes were flame sealed. All the tubes were placed at *ca.* 10 cm distance from the UV light source and then turned at regular intervals during the first 30 min, to obtain a more even exposure. After 24 hrs irradiation the tubes were cured for an additional 24 hours at elevated temperatures. The tubes were then crushed, the polymers were ground and sieved under water and the particle size fraction 25-36 µm was collected. This fraction was then repeatedly washed with 50 ml aliquots of CH_3OH/H_2O 1/1, CH_3OH, CH_3OH/CH_3COOH 80/20 and CH_3OH and then used for the chromatographic evaluation and the pore analysis.

The 25-36 µm particle fraction of each polymer batch was slurry packed into stainless steel HPLC columns (125 x 4 mm) using MeOH/H_2O 80/20 as pushing solvent at pressures up to 300 bar. The columns were then evaluated using $CH_3CN/H2O/CH_3COOH$ 92.5/2.5/5 or CH_3CN as mobile phase, at a flow rate of 1 ml/min. The wavelength of detection was 254 nm and the injection volume was 10 µl. 1 mM solutions of the analytes in the mobile phase were injected unless otherwise stated. The capacity factor k′ was calculated as $(t-t_0)/t_0$ where t is the retention time of the analyte and t_0 the retention time of a void marker (acetone)

Inverse Size Exclusion Chromatography

The previously described columns were used for the inverse size exclusion measurements. The measurements were performed using an Agilent 1100 HPLC system comprising a binary pump, an autosampler and a variable wavelength detector. THF was used as mobile phase at a flow rate of 0.2 ml/min. The wavelength of detection was again 254 nm. 1 mg/ml solutions of polystyrene standards of different molecular weights were in this case injected for the evaluation. Acetone was used as void marker.

The pore analysis based on the inverse size exlusion measurements was carried out by means of the PSS Porocheck Software. The pore size distributions were calculated as average on the volume.

Pore analysis (N₂ adsorption porosimetry)

Pore and surface area analysis were performed using a Quantachrome Autosorb 6B (Quantachrome Corporation, Boynton Beach, FL, USA). A sample of polymer (50 mg) was degassed at room temperature overnight under vacuum. The adsorption and desorption isotherms were then recorded using an 80-point pressure table and 15 s equilibration time.
Surface areas, pore volumes and pore size distributions were determined by means of the Autosorb Software for Windows version 1.11. The surface areas were determined using the BET model, pore volumes and pore size distributions using the BJH model.

DISCUSSION

Our initial aim was to gain knowledge about the initial stages of the thermal copolymerisation of MAA and EDMA in presence or absence of the template 9-ethyladenine. This template is known to interact strongly with carboxylic acids in aprotic solvents[20] and a significant part should exist in the complexed form prior to polymerisation, as indicated in Figure 1. Complexation was supported by pronounced shifts observed for the exocyclic amine and aromatic ¹H-NMR signals of the template upon addition of MAA (NH₂: -2,4 ppm; H₂: +0,1 ppm; H₈: -0,1 ppm). These signals appear in a region of the spectrum which is free from any other interfering signals arising from the monomers (figure 2). *In-situ* ¹H-NMR thus allowed the characteristic protons of the template as well as the vinyl protons of MAA and EDMA, to be monitored during the initial stage of the polymerisation (figure 2).
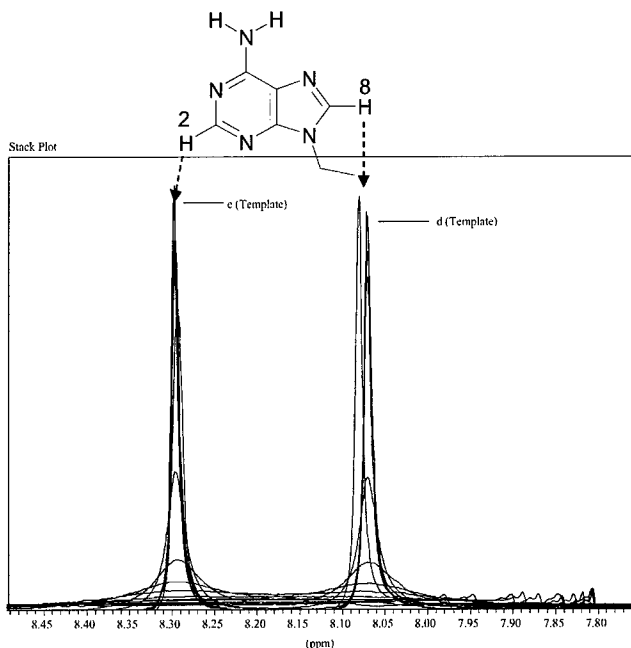
Diagram A
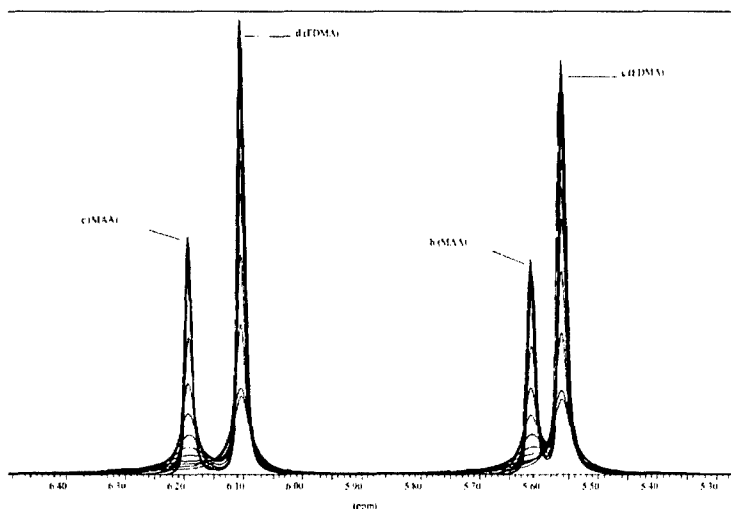
Diagram B

Figure 2. Characteristic proton signals of 9-ethyladenine (A) and the monomers (B) during the imprinting process

Concerning the template signals a slight upfield peak shift (0.01ppm) for H_8 was observed during the first 3 minutes of the polymerization. After that no significant peak shift could be observed. This indicates that the degree of monomer-template complexation is constant in this interval. The signals then experienced broadening early on during the polymerisation. Interestingly this broadening was more pronounced for the template than for the monomer related signals, indicating that the template mobility becomes severely restricted. Figure 3 shows the integral areas of the relevant signals plotted versus the time of polymerisation.

Integrals of the monomer signals could be obtained during the first two hours of the polymerisation. After this point pronounced broadening due to polymerisation occured. Thus, the integrals of these signals cannot be taken as a quantitative measure of the absolute conversion of the monomers. However, they do reflect the absolute and relative monomer reactivities during the initial polymerisation phase. In view of the relative initial slopes of the rate curves, the monomers appeared, in most cases, to be stoichiometrically incorporated in the polymer.
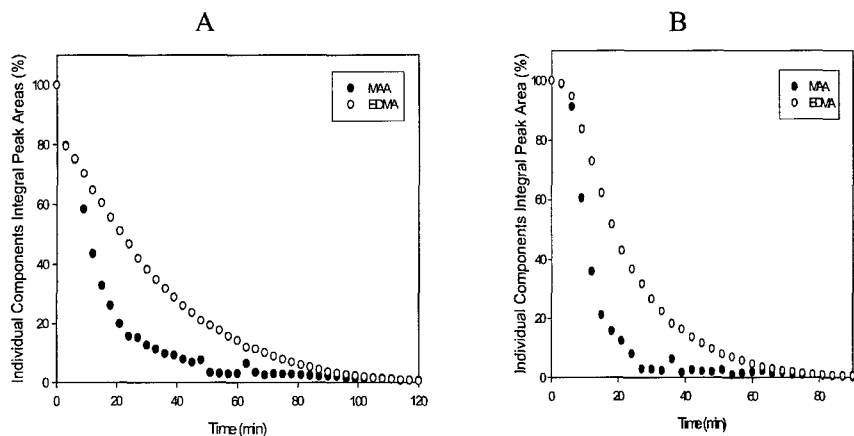
Figure 3. Integral areas from Figure 2 of the vinyl protons of MAA and EDMA as a function of polymerisation time in the absence (A) and in the presence (B) of the template (MAA/EDMA/9-ethyladenine: 5/5/1 in CDCl₃).

However, comparing the kinetics in the presence (figure 3, B) and absence of template (figure 3, A), a retardation of the onset of polymerisation was seen in the presence of template. After an initial lag time the monomers are converted at a rate that appears slightly faster than in absence of template. The origin of this phenomenon and its implication on the mechanism of site formation is still unclear. However it must be noted that the reactivity of MAA in free radical homopolymerisation depends on the extent and types of complexes present.[21] Further experiments are being performed which will be the topic of a forthcoming publication.[22], in particular different compositions of the polymerisation mixtures and different templates have been studied: in all cases the presence of the template significantly retarded the polymerisation.

The question arose with regards to what point in time the templated sites are irreversibly formed by crosslinking. To answer this question, another series of experiments was performed by adding the template after the start of the polymerisation. In order to minimise the dilution of the system upon each addition, this experiment required the use of a template that is highly soluble in the porogenic solvent. For this purpose the triazine ametryn was used. The polymers were prepared in standard scintillation vials (500 mg) by thermal initiation (ABDV, 40°C) and then tested *in situ* by studying the release and rebinding of the template under equilibrium conditions. The amount of template rebound to the MIP and to the NIP for the thermally initiated MIPs and NIPs are shown in figure 4.

◆ % Ametryn bound to the MIP   ● % Ametryn bound to the NIP
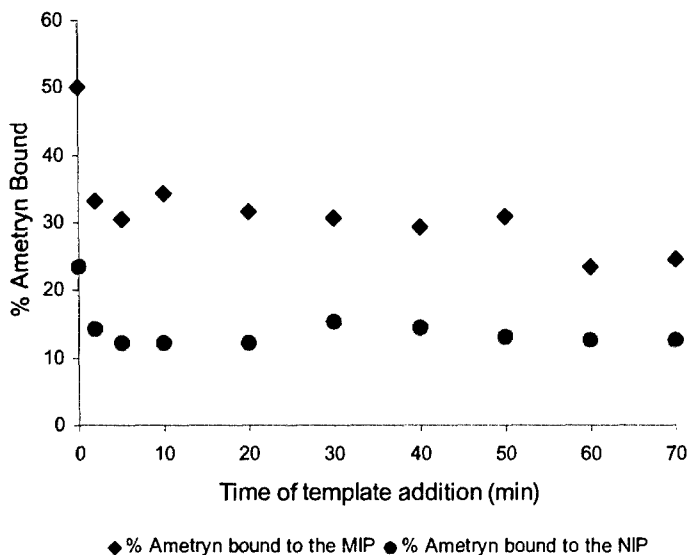
Figure 4. Percentage of template rebound in an equilibrium batch rebinding experiment performed on MIPs (diamonds) and NIPs (circles) prepared by delayed addition of template (for the conditions of the equilibrium batch rebinding see the Experimental details).

A pronounced imprinting effect was seen for all the materials prepared within the first hour after start of the polymerisation. Although the reference materials (t=0) adsorbed somewhat higher amounts of template (possibly related to radical quenching in the manipulated samples), the selectivity changed only slightly in this interval and started to decrease only after 60 minutes. Thus, templated sites exhibiting similar selectivity to that of the native material can be induced well after the gel point of the system has been passed (typically less than 30 minutes). These results may thus reveal the monomer conversion and critical crosslinking level required to stabilise the templated sites. Such studies are presently being performed.[22]

Given that templated sites can be induced well after the start of the polymerisation, the question arose of to what extent these sites collapse upon subsequent removal of the template and the thermal stability of the sites. In view of the large portion of unreacted double bonds present in typical MIPs, could the sites be further stabilised by post-treatment at higher temperatures in the presence of the template ? In an attempt to answer these questions MIPs and NIPs were prepared by photochemical initiation at 15°C in flame sealed vials which were subsequently cured for an additional 24 hrs at elevated temperatures between 80°C and 160°C . The materials were then worked up and evaluated as stationary phases in chromatography. Figure 5 shows the capacity factors of the template (terbutylazine) on the imprinted and non-imprinted polymers versus the temperature of curing.
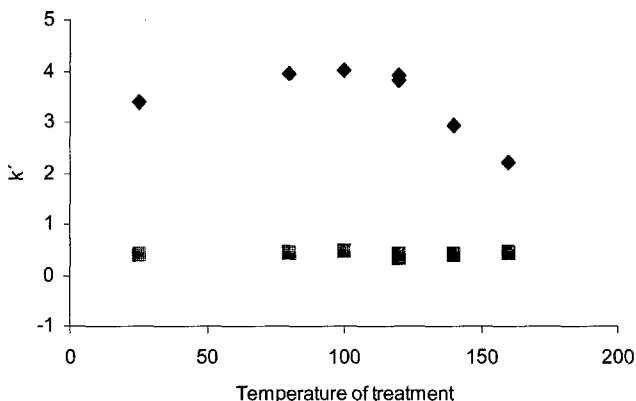
Figure 5. Capacity factors of terbutylazine ($10\mu l$ of a 1mM solution in the mobile phase $CH_3CN/CH_3COOH/H_2O$ 92.5/5/2.5) on columns packed with MIPs (diamonds) and NIPs (squares) cured at different temperatures.

A slight but significant increase in the retention is observed on the MIP when the curing temperature is increased up to 120°C. This behaviour is absent on the NIP and seems therefore to be related to the templated sites. Curing at higher temperatures leads to a loss in selectivity, very similar to our previous results from annealing experiments.[10] Interestingly the temperature interval where the decrease occurs agrees roughly with the glass transition temperature for linear poly(methylmethacrylate). Thus it may due to large conformational changes in less crosslinked regions of the network.

The polymers prepared using chloroform or dichloromethane are gel like and exhibit no porosity in the dry state.[9] Thus nitrogen sorption does not reveal any effect of the presence of template or curing on the pore size distributions and morphologies of the materials. For this purpose the porosity in the swollen state needs to be investigated. This can be done by inverse size exclusion chromatography (ISEC), providing the exclusion volume for polystyrene standards of known molecular radii. From the exclusion volumes, the accessible pore volume versus molecular radius can be modelled. As seen in figure 6, the polymers prepared using dichloromethane as porogen exhibit a large volume of pores with a diameter between 2 and 10 nm.
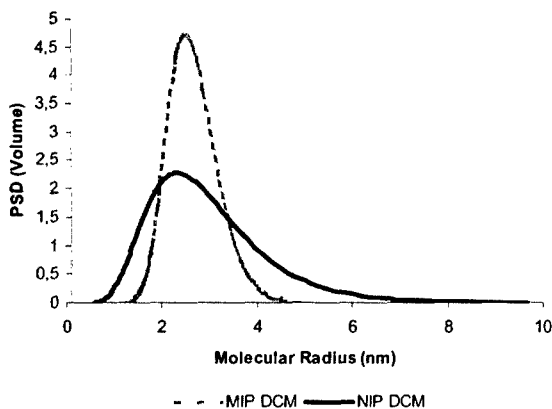
Figure 6. Pore size distributions obtained from ISEC measurements on an ametryn imprinted polymer (dotted curve) or non imprinted polymer (continuous curve) prepared using dichloromethane as porogen. The polymers were non porous in the dry state but gave a surface areas of 930 m^2/cm^3 (NIP) and 810 m^2/cm^3 (MIP) in the ISEC measurement.

This gives rise to a very high surface area for these materials of nearly 1000m^2/mL. The presence of template leads to a pronounced sharpening of the pore size distribution. The origin of this effect is unclear but the analogy with the role of templates in the synthesis of mesoporous materials is striking.[23]

CONCLUSIONS

The first studies on the formation and the nature of templated sites have shown this to be a slow process and that high affinity binding sites can be induced by delaying the addition of template. This may have practical implications concerning template bleeding and the kinetic properties of the materials. Thus template added at later stages is expected to be less embedded and to result in more accessible binding sites. From these sites it should also be easier to remove the template quantitatively. Curing of the materials at elevated temperatures up to 120°C seems to stabilise some sites and make them more accessible, whereas curing at even higher temperatures leads to destruction of sites.

REFERENCES

1. B. Sellergren, (ed) *Molecularly imprinted polymers. Man-made mimics of antibodies and their applications in analytical chemistry. Techniques and instrumentation in analytical chemistry, Vol. 23*, (Elsevier 2001).
2. K. J. Shea, T. K. Dougherty, *J. Am. Chem. Soc.* **108,** 1091-1093 (1986).
3. K. J. Shea, D. Y. Sasaki, G. J. Stoddard, *Macromolecules* **21,** 1722 (1989).
4. K. J. Shea, D. Y. Sasaki, *J. Am. Chem. Soc.* **111,** 3442-3444 (1989).
5. B. Sellergren, A. J. Hall, in *Molecularly imprinted polymers. Man-made mimics of antibodies and their applications in analytical chemistry., Vol. 23*, edited by B. Sellergren (Elsevier 2001), p. 21-57.
6. I. A. Nicholls, *Chem. Lett.* **11** 1035-6 (1995).
7. I. A. Nicholls, *Adv. Mol. Cell Biol.* **15B,** 671-679 (1996).
8. B. Sellergren, M. Lepistö, K. Mosbach, *J. Am. Chem. Soc.* **110,** 5853-60 (1988).
9. B. Sellergren, K. J. Shea, *J. Chromatogr.* **635,** 31 (1993).
10. Y. Chen, M. Kele, P. Sajonz, B. Sellergren, G. Guiochon, *Anal. Chem.* **71,** 928-938 (1999).
11. W. Y. Chen, C. S. Chen, F. Y. Lin, *J. Chromatogr.,* **A 923,** 1-6 (2001).
12. C. J. Allender, C. M. Heard, K. R. Brain, *Chirality* **9,** 238-242 (1997).
13. R. J. Umpleby, II, M. Bode, K. D. Shimizu, *Analyst* **125,** 1261-1265 (2000).
14. G. Wulff, B. Heide, G. Helfmeier, *J. Am. Chem. Soc.* **108,** 1089-1091 (1986).
15. C. Lübke, M. Lübke, M. J. Whitcombe, E. N. Vulfson, *Macromolecules* **33,** 5098-5105 (2000).
16. M. Quaglia, K. Chenon, A. J. Hall, E. De Lorenzi, B. Sellergren, *J. Am. Chem. Soc.* **123,** 2146-2154 (2001).
17. K. J. Shea, D. A. Spivak, B. Sellergren, *J. Am. Chem. Soc.* **115,** 3368-3369 (1993).
18. C. Dauwe, B. Sellergren, *J. Chromatogr.,* **A 753,** 191-200 (1996).
19. F. Lanza, B. Sellergren, *Anal. Chem.* **71,** 2092-2096 (1999).
20. G. Lancelot, *J. Am. Chem. Soc.* **99** 7037 (1977).
21. F.D. Kuchta, A.M.van Herk, A.L. German, *Macromolecules* 33, 3641-3649 (2000)
22. M. Rüther, F. Lanza, A. J. Hall, B. Sellergren (in preparation).
23. M. E. Davis, A. Katz, W. R. Ahmad, *Chem. Mater.* **8** 1820-1839 (1996).

Binding Studies on Resins Imprinted with (S)-naproxen

Yue Hu and Robert A. Orwoll
Departments of Applied Science and Chemistry
College of William and Mary
Williamsburg, VA 23187-8795, U.S.A.

ABSTRACT

Resins were prepared in a free-radical polymerization of 4-vinylpyridine and ethylene glycol dimethacrylate in the presence of (S)-(+)-6-methoxy-α-methyl-2-naphtaleneacetic acid ((S)-naproxen). Initially (S)-naproxen, the imprinted molecule template, was assembled with the monomer 4-vinylpyridine by non-covalent interactions. After the polymerization, stepwise removal of the template left binding sites that retain complementary specificity and affinity. Binding parameters including the maximum number of binding sites and dissociation constant were calculated from the amount of template removed using a two-site Scatchard equation. The results are typical of other systems reported in the literature.

INTRODUCTION

Molecularly imprinted polymers (MIPs) are synthetic polymers having tailor-made selectivity for a particular template species. They are prepared by self-assembly with a template bound to a monomer in the presence of a crosslinking monomer. Polymerization of the monomers typically results in a macroporous support with the binding monomer positioned for interaction with the template. After extraction of the template, molecular sites are positioned to readsorb the template.

Molecular imprinting has been a very active field since 1990. Although attempts have been made to acquire MIP particles dimensionally and morphologically homogeneous, the heterogeneity in the binding has been a significant problem to date in the synthesis of MIPs. The heterogeneity not only affects MIP's analytical applications, but also complicates MIP's characterization. Studying how the template molecule is captured by and released from the MIP during the prearrangement procedure, before the polymerization, and during the extraction procedures will help to better understand the heterogeneity in the binding sites. A known MIP system was used: (S)-naproxen as the template and 4-vinylpyridine as the functional monomer.

In an early study using (S)-naproxen as a template, Mosbach et al. [1] prepared MIP by a free radical polymerization followed by crushing, grinding, and sieving to produce packing material for high-performance liquid chromatography (HPLC). They found good retentivity and enantioselectivity. Then between 1997 and 2001 Haginaka et al. studied the similar system but developed a multi-step swelling and thermal polymerization method with water as a suspension medium followed by hydrophilic surface modification techniques to make uniformly sized MIP particles [2]. By their method, the separation factor for the enantioselectivity of (S)-naproxen (1.74) was obtained, an improvement over that of Mosbach (1.65).

In this study, we employed Mosbach's method to synthesize MIP. Washing analysis of the template from the MIPs yielded data for a Scatchard plot [3] and the determination

of binding parameters. They were compared with parameters reported in the literature for other systems.

EXPERIMENTAL

Imprinted polymer preparation and washing

(S)-(+)-6-methoxy-α-methyl-2-naphtaleneacetic acid ((S)-naproxen), 4-vinylpyridine (4-VP), ethylene glycol dimethacrylate (EGDMA) and 2,2´-azobisisobutyronitrile (AIBN) were purchased from Aldrich. All organic solvents were of analytical or HPLC grade. 4-VP and EGDMA were purified before using.

0.4600 g (S)-naproxen (2 mmol), 1.30 mL 4-VP (12 mmol) and 11.32 mL EGDMA (60 mmol) were dissolved in 8 mL tetrahydrofuran (THF). After stirring in a 4°C bath for 1 hour, 0.1150 g AIBN dissolved in 8 mL THF was added. This mixture was immediately purged with nitrogen for 15 minutes and then irradiated for 48 hours with UV light from an ACE 7825-34 mercury vapor UV lamp (450 watts). The resulting polymer was ground in a ball mill (SPEX 8000) and dry sieved to sizes between 63 and 125 μm.

Approximately 1 g MIP was stirred with 20 mL THF for 24 hours, thereby removing some template from the resin to the THF. After centrifuging, the supernatant was filtered through 0.45 μm syringe filter. Its UV absorbance was measured at 363.5 nm using a Perkin-Elmer Lambda 35 UV/VIS spectrophotometer. Washing was repeated three more times. The UV absorbance for the solutions was measured after calibrating the absorbance as a function of concentration over the range for 0.02 to 0.25 mg/mL. A background absorbance was determined in washings of a resin that had been prepared in the absence of template. This correction, which in no case exceeded 4%, was subtracted from the absorbance of the washings in order to eliminate the effects of any non-template UV-absorbing material. These washing experiments were performed on three different MIP-(S)-naproxen samples.

A reference non-imprinted polymer was prepared using the same procedure without addition of the template.

UV/VIS and Fourier transformation infrared spectra (FT-IR)

A series of solutions was prepared with a fixed concentration of (S)-naproxen (0.04 μmol/L) and varying amounts of 4-VP in THF. The UV/VIS absorption spectra of these solutions were compared with corresponding (S)-naproxen or 4-VP.

Resins with and without the template were prepared as KBr disks. The IR spectra were measured between 1000 and 4000 cm^{-1} with a 4 cm^{-1} resolution using a Perkin-Elmer Spectrum 1600 FT- IR instrument.

DISCUSSION

Interaction between monomer and template

The interactions between (S)-naproxen and 4-VP are important for understanding imprinting and recognition phenomena in MIP.

The UV spectrum in Figure 1 shows the prearrangement interaction between 4-VP and (S)-naproxen. As the concentration of 4-VP was increased, the wavelength λ_{max} of maximum adsorption by (S)-naproxen shifted to greater λ, and the maximum absorbance at the maximum wavelength increases with the addition of 4-VP.

The interaction of the template with the polymer causes a shift in the infrared absorption for the carbonyl stretching in the EGDMA units of the resin. Figure 2 shows the spectrum of the 4-VP and EGDMA resin (A) in the absence of (S)-naproxen, (B) with the naproxen template in place after polymerization, and (C) after extraction of (S)-naproxen. The $\tilde{\nu}_{max}$ moves from (A) 1739 to (B) 1726 to (C) 1734 cm^{-1}. Such transitions to lower $\tilde{\nu}$ are characteristic of carbonyl oxygen in a hydrogen bond. This suggests that the template molecule may interact through hydrogen bonding in this MIP network and the hydrogen bonding may be more responsible for the selectivity of the template.
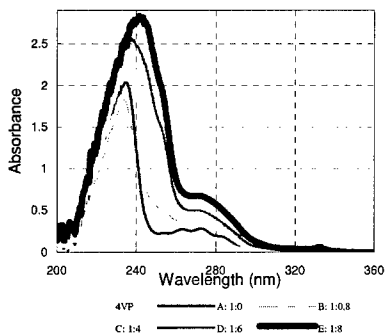
Figure 1. UV adsorption spectra of (S)-naproxen and 4-VP system in THF. Concentration of (S)-naproxen is 0.04 μmol/L; concentration of 4-VP (μmol/L): B: 0.032; C: 0.16; D: 0.24; E: 0.32.
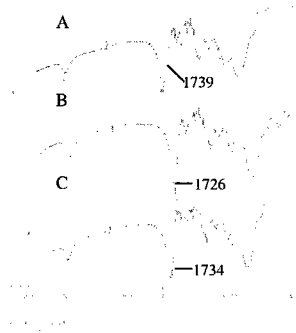
Figure 2. FT-IR Spectra for (A) MIP without (S)-naproxen as the template; (B) MIP before (S)-naproxen extraction; (C) MIP after (S)-naproxen extraction. Wave numbers are reported in cm^{-1}.

Washing analysis by Scatchard equation

Washing the template from the resin is an important step in preparing MIP systems for analytical applications. In this study, (S)-naproxen was extracted from the template-containing resin using several washings with THF. Although others [1] reported washings using THF with acetic acid added to promote the release of the (S)-naproxen, we found no difference with or without the acid. The molar concentration of template [T] in the wash solutions was measured directly from the UV absorbance of those solutions. The amount of (S)-naproxen remaining in the resin, [MT] measured in mmoles per gram of resin, was determined by difference from the amount of (S)-naproxen initially present in the polymerizing mixture. Four successive washings of each of three resin samples yielded 90-94% recovery of the template initially present. The data were fit to the two-

site Scatchard Equation $[MT] = \dfrac{n_{max,H}[T]}{K_{d,H}+[T]} + \dfrac{n_{max,L}[T]}{K_{d,L}+[T]}$ using an iterative spreadsheet procedure that minimized the sum of the square of the difference between the measured and calculated concentrations [MT] of bound (S)-naproxen by adjusting the parameters for the maximum number of binding sites $n_{max,H}$ and $n_{max,L}$ and dissociation constants $K_{d,H}$ and $K_{d,L}$. Here the subscripts H and L refer to high- and low-affinity binding sites.

Two of these sets of four washings yielded good fits. The third required a negative $K_{d,H}$ to fit the four data points to the four parameters. The mean values and their spreads for the two good data sets are $n_{max,H} = 13\pm1$ μmoles of sites per gram of resin, $n_{max,L} = 110\pm30$ μmol/g, $K_{d,H} = 0.003\pm0.002$ mmol/L, and $K_{d,L} = 14\pm5$ mmol/L. The data for one set of washings are depicted in Figure 3. The two-site Sactchard analysis shows the strong binding sites to be saturated at solution concentrations [T]>0.4 mmol/L. A more precise value for $K_{d,H}$ would require more data at concentrations below saturation than were obtained in these washing experiments.
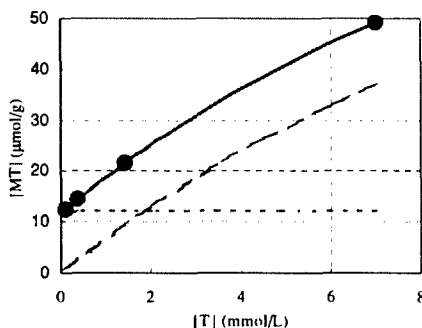
Figure 3. Two-site Scatchard plot showing the quantity of (S)-naproxen absorbed at the weak (dashed line) and strong (dotted line) binding sites. Measured values for the four washings are shown. The solid line is the calculated fit for the total amount bound.

Literature review

Researchers have interpreted binding in MIP systems in terms of the Scatchard equation. We summarize these studies and compare them with the results of the washing measurements of the present study.

The most common method for investigating the capacity of MIPs to absorb template from solutions is the rebinding experiment. After the template has been extracted, the MIP is immersed in solutions of varying concentration of the template. The change in concentration of the solution as the template is reabsorbed is measured, typically using HPLC or UV spectroscopy. Two kinds of binding sites with differing strengths were observed in the ten studies summarized in the beginning of Table 1. As described above, this behavior is consistent with a small equilibrium dissociation constant K_d for the template-specific binding sites and a large K_d for more general adsorption of template onto the resin.

In Table 1 the identities of the template, functional monomers, and crosslinking reagents are listed. The moles of monomer and of crosslinker relative to the number of moles of template is in the fourth column. The solvents used in the polymerization, the extraction of the template from the MIP, and the rebinding are identified in columns 5-7. The dissociation constants and concentrations of binding sites in the resins are tabulated in columns 8-11. In the six studies listed at the bottom of Table 1, only a single line was obtained in the Scatchard plot and so only single values are listed for K_d and n_{max}.

Because of the variability of chemical environments around the binding sites in an MIP resin, the dissociation constants associated with those binding sites should also vary. It is remarkable then that so many systems exhibit a bimodal distribution of binding constants such that the binding behavior can be represented accurately with double Scatchard plots. A continuous distribution function has been proposed [19] for more detailed analyses of bindings.

CONCLUSIONS

The 4-VP+EGDMA resin prepared in the presence of (S)-naproxen yielded K_ds for high-affinity (0.04 mmol/L) and low affinity (3 mmol/L) sites that are comparable to those reported in other systems, *i.e.,* 10^{-3}-1 mmol/L (high affinity) and 0.1-3 mmol/L (low affinity). Spectroscopic evidence obtained on this system is consistent with hydrogen bonding between the template and functional monomer.

REFERENCES

1. M. Kempe and K. Mosbach, *J. Chromatogr. A*, **664**, 276, (1994).
2. J. Haginaka, H. Takehira, K. Hosoya and N. Tanaka, *J. Chromatogr. A*, **849**, 331, (1999); J. Haginaka and H. Sanbe, *Anal. Chem.*, **72**, 5206, (2000).
3. K. A. Connors, *Binding Constants*, (John Wiley & Sons Publication, New York, 1987) Chapter 2.
4. H. Guo, X. He and H. Liang, *Fresenius J. Anal. Chem.*, **368**, 763, (2000).
5. T. Zhang, F. Liu, W. Chen, J. Wang and K. Li, *Anal. Chim. Acta*, **450**, 532 (2001).
6. H. Guo and X. He, *Fresenius J. Anal. Chem.*, **368**, 461, (2000).
7. H. Guo and X. He, *Chinese J. Anal. Chem.*, **28**, 1214, (2000).
8. H. Guo, X. He, J. Zhou and H. Liang, *Chinese J. Anal. Chem.*, **29**, 128, (2001).
9. J. Zhou, X. He and Y. Li, *Anal. Commun.*, **36**, 243, (1999).
10. H. Guo, X. He, Y. Jing and H. Liang, *Chem. J. Chinese Univ.*, **22**, 739, (2001).
11. J. Zhou, X. He and Y. Li, *Anal. Chim. Acta*, **394**, 353 (1999).
12. O. Ramström, L, Ye and K. Mosbach, *Chemistry & Biology*, **6**, 471, (1996).
13. J. Zhou and X. He, *Anal. Chim. Acta*, **381**, 85, (1999).
14. H. Guo, X. He, C. Deng and Y. Li, *Chem. J. Chinese Univ.*, **21**, 363, (2000).
15. S. Cheong, A. E. Rachkov, J. Park, K. Yano and I. Karube, *J. Polym. Sci.: Part A: Polym. Chem.*, **36**, 1725 (1998).
16. J. Zhou, X. He, J. Zhao and H. Shi, *Chem. J. Chinese Univ.*, **20**, 204, (1999).
17. H. Guo, X. He, Y. Gan, W. Li and H. Liang, *Acta Chim. Sinica*, **59**, 262, (2001).

18. T. Takeuchi, T. Mukawa, J. Matsui, M. Higashi and K. D. Shimizu, *Anal. Chem.*, **73**, 3869, (2001).
19. R. J. Umpleby, S. C. Baxter, Y. Chen, R. N. Shah and K. D. Shimizu, *Anal. Chem.*, **73**, 4584, (2001).

Table 1. Summary of Scatchard analyses from the literature.

Template	MIP Synthesis				Extraction Solvent[d]	Rebinding Solvent[d], conc (mM)	High Affinity		Low Affinity		Ref
	Mono.[a]	Xlink[b]	M:X:T[c]	Solvent[d]			K_d (mmol/L)	n_{max} (μmol/g)	K_d (mmol/L)	n_{max} (μmol/g)	
4-aminopyridine	maa	egdma	4:20:1	dmf	ma/aa	membrane; w, 0.1-4.0	0.54	49	3.2	50	[4]
4-hydroxybenzoic acid	a	egdma	6:30:1	acn	ma/aa	acn, 0-2.5	0.18	9	1.4	22	[5]
cefalexin	tfmaa	egdma	4:20:1	ma	ma/aa	w, 0.1-4.5	0.14	30	2.4	130	[6]
cefalexin	tfmaa+4vp	egdma	12:30:1	ma	ma/w	w, 0-4.5	0.14	28	2.8	157	[7]
norfloxacin	maa	egdma	6:30:1	c/dmf	ma/aa	c/dmf, 0-4.5	0.09	23	1.9	128	[8]
(5R)-5-benzylhydantoin	a	egdma	4:20:1	acn	ma/aa	acn, 0-30	0.05	40	0.13	48	[9]
4-aminopyridine	maa	egdma	4:30:1	c	ma/aa	acn, 0-4.5	6.2×10^{-3}	78	0.43	223	[10]
5,5-diphenylhydantoin	a	egdma	4:20:1	thf	ma/aa	acn, 0.05-4.0	2.1×10^{-3}	17	1.6	104	[11]
cortisol	maa	egdma	13:65:1	thf	ma/aa	thf, 0.03-20 mg/mL	0.6	0.2	1.6	280	[12]
corticosterone	maa	egdma	13:65:1	thf	ma/aa	thf, 0.03-20 mg/mL	1.2	0.4	0.8	130	[12]
2-aminopyridine	maa	egdma	4:30:1	c	ma/aa	acn, 0-4.0	2.6	136	--	--	[13]
paracetamol	a	egdma	4:40:1	acn	ma/aa	acn, 0-4.5	2.3	126	--	--	[14]
testosterone	maa	egdma	8:25:1	c	acn	acn, 0-1.5	1.1 (UV), 0.8 (HPLC)	1.6 (UV), 2.5 (HPLC)	--	--	[15]
trimethoprim	maa	egdma	6:30:1	c	acn/aa	c, 0.5-9.0	0.2	202	--	--	[16]
trimethoprim	maa	trim	4:4:1	acn	acn	membrane; acn, 0-4.5	0.05	290	--	--	[17]
(-)-cinchonidine	maa	egdma	2.5:75:1	c	acn/ma	dcm; 0-2.0	1.5×10^{-4}	4.0	--	--	[18]
	zp	egdma	2.5:75:1	c	acn/ma	dcm; 0-2.0	6.9×10^{-4}	3.8	--	--	
	maa +zp	egdma	3.5:75:1	c	acn/ma	dcm; 0-2.0	8.8×10^{-5}	5.3	--	--	

[a]Monomer abbreviations: a, acrylamide; maa, methacrylic acid; tfmaa, 2-(trifluoromethyl)acrylic acid; 4vp, 4-vinylpyridine; zp, zinc porphyrin.
[b]Crosslinker abbreviations: egdma, ethylene glycol dimethacrylate; trim, tris(hydroxymethyl) propane trimethacrylate.
[c]Molar proportions of monomer:crosslinker:template.
[d]Solvent abbreviations: aa, acetic acid; acn, acetonitrile; c, chloroform; dmf, dimethyl formamide; dcm, dichloromethane; ma, methyl alcohol; thf, tetrahydrofuran; w, water

111

Covalent and Non-Covalent Imprinting

Molecularly Imprinted Polymers Used as Optical Waveguides
for the Detection of Fluorescent Analytes

Jennifer J. Brazier, Mingdi Yan, Scott Prahl, and Yin-Chu Chen
Chemistry Department, Portland State University,
Portland, OR 97207- 0751, U.S.A.

ABSTRACT

This article demonstrates the novel approach of fabricating molecularly imprinted polymers (MIPs) as fiber optic waveguides for the detection of fluorescent analytes. Combining a polyurethane system and the soft lithography technique of micromolding in capillaries (MIMIC), polymer waveguides of 50 μm and 100 μm dimensions were patterned onto a silicon substrate. Laser coupling into small waveguide segments has been verified visually. Binding experiments using the waveguides are currently being explored. Some preliminary binding studies have been performed, however, for smaller, freestanding filaments of sizes consistent with conventionally prepared MIP particles. Using fluorimetry measurements, templated fibers of 20 μm dimension preferentially bound the analyte molecules by a factor of 1.5 as compared to control polymers.

INTRODUCTION

Molecularly imprinted polymers are biomimetic materials used for the sensitive and selective detection of small organic molecules. Through host-guest interactions, imprinted polymers often display recognition capabilities comparable to those of antibody-antigen systems.[1] The imprinted polymers, however, are much more stable to organic solvents, pH, and temperature than their biological counterparts. With such benefits, this technology has found a niche in various separation techniques such as HPLC, CEC, TLC,[2-4] and in many sensor applications.[5-6]

Traditionally, molecularly imprinted polymers are synthesized in bulk and then subjected to a grinding and sieving process that results in particles of 25 μm or larger dimension. This process, however, is tedious and often creates particles of irregular shape and size. Furthermore, many of the imprinted sites are destroyed during the grinding procedure. Because of these drawbacks, various other synthetic techniques have been employed to create polymers ranging from thin films to small beads.[7-8] This article demonstrates the novel approach of fabricating imprinted polymers in the form of fiber optic filaments for the detection of fluorescent polyaromatic hydrocarbons.

EXPERIMENTAL DETAILS

Materials

PDMS (Sylgard 184 elastomer, Dow Corning) and its corresponding curing agent were purchased from K.R. Anderson, Inc. (Kent, WA). A silicon master was patterned via conventional photolithography using SU-8 photoresist (Microchem Corporation, Newton, MA). Bisphenol A, phlorglucinol, and anthracene were purchased from Aldrich and were used as

Silicon | Pour PDMS and | Remove stamp and | Fill capillaries and | Peel stamp
Master | cure at 70°C, 4h | place on substrate | cure polymer
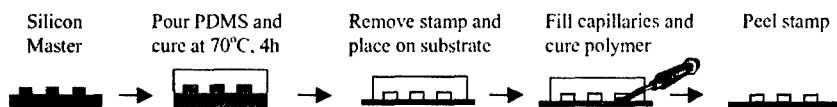
Figure 1. The process of micromolding in capillaries.

received. A mixture of *p,p'*-diisocyanatodiphenylmethane and 30% *p,o,p'*-triisocyanatodiphenylmethane were purchased from Merck-Schuchardt (Hohenbrunn, Germany) and stored under nitrogen after use. Dimethylformamide, was distilled over MgSO$_4$ under reduced pressure and was stored over molecular sieves.

Fabrication of MIP waveguides

Fabrication of polymer waveguides utilized the soft lithography technique of micromolding in capillaries, MIMIC,[9] shown in Figure 1. In this process, a master pattern comprised of lines (50 μm in height by 50 μm in width and 7.5 cm in length) was fabricated through conventional photolithography using SU-8 photoresist. A mixture of poly(dimethylsiloxane), PDMS, and its corresponding curing agent (1:0.07, wt/wt) was poured over this master pattern and allowed to cure at 70°C for 4 hours. The PDMS stamp was then peeled from the master, thereby producing a negative image of the original pattern. The ends of the stamp were then carefully cut with a razor blade to open up the channels and each stamp was cleaned via sonication in ethanol.

When placed on a substrate, the stamp formed small microchannels that were filled with an imprinting solution by capillary action. Prepolymer solutions were generated by mixing monomers (0.375 mmol bisphenol A and 0.455 mmol *p,p'*-diisocyanatodiphenylmethane), crosslinkers (0.250 mmol trihydroxybenzene and 0.195 mmol *p,o,p'*-triisocyanatodiphenylmethane), template molecules (0.0485 mmol anthracene) and porogen (dimethylformamide). Each mixture contained a 1:1 mol ratio of hydroxy to isocyanate functional groups and a 35% mol ratio of cross-linking components to polymer monomers. The templated polymers contained approximately 4 mol % of anthracene, which interact with the aromatic monomers through noncovalent, Π-Π interactions. Control polymers were prepared identically except for the anthracene.

To ensure covalent attachment of the polymer to the substrate, the silicon wafers were previously cleaned in piranha solution (3:1 v/v, conc. H$_2$SO$_4$ / 30% H$_2$O$_2$) and were silanized with 3-aminopropyltrimethoxysilane. Subsequent overnight polymerization under ambient conditions and stamp removal left behind imprinted filaments attached to the wafer support. Filaments were visually inspected via an Olympus BHM optical microscope. Filament segments, which appeared to be uniform in composition and geometry, were cleaved for laser coupling experiments using a 543 nm laser.

Synthesis of freestanding filaments

Freestanding filaments of 20 μm dimension were prepared similarly except that the wafer substrates were spin-coated with PDMS at 1300 rpm for 40 s rather than being silanized. This

thin layer of PDMS (cured at 70°C for 4 h) allows for the easy removal of the 20 µm polymer filaments. Elastomeric stamps were produced as previously discussed using a master pattern with line dimensions of 20 µm height and 20 µm width. Stamps were placed on the PDMS coated substrate and filled with either a control or templated prepolymer solution by capillary action.

Following overnight polymerization at room temperature, stamps were peeled from their PDMS support and immersed in a bath of toluene for isolation and extraction. Fresh volumes of toluene were repeatedly added to the filaments until no further anthracene could be detected. The filaments were then dried under vacuum for 48 hours and massed. These filaments were subsequently shaken with a known concentration of anthracene for 24 hours. The fluorescence of the anthracene solutions was measured using an excitation at 358 nm and an emission at 403 nm, both before and after rebinding. The decrease in fluorescence intensity was correlated to amount of anthracene bound by the polymer through a linear calibration curve.

RESULTS AND DISCUSSION

In this study, polyurethane filaments imprinted with anthracene were fabricated for use as optical waveguides. The imprinting system was adapted from the work of Dickert, where imprinted polyurethane was applied as thin films for the selective detection of polyaromatic hydrocarbons using quartz microbalance (QMB), surface acoustic wave (SAW), and planar waveguide sensors.[10-13] In these studies, Dickert was able to optimize the polyurethane imprinting conditions such that selective detection of various polyaromatic hydrocarbons in the ppt range was observed. The fabrication method used in this study offers the possibility of an array of polyurethane MIPs on a single chip that may lead to simultaneous analysis of multiple analytes.

Imprinted waveguides

Initial attempts at waveguide fabrication proved unsuccessful. The 7.5 cm long capillaries (both 50 µm and 100 µm dimension) would not fill by capillary action alone. They could be forcibly filled, however, with the aid of a small vacuum. Via water aspiration, the vacuum was able to draw the prepolymer solution through the capillaries. Unfortunately, the filaments that resulted were of poor quality. As shown in Figure 2 a-b, the filaments were often cracked, filled with small inclusions, and of varying morphology. It was determined that surface impurities and defects in the original photolithography master played key roles in the quality of the filaments. By making sure that the stamps produced were without defects and that all surfaces (stamp and substrate) were free from particulate matter, the homogeneity of the filaments was dramatically improved.

Prepared under more rigorous standards, the new capillaries filled freely and immediately without vacuum assistance. As shown in Figure 2c, the quality of these filaments was also improved. Filaments appeared to be of uniform geometry and composition. However, the length of these filaments was much shorter than expected.

During polymerization, the polyurethane would shrink laterally from the open end of the 7.5 cm long capillary. As solvent evaporated and cross-linking progressed, an approximate 75% reduction in length would occur thereby producing a filament of only 2-3 cm.

To prevent this length reduction, the catalyst TMED, *N,N,N',N'*-tetramethylethylenediamine, was placed at both ends of a filled capillary. This caused
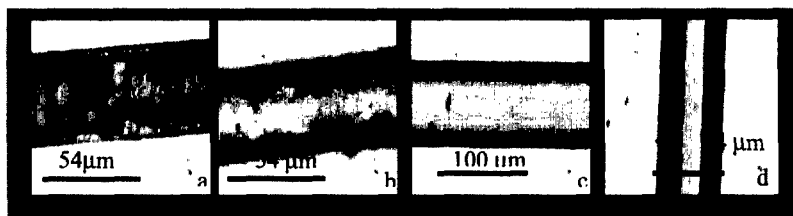
Figure 2. Optical micrographs showing various filament morphologies.

immediate polymerization of the polymer at both capillary ends, thereby making solvent evaporation much more difficult. When the stamp was finally peeled from the substrate, a 7.5 cm length filament was observed along with a significant amount of unevaporated solvent. Although the length of the filament was maintained, it was at the expense of the overall geometry of the filament. As shown in Figure 2d, trapezoidal fibers were often the result of these experiments. For this reason, fiber quality was chosen at the expense of length and the filaments were allowed to shrink. Small segments of imprinted filaments containing no inclusions or defects were cleaved and tested for performance.

In theory, a single wavelength laser can be coupled into such polymer filaments as long as the polymer index of refraction is lower than the index of refraction of the surrounding media and the filament is of high quality. Previous work has already shown successful waveguide performance by nonimprinted polyurethane filaments fabricated through microcontact printing on a silicon substrate.[14] If light can be coupled into the imprinted waveguides, the degree of analyte binding may be measured. As the light is guided through the filament via multiple internal reflections, it can excite and cause an emission from fluorescent molecules, such as anthracene, that bind to the imprinted polymer matrix. The emitted fluorescence from the analytes can be measured and correlated to analyte concentration.

While binding tests have not yet been performed, coupling of a 543 nm and 632 nm He-Ne laser into 0.5 cm long waveguide segments has been verified visually. A lens with a focal length of approximately 10 cm was used to focus the laser into the waveguide. Coupling was verified by rotating the waveguide relative to the optical axis such that the light emitted from the fiber was aimed in a direction that was distinct from the illumination light. The distal end of the waveguide lit up as well. Quantitative tests are currently being performed.

Freestanding Filaments

Freestanding filaments were prepared in a manner similar to the polymer waveguides. The main fabrication difference was that the substrate surface was coated with a thin layer of PDMS to facilitate removal of the freestanding filaments during isolation. Therefore, the imprinting solution was sandwiched between PDMS on the substrate support and the PDMS stamp. After polymerization, the PDMS stamp was easily peeled from the substrate resulting in well-formed 20 µm filaments inside the PDMS stamp as shown in Figure 3a.

Previous studies involving MIMIC and freestanding MIP filaments employed tetrabutylammonium fluoride, TBAF, in the isolation procedure.[15] TBAF is known to
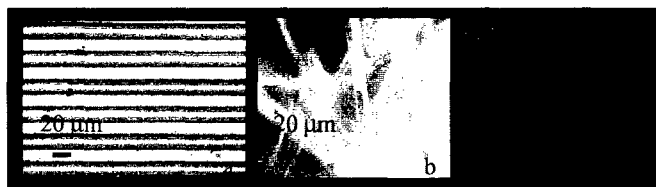
Figure 3. Optical micrographs of a) filaments still in the PDMS stamp b,c) freestanding MIP filaments.

attack PDMS.[16] Therefore, if a stamp and its polymer-filled channels were placed in a bath of TBAF, the stamp should be dissolved and free-floating MIP filaments should be obtained. Unfortunately, TBAF reacted poorly with the polyurethane filaments. The TBAF solution caused the filaments to shrink into small, viscous masses.

This problem was avoided by submerging the stamp and its polymer filaments directly into the extraction solvent, toluene. When introduced to toluene, the PDMS stamp swelled enough that the filaments were removed from the stamp. Figure 3b-c show freestanding 20 μm filaments, which had been isolated, extracted, and dried.

Dried fibers were vortexed with a known concentration of anthracene for 24 hours. The fluorescence intensity of the solution was measured before and after rebinding. The decrease in fluorescence intensity was then correlated to the amount of anthracene absorbed by the polymer filaments.

Initial studies have shown a preference for the templated filaments towards anthracene 1.5 times greater than the control polymers as shown in Figure 4. While, the amount of analyte absorbed by the templated polymer (2.2 μmol/g) is more than the control (1.5 μmol/g), the difference is much less than that previously reported by Dickert.[17] Using thin imprinted films and planar waveguide fluorescence measurements, Dickert reported a less than 1% response of the control polymer to the analyte when compared to the templated polymer. A difference in imprinting conditions as well as the method used to evaluate rebinding may account for this discrepancy. Further optimization of the imprinting parameters are currently being explored.
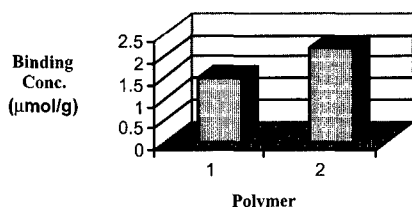
Figure 4. Templated (2) versus control (1) polymers for anthracene binding.

CONCLUSIONS

While optical waveguides have previously been produced via soft lithography techniques,[18] this study combines MIMIC and molecularly imprinted polymers to fabricate imprinted optical waveguides. The preferential binding of imprinted polymers compared to control polymers for freestanding filaments as well as the fabrication of high-quality filaments capable of coupling light is promising. Studies are underway to test the performance of these waveguides and to further optimize imprinting conditions.

ACKNOWLEDGMENTS

REFERENCES

1. G. Vlatakis, L.I. Andersson, R. Muller, and K. Mosbach, Nature **361**, 645 (1993).
2. N. Masque, R. Marce, F. Borrull, P.A.G. Cormack, and D. Sherrington, Anal. Chem. **72**, 4122 (2000).
3. L. Schwartz, M. Petersson, T. Johansson, and S. Nilsson, Journal of Chromatography A **892**, 203 (2000).
4. D. Kriz, C. Berggren, L.I. Andersson, and K. Mosbach, Anal. Chem. **66**, 2636 (1994).
5. F.L. Dickert and O. Hayden, Trends Anal. Chem. **18**, 192 (1999).
6. D. Kriz, O. Ramstrom, and K. Mosbach, Clin. Chem. **69**, 345A (1997).
7. J. Mathew-Krotz and K.J. Shea, J. Am. Chem. Soc. **118**, 8154 (1996).
8. R.J. Ansell and K. Mosbach, J. Chromatogr. A **787**, 55 (1997).
9. G.M. Whitesides and Y. Xia, Angew. Chem., Int. ed. Engl. **37**, 550 (1998).
10. F.L. Dickert, P. Forth, P. Lieberzeitz, and M. Tortschanoff, Fresenius J. Anal. Chem. **360**, 759 (1998).
11. F.L. Dickert and O. Hayden, Adv. Mater. **14**, 311 (2000).
12. F. L. Dickert, M. Tortschanoff, W. Bulst, and G. Fischerauer, Anal. Chem. **71**, 4559 (1999).
13. F.L. Dickert and S. Thierer, Adv. Mater. **8**, 987 (1996).
14. E. Kim, G.M. Whitesides, L. Lee, S.P. Smith, and M. Prentiss, Adv. Mater. **8**, 139 (1996).
15. M. Yan and A. Kapua, Analytica Chimica Acta **435**, 163 (2001).
16. B. Xu, F. Arias, and G.M. Whitesides, Adv. Mater. **11**, 492 (1999).
17. F.L. Dickert, H. Besenbock, and M. Tortschanoff, Adv. Materials **10**, 149 (1998).
18. P. Yang, G. Wirnsberger, H. Huang, S. Cordero, M. McGehee, B. Scott, T. Deng, G.M. Whitesides, B. Chmelka, S. Buratto, and G. Stucky, Science **287**, 465 (2000).

SYMPOSIUM O

Sensor Arrays and Devices

Thin film micro arrays with immobilized DNA for hybridization analysis

F. Fixe[1,2], A. Faber[1], D. Gonçalves[1], D.M.F. Prazeres[1], R. Cabeça[2], V. Chu[2], G. Ferreira[3] and J.P. Conde[4]
[1] Center for Biological & Chemical Engineering, Instituto Superior Técnico, Lisbon, Portugal
[2] INESC Microsystems and Nanotechnologies, Lisbon, Portugal
[3] Faculdade de Engenharia de Recursos Naturais, Universidade do Algarve, Faro, Portugal
[4] Department of Materials Engineering, Instituto Superior Técnico, Lisbon, Portugal

ABSTRACT

In this work, a procedure to immobilize DNA probes on a microarray patterned on a flexible plastic substrate is developed. The method involves the chemical activation of a thin film surface, the introduction of amine functionality via a silanization step, the coupling of an adequate crosslinker and finally the immobilization of the DNA probe. The response of different thin-film materials and plastic substrates to the immobilization procedure is discussed. The DNA probes immobilized in the patterned pixels were then allowed to hybridize with complementary target DNA labeled with a fluorescent molecule. A prototype array of thin film pixels of SiO_2 functionalized by silanization deposited over a polyimide substrate is demonstrated.

INTRODUCTION

Biochips, particularly those based on DNA, are powerful devices that integrate the specificity and selectivity of biological molecules with electronic control and parallel processing of information. This combination will potentially increase the speed and reliability of biological analysis [1]. Thin-film microelectronic technology is especially suited for this purpose since it enables low-temperature processing and thus allows fabrication of electronic devices on a wide variety of substrates (glass, stainless steel, plastic, etc. [2]). Examples of current applications of DNA chips include genomic analysis to screen and identify single nucleotide polymorphisms (SNPs) or to sequence gene fragments, pathogen identification, and gene expression profiling [1].

The core of a DNA chip is a surface, usually flat, with DNA probe molecules spatially resolved and attached to it. This separation can be accomplished by using immobilization procedures that localize the probes to their exact site such as fine spotting [3], piezoelectric printing [4], electronic [5] and electrochemical addressing [6]. Alternatively, thin-film microelectronics technology can be used to deposit a material suitable for DNA attachment on an inert surface according to a given pattern. The use of passivation layers, although not described so often, can also be considered [7]. Other possible features of a DNA chip surface include the presence of microelectrodes beneath the DNA-containing areas. These can be used as sensing devices and to generate electric fields that promote the migration of oligonucleotides [5], hybridization and covalent binding [8]. Overall, the structure of a DNA chip is complex and its fabrication may include surface activation, passivation, patterning, and introduction of sensing devices and immobilization aids such as microelectrodes.

EXPERIMENTAL
Materials: Glass slides were obtained from Corning (7059). Polyimide (PI), polyethylene terephtalate (PET), polyetherether ketone (PEEK), polyethersulfone (PES), polycarbonate (PC)

and (PEN) plastic slides were obtained from Goodfellow. Oligonucleotides (both probes and targets) were purchased from Interactiva (Germany).

Silanization: The substrates and thin films tested were first cleaned with HNO_3, 5%(v/v), for 1 hr at 90°C. In a later stage, a procedure using the less corrosive cholic acid (12 hr at room temperature) was developed to replace HNO_3, in order to minimize damage to thin film materials already present on the chip during the cleaning process. The surfaces were then silanized with 3-aminopropyltriethoxysilane (APTES) for 2 hr at 85°C (figure 1).

Oxidation   Silanization
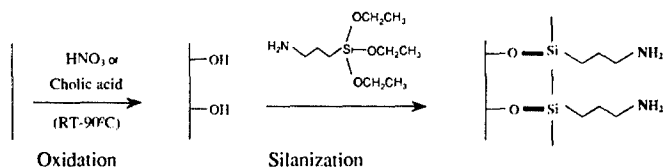
Figure 1. Introduction of amine functionality by surface modification with 3-aminopropyltriethoxysilane (APTES) after surface oxidation with HNO_3 or cholic acid.

Detection methods: The presence of NH_2 groups was evaluated by incubating the surfaces with 0.1 mg/ml fluorescein-5-isothiocyanate (FITC) for 30 min, followed by inspection with fluorescence microscopy. X-Ray Photoelectron Spectroscopy (XPS) and UV-VIS spectroscopy were also used to complement surface characterization.

Immobilization of DNA: After selecting the materials that could be silanized, DNA probes (17 bp) were immobilized using two chemical strategies. In the first strategy (figure 2a) surfaces were modified with the crosslinker glutaraldehyde. Next, DNA probes labeled with FITC and modified at the 5´-end with an amino group were linked to the terminal aldehyde group of the crosslinker (1 hr at room temperature). The second strategy (figure 2b) involved the modification of the activated films with the hetero-bifunctional cross-linker, sulpho succinimidyl 6-maleimidylhexanoate (sulpho-EMCS), for 2 hr at room temperature. Next, DNA probes labeled with FITC at the 3´-end and modified with a thiol group on the 5´-end were linked to the maleimide residues of the crosslinker. After immobilization for 3 hr the DNA probes were detected by fluorescence microscopy.

Hybridization: Non-labeled DNA probes were immobilized as described above using the cross-linker sulpho-EMCS. The surfaces were pre-hybridized with a solution containing Bovine Serum Albumin in order to avoid non-specific adsorption of the DNA target [9]. Hybridization was then carried out with a complementary (positive control) and a non-complementary (negative control) strand of DNA (target) labeled with FITC. The reaction was carried in 50 mM L-histidine at 37°C overnight, followed by two washing steps with SSC (2x) + 0.1 % SDS. The detection was made by fluorescence microscopy.

Patterning: Arrays of SiO_2 on polyimide substrates were prepared in a clean room environment by direct write photolithography using a HeCd laser ($\lambda = 440$ nm) and reactive ion etching using a RF plasma of CF_4, O_2 and Ar.

Thin Film Deposition: The thin film deposition techniques used were plasma-enhanced chemical vapor deposition (silicon dioxide (SiO_2), amorphous silicon (a-Si:H), microcrystalline silicon (μc-Si:H), amorphous carbon (a-C:H), silicon nitride (SiN_x)) and magnetron sputtering (Al_2O_3, TiO_2, ZnO, SnO_2). All films were deposited at temperatures $\leq$ 150 °C. A combination of

these layers allowed the definition of either functionalized islands on an inactive surface or windows of functionalized areas cut out of a passivation overlayer.
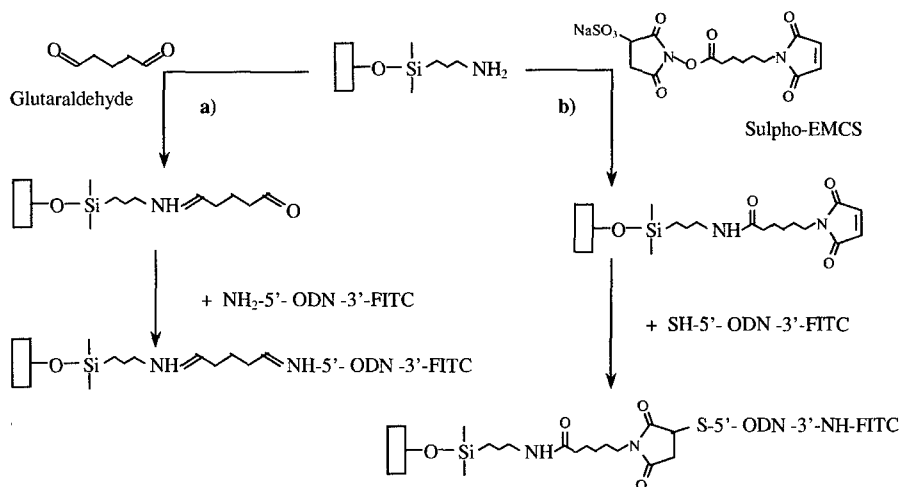
Figure 2 (a) and (b). Immobilization of FITC-labeled DNA probes onto silanized surfaces: modified with an amino group at the 5´-end were coupled via glutaraldehyde, and probes modified with a thiol group at the 5´-end were coupled via sulpho-EMCS, respectively.

RESULTS AND DISCUSSION

Activation (functionalization) and passivation layers: All substrates and thin films studied were subjected to the silanization procedure described in the previous section. The surfaces were then probed for NH_2 groups with FITC. The results obtained with different materials are described in table 1.

Table 1. Materials tested for activation by silanization (results obtained by fluorescence microscopy with FITC) (++: strong activation; +: activation; -: inert;?: auto-fluorescent substrate).

Substrate	Activation	Film*	Activation	Film*	Activation
Glass	++	SiO$_2$	++	SiNx	-
PI	-	TiO$_2$	++	Al$_2$O$_3$	-
PET	+	ZnO	++	C-Si p	-
PEEK	-	SnO	++	C-Si n	-
PES	-	a-Si:H	-	C-Si i	-
PC	?	a-C:H	-	Photoresist	-
PEN	-	µC-Si	-		

*The supporting substrate was either glass or PI

The results indicate that, apart from PET, all plastics tested are inert to the activation protocol used. These plastics are therefore appropriate substrates for the deposition of films of different materials. Polyimide was further selected for future work due to its good chemical and physical stability, as well as availability. A range of different thin film materials were deposited on top of PI and tested with the activation protocol. Only the oxide films were activated (i.e., functionalised by silanization), with the exception of Al_2O_3. These materials, and particularly SiO_2, were therefore selected as adequate surfaces for the attachment of DNA probes. On the other hand, Al_2O_3, silicon nitride and amorphous carbon (a-C:H) were chosen as passivation layers.

Most of the oxide films were also analysed by X-ray photoelectron spectroscopy (XPS), before and after silanization. As an example, figure 3 shows a XPS spectrum obtained for a silanized SiO_2 thin film deposited over PI. The binding energy for N (1s) (399,7 eV) is typical of NH_2 groups [10] and the binding energies of the others atoms C (1s), Si (2p) and O (1s) also confirm the functionalization of the silanized SiO_2 film surface, when compared with the XPS spectrum for non-silanized SiO_2.
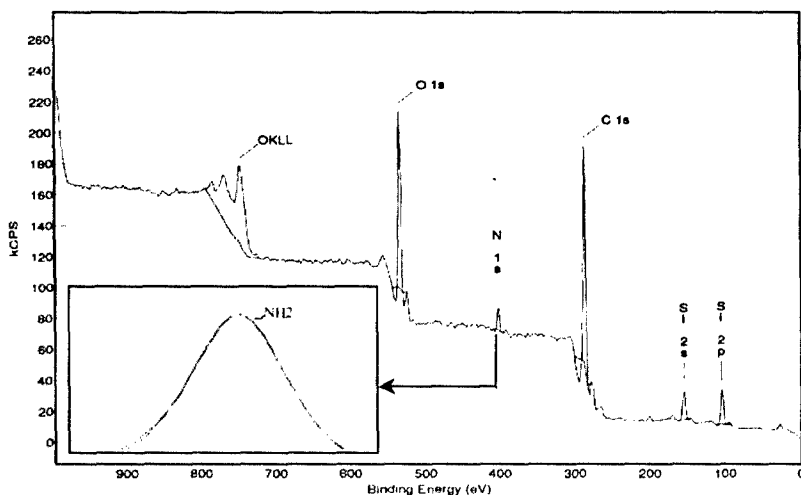
Figure 3. XPS scanning of a silanized SiO_2 thin film deposited over PI, showing the presence of nitrogen in the form of NH_2.

Patterning of thin film layers: After selecting the thin films that are functionalized by silanization and the substrates that are inert to this chemical procedure, two patterned surfaces were designed with islands of activated SiO_2 on PI (figure 4a) and active squares of glass delimited by a passivation layer of silicon nitride (figure 4b).

Immobilization of DNA probes: DNA probes were immobilized using two different cross-linkers, glutaraldehyde and sulpho-EMCS. In either case it was possible to attach the probes on non-patterned surfaces and on selectively activated areas defined by patterning (figure 5).
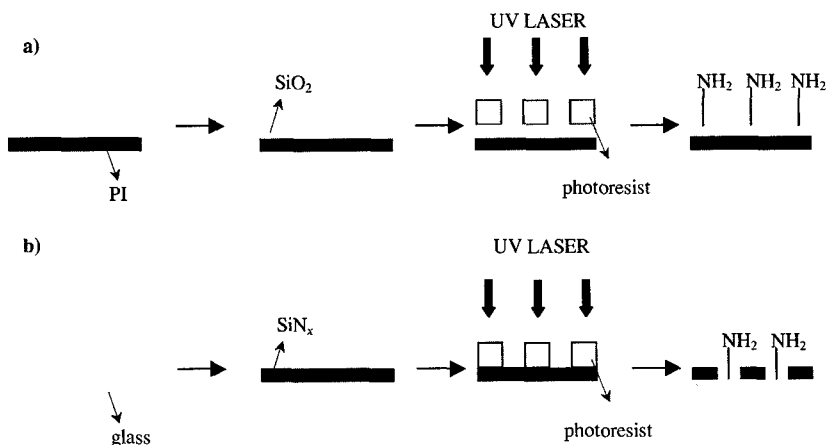
Figure 4 (a) and (b). Patterned surfaces, by photolithography, of active thin film layers (SiO$_2$) on the top of an inactive substrate (PI), or inactive layers (SiN$_x$) on an active (i.e., functionalized by silanization) substrate (Glass), respectively.
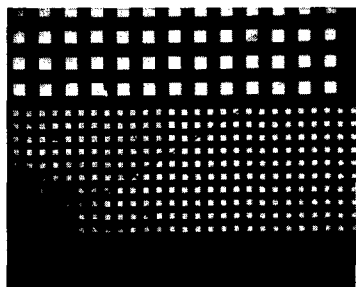
Figure 5. DNA probes immobilized on patterned active islands of SiO$_2$ deposited over PI. Sulpho-EMCS was used as a spacer arm and the probes were detected by fluorescence microscopy. The concentration of DNA was 1 µM and the immobilization time was 3 hr at room temperature.

Hybridization: Hybridization studies were made with DNA sequences complementary (positive control) and non-complementary (negative control) to the immobilized DNA probe. This was done in order to check if the immobilized probe can hybridize freely with a complementary strand, and also to make sure that the fluorescence signal obtained is due to hybridization alone and not to unspecific adsorption of the DNA target to the surface (Figure 6). The presence of fluorescence on the surface incubated with the complementary DNA target clearly indicates that hybridization has occurred. Furthermore, the absence of fluorescence in the surface that was incubated with the non-complementary DNA rules out the possibility of non-specific adsorption as a source of fluorescence.
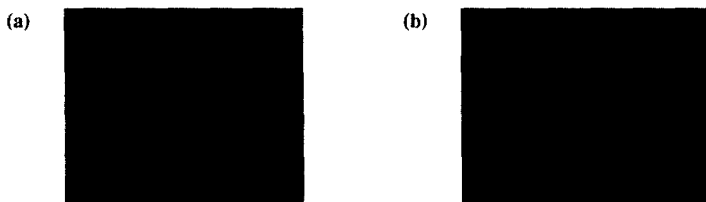
Figure 6 (a) and (b). Hybridization of complementary and non-complementary DNA target, respectively, to DNA probes immobilized with sulpho-EMCS on a pattern of active glass exposed through windows in a passivating SiN_x passive layer

CONCLUSIONS

The work presents an enabling technology which applies low temperature thin film microelectronics processing to DNA chip and potentially other types of biological applications. Different materials were screened by a silanization chemistry for their ability to attach DNA probes. Glass and oxide films (SiO_2, TiO_2, ZnO, SnO_2) were modified, while plastic substrates such as polyimide (PI), thin films of silicon nitride, Al_2O_3, amorphous carbon and amorphous silicon were inert to the silanization procedure. On the basis of these results, chip prototypes were fabricated by photolithography, consisting of patterned arrays of functionalized thin film SiO_2 on a plastic substrate (PI) and islands of silanized glass passivated by a silicon nitride. DNA probes were then attached to the silanized areas using sulpho-EMCS as a hetero-bifunctional crosslinker. Hybridization of the DNA probes on the pixels with complementary DNA was demonstrated. This technology provides the basic building blocks for the integration of thin film electronic sensing and control with biological applications.

ACKNOWLEDGEMENTS

REFERENCES

1. Ramsay, G. (1998), *Nature Biotechnol.*, **16**, 40-44.
2. Street, R.A."Hydrogenated Amorphous Silicon", Cambridge Univ. Press, Cambridge, 1991.
3. Kumar, A. and Liang, Z. (2001), *Nucleic Acids Res.*, **29**, e2.
4. Brennan, T. M. (1995) US Patent 5 474 796.
5. Edman, C.F., Raymond, D.E., Wu, D.J., Tu, E., Sosnowski, R.G., Butler, W.F., Nerenberg, M. and Heller, M.J. (1997), *Nucleic Acids Res.*, **25**, 4907-4914.
6. Bidan, G., Billon, M., Galasso, K., Livache, T., Mathis, G., Roget, A., Torres-Rodriguez, L.M. and Vieil, E. (2000), *App. Biochem. Biotechnol.*, **89**, 183-193
7. Shoffner, M.A., Cheng, J., Hvichia, G.E., Kricka, L.J. and Wilding, P. (1996), *Nucleic Acids Res.*, **24**, 375-379.
8. Peterson, Q.W., Heaton, R.J. and Georgiadis, R.M. (2001), *Nucleic Acids Res.*, **29**, 5163-5168.
9. Okamoto, T., Suzuki, T. e Yamamoto, N., (2000), *Nature Biotechnol.*, **18**: 438-441.
10. Dang, T. A. and Gnanasekaran, R., (1990), *Surf. Int. Analysis,* **15**: 113-118.

O3.1

A Highly Sensitive and Selective Surface-Enhanced Nanobiosensor

Amanda J. Haes and Richard P. Van Duyne
Department of Chemistry, Northwestern University,
Evanston, IL 60208-3113, USA

ABSTRACT

Nanosphere lithography (NSL) derived triangular Ag nanoparticles were used to create an extremely sensitive and specific optical biological and chemical nanosensor. Using simple UV-vis spectroscopy, biotinylated surface-confined Ag nanoparticles were used to detect streptavidin down to one picomolar concentrations. The system was tested for nonspecific binding interactions with bovine serum albumin and was found to display virtually no adverse results. The extremely sensitive and selective response of the Ag nanoparticle sensor indicates an exciting use for biological and chemical sensing.

INTRODUCTION

Currently, there is great interest in the optical properties of noble metal nanoparticles. Early work with size tunable Ag nanoparticles fabricated by nanosphere lithography (NSL) demonstrated that the localized surface plasmon resonance (LSPR) could be tuned throughout the visible region of the electromagnetic spectrum [1]. The LSPR, the signature optical property of noble metal nanoparticles, arises when electromagnetic radiation excites the conduction electrons of the metal and causes them to oscillate collectively. The primary consequences of this excitation include (a) localized electromagnetic field enhancement and is responsible for the intense signals observed in surface-enhanced spectroscopies and (b) selective photon absorption/scattering (extinction) and can be easily monitored using UV-vis spectroscopy [2].

The formation of alkanethiol self-assembled monolayers (SAMs) on metal surfaces (i.e. nanoparticles) offers a simple and attractive method of surface modification. SAMs are used in many chemical and biological sensor technologies because they can functionalize a metal nanoparticle for specific analyte capture and protect fragile biological molecules from denaturing upon exposure to bare metal surfaces [3-5]. These systems have been implemented in various detection schemes with the goal of creating biosensing systems.

SAMs have been used to link molecules from solution onto nanoparticles and bulk surfaces [6-8]. The extremely high binding affinity of the biotin-streptavidin complex ($\sim 10^{13} - 10^{15}$ M^{-1}) [9] makes SAM modified Ag nanoparticles ideal for model biosensing experiments . The detection of low concentrations of biomolecules with minimal nonspecific binding responses is an elusive goal in many biosensor technologies. Streptavidin (SA), a tetrameric protein, can bind up to four biotinylated molecules (i.e. antibodies, inhibitors, nuclei acids, etc.) with minimal impact on its biological activity [10]. These complexes are extremely stable over a wide range of pH and temperature; accordingly, this system is often used to test potential biosensor systems.

Surface plasmon resonance biosensors have been used to characterize the specific binding of a biomolecule to its immobilized binding partner. These propagating surface plasmon polariton (SPP) sensors, which operate on real-time refractive index changes, offer a label-free method for the detection of biomolecules [11-13].

Recently, we demonstrated that NSL-derived Ag nanoparticles can be used as biological and chemical optical nanosensors by monitoring the peak extinction, λ_{max} [8]. These experiments indicated that Ag nanoparticles could be used in sensor applications much like the widely available SPP biosensors. Similar to the SPP sensor, the LSPR nanosensor operates by detecting refractive index changes near the metal surface. NSL-generated nanoparticles are ideal for optical nanosensor applications for the following reasons: (a) the nanoparticles are confined to a surface at a large enough fixed interparticle spacing so that they function independently rather than as an array [14], (b) the nanoparticles are homogenous in size and shape [15], and (c) the dielectric environment surrounding the particles is easily controlled [8]. In this study, the specific binding of SA to biotinylated Ag triangular nanoparticles was explored. Additionally, detection limits and sensor specificity were determined.

EXPERIMENTAL DETAILS

Materials

11-Mercaptoundecanoic acid (11-MUA), 1-octanethiol (1-OT), hexanes, and methanol were acquired from Aldrich (Milwaukee, WI). 1-Ethyl-3-[3-dimethylaminopropyl]carbodiimide hydrochloride (EDC), bovine serum albumin (BSA), streptavidin (SA), 10 mM and 20 mM phosphate buffered saline (PBS), pH = 7.4 was obtained from Sigma (St. Louis, MO). (+)-Biotinyl-3,6-dioxaoctanediamine (biotin) was purchased from Pierce (Rockford, IL). Absolute ethanol was purchased from Pharmco (Brookfield, CT). Ag wire (99.99%, 0.5 mm diameter) was obtained from D. F. Goldsmith (Evanston, IL). Borosilicate glass substrates, Fisher brand No. 2 18 mm circle cover slips were purchased from Fisher Scientific (Pittsburgh, PA). Tungsten vapor deposition boats were acquired from R. D. Mathis (Long Beach, CA). Polystyrene nanospheres with diameters of 400±7 nm were received as a suspension in water (Interfacial Dynamics Corporation, Portland, OR) and were used without further treatment. Millipore cartridges (Marlborough, MA) were used to purify water to a resistivity of 18 MΩ. All materials were used without further purification.

Substrate preparation

Glass substrates were cleaned in a piranha solution (1:3 30 % H_2O_2:H_2SO_4) at 80°C for 30 minutes. Once cooled, the glass substrates were rinsed with copious amounts of water and then sonicated for 60 minutes in 5:1:1 H_2O:NH_4OH:30% H_2O_2. Next, the glass was rinsed repeatedly with water and was stored in water until used.

Nanoparticle preparation

NSL was used to fabricate monodisperse, surface-confined Ag nanoparticles [16]. For these experiments, single layer colloidal crystal nanosphere masks were prepared by drop coating ~2 μL of nanosphere solution onto glass substrates. Once the nanosphere masks were dry, the substrates were mounted into a Consolidated Vacuum Corporation vapor deposition system. A Leybold Inficon XTM/2 quartz crystal microbalance (East Syracuse, NY) was used to measure the thickness of the Ag film deposited over the nanosphere mask. Ag films were

deposited to a 50.0 nm thickness for all samples in this study. Following Ag deposition, the nanosphere mask was removed by sonicating the sample in ethanol for 3 minutes.

Ultraviolet-visible extinction spectroscopy

Macroscale UV-vis extinction measurements were collected using an Ocean Optics (Dunedin, FL) SD2000 fiber optically coupled spectrometer with a CCD detector with a resolution of ~0.6 nm. All spectra were collected in standard transmission geometry with unpolarized light. The probe beam area was approximately 12 mm^2.

Nanoparticle modification

A home built flow cell [8] was used to control the external environment of the Ag nanoparticle substrates. Prior to modification, the Ag nanoparticles were solvent annealed [8]. Dry N_2 gas and solvent were cycled through the flow cell until the λ_{max} of the sample stabilized. The UV-vis extinction maxima, λ_{max}, of identically-prepared bare Ag nanotriangles, varies slightly due to small differences in nanoparticle size and roughness [8]. This difference, however, does not affect the overall sensitivity of the nanoparticle sensor. As a result, the λ_{max} must be recorded before and after chemical modification. Once solvent annealed, samples were then incubated in 1 mM 3:1 1-OT:11-MUA ethanolic solutions for 24 hours. After incubation, the nanoparticle samples were rinsed with ethanol and dried by flowing N_2 gas through the sample cell. Next, 1 mM biotin in 10 mM PBS was covalently linked to the surface carboxyl groups using EDC coupling over a 3 hour period. Following thorough rinsing and N_2 drying, the samples were incubated in SA solutions in 10 mM PBS for 3 hours. Samples were rinsed thoroughly with 10 mM PBS, 20 mM PBS, and water to remove electrostatically bound molecules.

Atomic force microscopy (AFM)

AFM images were collected using a Digital Instruments Nanoscope III microscope operating in tapping mode. Etched Si nanoprobe tips (TESP, Digital Instruments, Santa Barbara, CA) were used. These tips had resonance frequencies between 280 and 320 kHz and are conical in shape with a cone angle of 20• and an effective radius of curvature at the tip of 10 nm. All images shown here are unfiltered data that were collected in ambient conditions.

DISCUSSION

NSL-derived Ag nanoparticles with an in-plane dimension, a=93 nm and an out-of-plane height, b=50.0 nm were synthesized and solvent annealed (Figure 1). The Ag nanoparticles were then functionalized with a mixed monolayer of 11-MUA/1-OT resulting in a surface coverage of $\Box$ = 0.1 [17] of carboxylate binding sites. Next, biotin was covalently attached via amide bond formation to carboxylated surface sites. Upon exposure to 10 pM SA, the LSPR extinction maximum shifted +15.3 nm (Figure 2). It should be noted that the signal transduction mechanism in this sensor is unique in that it is a reliably measured wavelength shift rather than an intensity change.

Figure 1. Tapping mode AFM image of the Ag nanoparticle LSPR nanosensor. After solvent annealing, the resulting nanoparticles have in plane widths of ~100 nm and out-of-plane heights of 51 nm. Defects are present in sensing probe volume but do not contribute to the optical sensing events.

The sensitivity limits of the biotinylated Ag nanoparticle biosensor were also examined. By varying the concentration of SA, the detection limit of LSPR shift versus SA concentration was determined (Table 1). In these studies, the SA concentration was varied from 1×10^{-15} M to 1×10^{-6} M. The LSPR shift response remained constant for concentrations between 1×10^{-10} M and 1×10^{-6} M. The LSPR response drops off drastically between 1×10^{-13} M and 1×10^{-10} M. Overall, it was found that the maximum SA response of +26.5 nm decreased rapidly to a detectable +4 nm shift for 1 pM SA. Fitting the SA response to the function yields a value for the saturation response, $R_{TOT} = 26.5$ nm, and the surface-confined thermodynamic affinity binding constant, $K_{a,surf} = 10^{11}$ M^{-1} [18]. This value is smaller than the widely accepted $K_{a,surf}$ value [9]. By adjusting the length of the biotin tether, the $K_{a,surf}$ value will approach the widely accepted value of 10^{13}-10^{15} M^{-1} [9].

It is important to realize that the maximum number of SA molecules detected at saturation coverage is approximately 600 per nanoparticle. At 1 pM SA concentration, a maximum of 60 SA molecules per nanoparticle is being detected. Previously, it has been demonstrated that the macroscopic measurements (12 mm^2 spot size) are equivalent to
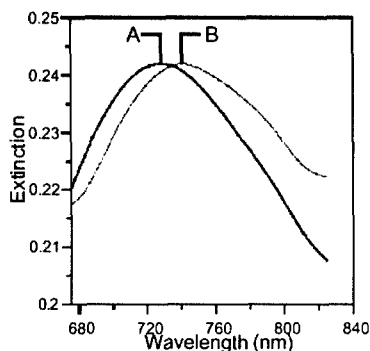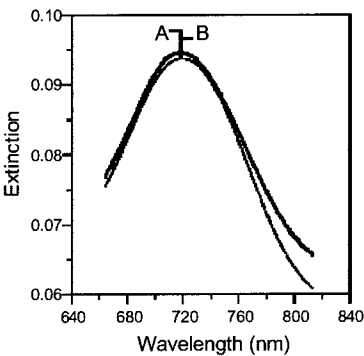

Figure 2. UV-vis extinction spectra of Ag nanoparticles before and after modification with 10 pM SA in a N_2 environment. (A) Ag nanoparticles after modification with 1 mM biotin, $\lambda_{max} = 727.5$ nm. (B) Ag nanoparticles after modification with 10 pM SA, $\lambda_{max} = 742.8$ nm.

Table 1. SA concentration vs LSPR shift (SA-biotin) obtained for Ag nanoparticles in a N_2 environment.

[SA] (M)	LSPR Shift (nm)
1×10^{-6}	23.9
1×10^{-7}	26.5
1×10^{-9}	26.4
1×10^{-10}	26.5
1×10^{-11}	15.3
1×10^{-12}	3.8
1×10^{-13}	0.6
1×10^{-14}	0.1
1×10^{-15}	0.3

microscopic measurements (12 μm^2 spot size) [19]. Based on the previous result and the principle that the individual nanoparticles act independently, the extinction spectrum of an array of nanoparticles is equivalent to the extinction spectrum of one nanoparticle. As the experiments near the 1 nanoparticle limit, a reasonable extrapolation of the data indicates yoctomole sensitivity.

Additionally, control experiments were performed to verify that the induced LSPR shifts are a result of SA binding to a biotinylated surface [18]. To test nonspecific protein interactions with a biotinylated Ag nanoparticle surface, BSA interactions with the Ag nanoparticle surface were tested (Figure 3). Ag nanoparticles were functionalized with a mixed monolayer of 11-MUA/1-OT. Next, biotin was covalently attached using EDC coupling. The biotinylated LSPR nanosensor is now ready for nonspecific binding tests. For this study, 1.5×10^{-5} M BSA was exposed to the biotinylated surface. A 0.6 nm LSPR shift was detected from this exposure. Because this shift is insignificant (i.e. less than the detection limit of the system) [18], this suggests that there is no non-specific binding occurring on the nanoparticle biosensor.

Figure 3. UV-vis extinction nonspecific binding measurements for Ag nanoparticles before and after modification with BSA. Ag nanoparticles (A) after modification with 1 mM biotin, $\lambda_{max} = 718.3$ nm and (B) after modification with 1.5×10^{-5} M BSA, $\lambda_{max} = 718.9$ nm.

CONCLUSION

In conclusion, Ag nanoparticles were fabricated using the technique of NSL. Using the model system of biotin-SA, several exciting features of this novel nanoparticle-based biosensor was demonstrated: 1) the extinction maximum, λ_{max}, of the LSPR shifts +26.5 nm for a complete monolayer coverage of streptavidin and shift +15.3 nm for 10 pM SA; 2) the limit of detection of this ultrasensitive nanoparticle based system is 1 pM streptavidin; and 3) a nonspecific binding tests using BSA yielded desirable results. Current work is aimed at studying systems with weaker binding constants than the biotin-SA system. All in all, a new class of nanobiosensors is being developed using triangular Ag nanoparticles modified with biomolecules. These nanosensors work by detecting shifts in the LSPR induced by changes in the local refractive index caused by analyte binding events. We anticipate the findings reported here will have a significant impact on biological and chemical sensing technologies.

ACKNOWLEDGMENTS

REFERENCES

1. T. R. Jensen, M. D. Malinsky, C. L. Haynes, R. P. Van Duyne, *J. Phys. Chem. B* **104**, 10549-10556 (2000).
2. U. Kreibig, M. Vollmer, *Optical Properties of Metal Clusters* (Springer-Verlag, Heidelberg, Germany, 1995), Vol. 25.
3. P. Schuck, *Annu. Rev. Biophys. Biomol. Struct.* **26**, 541-566 (1997).
4. E. Sackmann, *Science* **271**, 43-48 (1996).
5. W. Knoll, M. Liley, D. Piscevic, J. Spinke, M. J. Tarlov, *J. Adv. In Biophys.* **34**, 231-251 (1997).
6. R. M. Bright, M. D. Musick, M. J. Natan, *Langmuir* **14**, 5696-5701 (1998).
7. C. A. Mirkin, R. L. Letsinger, J. J. Storhoff, R. C. Mucic, *Nature* **382**, 607-609 (1996).
8. M. D. Malinsky, K. L. Kelly, G. C. Schatz, R. P. Van Duyne, *J. Am. Chem. Soc.* **123**, 1471-1482 (2001).
9. N. M. Green, *Adv. In Protein Chem.* **29**, 85-133 (1975).
10. M. B. Wilchek, A. Edward, in *Avidin-biotin immoblization systems* T. L. Cass, S. Frances, Ed. (Oxford University Press, Oxford, UK, 1998) pp. 15-34.
11. J. M. Brockman, B. P. Nelson, R. M. Corn, *Ann. Rev. of Phys. Chem.* **51**, 41-63 (2000).
12. B. L. Frey, R. M. Corn, *Anal. Chem.* **68**, 3187-3193 (1996).
13. L. S. Jung, K. E. Nelson, P. S. Stayton, C. T. Campbell, *Langmuir* **16**, 9421-9432 (2000).
14. T. R. Jensen, G. C. Schatz, R. P. Van Duyne, *J. Phys. Chem. B* **103**, 2394-2401 (1999).
15. J. C. Hulteen, *et al.*, *J. Phys. Chem. B* **103**, 3854-3863 (1999).
16. C. L. Haynes, R. P. Van Duyne, *J. Phys. Chem. B* **105**, 5599-5611 (2001).
17. C. D. Bain, G. M. Whitesides, *J. Am. Chem. Soc.* **110**, 6560-6561 (2001).
18. A. J. Haes, R. P. Van Duyne, *manuscript in preparation.*

Sensing With Bilayers, Cells, and Polymers

Cells in Micropatterned Hydrogels: Applications in Biosensing

Won-Gun Koh and Michael Pishko

Department of Chemical Engineering, The Pennsylvania University, 104 Fenske,
University Park, PA 16802-4420

ABSTRACT

Here we will discuss the development of arrays of mammalian cells of differing
phenotype integrated with microfluidics and microsensors for applications such as drug
screening and used to monitor cellular effects of multiple chemical and biological
candidates. To fabricate these arrays, we immobilized either single or small groups of
cells in 3-dimensional poly(ethylene glycol) hydrogel microstructures fabricated on
plastic or glass surfaces. These microstructures were created using either
photolithography or printed using microarray robots. The resulting hydrogel
microstructures were fabricated to dimensions as small as 10 microns in diameter with
aspect ratios as high as 1.4. The gels were highly swollen with water to permit mass
transfer of nutrients and potential analytes to the cells, and cell adhesion molecules were
immobilized in the gel to allow cell attachment and spreading. Cell viability was
confirmed using fluorescent assays and ESEM used to verify complete cell encapsulation.
The specific and non-specific response of these cells to target molecules was monitored
using optical or electrochemical detectors and analyzed to quantify the effect of these
agents on the different phenotypes present in the array.

INTRODUCTION

Cell-based biosensing devices for applications such as high-throughput drug
screening require accurate positioning of cells into arrays that can be addressed
(preferably using optical methods) and integrated with microfluidic channels for sample
introduction.[1-4] Much research has been conducted in the area of cell patterning using
chemical or lithographic methods for the spatial control of cell adhesion and growth. In
most of these applications, anchorage dependent cells are immobilized on a two-
dimensional substrate. However, in a two-dimensional system, non-adherent cells are
difficult to immobilize and adherent cells such as fibroblasts and hepatocytes are in an
unnatural environment, i.e. in tissue they exist in a three-dimensional hydrogel matrix
consisting of other cells, proteins, and polysaccharides. As the result, the response of
these cells to drug candidates may be very different than that of the same cells in their
native tissue.

One strategy to overcome the problems associated with a two-dimensional culture
system is to encapsulate cells inside a three-dimensional hydrogel matrix. Originally cell
encapsulation technologies using hydrogels were developed for tissue engineering or
therapeutic cell transplantation to prevent rejection of the transplanted cells by the host's
immune system.[5-7] Hydrogels have been widely used because of their high water
content, softness, pliability, biocompatibility, and easily controlled mass transfer
properties, essential for allowing the transport of nutrients to and waste products from the

cells.[8, 9] In this paper, we described the fabrication using photolithography of poly (ethylene glycol) (PEG)-based hydrogel microstructures encapsulating viable mammalian cells on glass or silicon substrates, which could be combined with microfluidic system for the cell-based biosensor application.

EXPERIMENTAL DETAILS

Functionalized silicon or glass substrates were prepared as described previously.[10] Briefly, square silicon wafers with area ranging from 0.25 in^2 to 1 in^2 were placed in 'piranha' solution consisting of 3:1 ratio of 30 % w/v H_2O_2 and H_2SO_4 for 1 min. This step was followed by immersion of silicon wafers in 1mM solution of 3-(trichlorosilyl)propyl methacrylate (TPM) in a 4:1 mixture of heptane/carbon tetrachloride for 5 min., at room temperature. As result, substrate surface became functionalized with self-assembled monolayers of TPM. After functionalization, silicon wafers were washed with ethanol and D. I. water.

Murine fibroblasts were cultured in Dulbecco's modified Eagle's medium (DMEM) containing 10% fetal bovine serum and 1% antibiotic/antimycotic in a $75cm^2$ cell culture flask. Confluent fibroblasts were subcultured every 2 to 3 days by trypsinization with 0.25% (w/v) trypsin and 0.13% (w/v) EDTA. Cell culture was incubated at 37^oC in 5% CO_2 and 95% air.

Hydrogel microstructures encapsulating murine 3T3 fibroblasts were fabricated using proximity photolithography. A sterilized poly(ethylene glycol) diacrylate or PEG-DA precursor solution containing 0.5% (w/w) Darocur 1173 as a photoinitiator was mixed with a cell suspension in PBS (phosphate buffered saline) to produce a cell density about 4 to 5 x 10^6 cells/mL in the gel precursor solution. The cell-containing polymer suspension was spin-coated onto functionalized substrates at 1500 rpm for 10 seconds to form uniform fluid layer. This layer was covered with a photomask and exposed to 365 nm UV light (300 mW/cm^2) for 0.5 seconds through the photomask. Upon exposure to UV light, only exposed regions underwent free-radical induced gelation and became insoluble in common PEG solvents such as water. As a result, desired microstructures were obtained by washing away unreacted precursor solution with PBS or cell culture medium so that only the hydrogel microstructures remained on the substrate surface. During the UV light in gelation process, cells present in the polymer precursor solution were encapsulated in the resultant hydrogel microstructures. After encapsulation, surfaces with cell-containing microstructures were immersed in DMEM with 10% fetal bovine serum and incubated in a 5% CO_2 atmosphere at 37^oC for 24 hours prior to examination. As a control, cell-containing microstructures were incubated with 0.05% sodium azide in same cell culture medium. ESEM and bright field optical microscopy were used to observe pattern morphology and verify presence of cells in the hydrogel arrays.

A Live/Dead Viability/Cytotoxicity fluorescence assay was used to investigate the cell viability after encapsulation of cells in the hydrogel microstructure. This assay uses SYTO 10 and Dead Red as fluorophores to distinguish living cells and dead cells. SYTO 10 stains live cells green and Dead Red stains dead cells red. For this assay, 2 μL of two fluorophores were added to 1mL HEPES-buffered saline solution (HBSS) to make the staining solution. The staining solution was placed on the hydrogel microstructure and

incubated for 15 minutes in the dark, at room temperature. Viability of cells encapsulated in hydrogel arrays was examined with fluorescence microscope.

Microchannels in polydimethyl siloxane (PDMS) were obtained by curing 10: 1 mixture of PDMS prepolymer and curing agent against Si master which has a negative pattern of the desired microchannel defined with photoresist. After cured for 24 hr at 60°C, PDMS replica was peeled from master and oxidized in an oxygen plasma with glass slide for 1 min. Bringing the oxidized PDMS and glass slide into conformal contact resulted in irreversible seal and forms a enclosed microchannel. To make inlet and outlet port of microfluidic device, several holes were made in PDMS replica using 16-gauge needle and tubes were hooked up inside these holes.

DISCUSSION

Cell encapsulation inside the hydrogel matrices is based upon free-radical polymerization of PEG-DA, a main constituent of the precursor solution. When exposed to UV light in the presence of photoinitiator, acrylate groups form unstable active sites which react with each other, thus creating insoluble, cross-linked, three-dimensional structures. Our group combined photopolymerization through photomask with surface modification to create surface bound, hydrogel structures of various geometries on SiO_2/Si substrates. It is hypothesized that methacrylate moieties on the substrate surface also participate in the free radical polymerization and create covalent bonding between acrylate groups present in the bulk gel and those on the surface, thus fixing hydrogel structures to the substrate. Long term adhesion of cell-containing hydrogel arrays to silicon surface was verified by placing hydrogel elements into aqueous environment for over a week. Upon hydration, PEG hydrogels may expand in volume by over 100%. In the absence of covalent attachment to the substrate, the mechanical forces associated with swelling are sufficient to cause the gels to delaminate from the surface. Here, the TPM monolayer binds the gel to the surface and prevents delamination while still allowing the gel to swell with aqueous media. However, the bound gel tends swell anisotropically, i.e. the dimensions at the base of the gel do not change but rather the gel swells upward away from the surface. Here, the gels were fabricated with approximately their equilibrium water content because of the PBS added along with the cells. Thus the gels would not physically swell with additional water. However, covalent attachment of the gels to the substrate surface was still necessary as unattached gels were easily washed from the surface.

To optimize the size of the cell-containing microstructures, various spin-coating rates were tested in an effort to create thicker gels and microstructures with greater aspect ratios. As expected, the thickness of the deposited layer of precursor solution was found to be inversely proportional to the spin-rate, and thus allowed control over the height of hydrogel microstructures. Spin-rates of 4000 rpm resulted in cylindrical hydrogels of about 10 μm in height as measured by profilometry, while polymer layer spun at 1500 rpm yielded hydrogel elements about 70 μm in height as observed by environmental scanning electron microscopy (ESEM). Hence, both lateral and height dimensions of hydrogel microstructures could be controlled, the latter by feature size of the photomask (to a minimum size of 7 μm)and the former by the spin-coating rate. By using masks

with different feature sizes and using different spin-coating rates, we were able to create cell-containing microstructures with aspect ratios ranging from 0.12 to 1.4.

Figure 1 (a) shows the optical bright-field micrographs of an array of 600 μm diameter hydrogel microstructures containing mouse 3T3 fibroblasts. The cells were completely encapsulated within the microstructures with no cells or cell processes evident outside the gel. The transparent nature of PEG-based hydrogel allowed us to observe cells in the hydrogel structure through optical microscopy and approximately an equal number of cells (30 per microstructure) were observed in each of the several hydrogel elements. Even though the image resolution of proximity lithography is larger than that of contact lithography, we were able to obtain high-quality hydrogel microstructures of 50 μm diameter as shown Figure 1 (b). These cylindrical microstructures were of an obviously three-dimensional nature and were arranged in a 20×20 square with 50 μm spacing between elements so that as many as 400 microstructures could be reproducibly fabricated in a 2 mm^2. As is apparent from Figure 1 (b) the fact that these microstructures contain cells is not readily evident by electron microscopy because the cells are completely encapsulated within the gel.


(a)   (b)
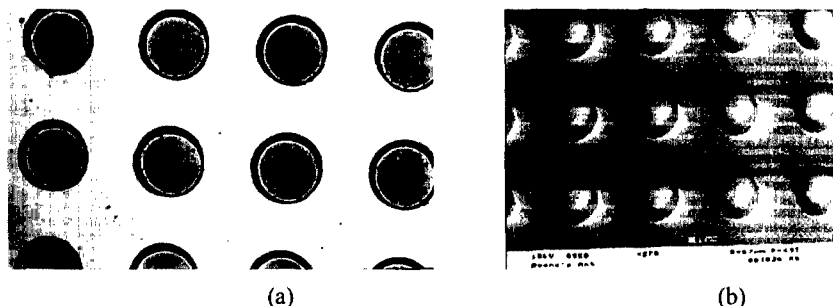
Figure 1. Hydrogel microstructures on the glass substrate: (a) optical bright-field micrograph of 600 μm diameter hydrogel microstructures encapsulating 3T3 fibroblasts; (b) ESEM micrograph of 50 μm diameter hydrogel microstructures

Cells must survive and maintain their normal function after encapsulation. We investigated the viability of cells encapsulated in the circle hydrogel arrays with diameters of 600 μm and 50 μm using a LIVE/DEAD viability assay. As was evident by the green emitted light, encapsulated cells were viable in both arrays. While 600 μm hydrogel microstructures contained numerous cells, 50 μm diameter microstructures had only 1 to 3 cells encapsulated per structure, with some microstructures absent of cells. Cell viability was influenced by photopolymerization condition such as concentration of photoinitiator and intensity and exposure time of UV light. The viability of cells encapsulated in hydrogel was also measured using an MTT (3-(4,5-dimethylthiazol-2-yl)-2,5-diphenyl tetrazolium bromide) assay. In this assay, viable cells generated purple formazan crystals and confirmed that cells within the microstructures were viable.

Based on previous results, we prepared cell-containing hydrogel microstructures inside PDMS microfluidic channels. Recently, PDMS has been widely used as a material for the microfluidic system, because it is less expensive and less fragile than glass or Si/SiO₂. Furthermore, being based on replication, fabrication processes in PDMS are much faster and more convenient than those in glass or Si/SiO₂.

In our experiment, we first fabricated hydrogel microstructure inside an approximately 100 μm wide, 50 μm deep PDMS microchannel. Microchannel was filled with hydrogel precursor solution and then exposed to UV light through a photomask. Only exposed regions underwent photopolymerization and gelled inside the microchannel. Finally, by flushing the channel with PBS, we obtained the desired hydrogel microstructure inside a microfluidic channel as shown in Figure 2(a). To obtain cell-containing hydrogel microstructure inside microchannel, cell suspension in PBS was added to polymer precursor solution and this solution was injected to the microchannel. Figure 2(b) shows the cell-containing hydrogel microstructures inside a microfluidic channel fabricated by same procedure.

(a)   (b)
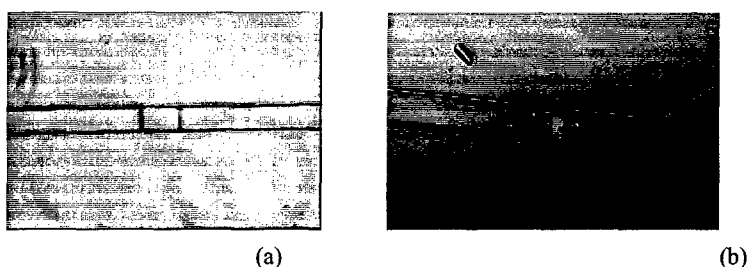
Figure 2. Hydrogel microstructure fabricated in PDMS microchannel: (a) hydrogel microstructure without encapsulated cells; (b) cell-containing hydrogel microstructure inside microchannel.

CONCLUSIONS

In conclusion, we presented an easy and effective method for encapsulation of cells inside PEG-based hydrogel microstructures form using photolithography. High-density arrays of three-dimensional microstructures have been fabricated on substrates using this method. Cells were encapsulated in cylindrical hydrogel microstructures of 600 and 50 μm in diameter. Reducing lateral dimension of the individual hydrogel microstructure to 50 μm allowed us to isolate 1 to 3 cells per microstructure. Viability assays demonstrated that cells remained viable inside these hydrogels after encapsulation. While more thorough investigation of the optimal conditions for sustaining cell survival inside the hydrogel microstructures is needed, our preliminary results are very encouraging. Future work will be focused on further investigation of cell viability and function with these gels and the formulation of gel chemistries designed to improve cell function, perhaps through the inclusion of cell adhesion molecules in the gel formulation.

In addition, the microstructures presented here could be combined with a microfluidic device to create optical biosensor arrays of individually addressable single or multiple cell-containing hydrogel microstructures with potential applications in drug screening or pathogen detection.

ACKNOWLEDGEMENTS

REFERENCES

1. Kane, R.S., S. Takayama, E. Ostuni, D.E. Ingber, and G.M. Whitesides, *Patterning proteins and cells using soft lithography.* Biomaterials, 1999. **20**: p. 2363-2376.
2. Singhvi, R., A. Kumar, G. Lopez, G. Stephanopoulos, D. Wang, G. Whitesides, and D. Ingber, *Engineering Cell Shape and Function.* Science, 1994. **264**: p. 696-698.
3. Takayama, S., J. McDonald, E. Ostuni, M. Liang, P. Kenis, R. Ismagilov, and G. Whitesides, *Patterning cells and their environments using multiple laminar fluid flows in capillary networks.* Proc. Natl. Acad. Sci. USA, 1999. **96**: p. 5545-5548.
4. Xia, Y. and G. Whitesides, *Soft Lithography.* Angew. Chem. Intl. Ed., 1998. **37**: p. 550-575.
5. Cruise, G.M., O.D. Hegre, F.V. Lamberti, S.R. Hager, R. Hill, D.S. Scharp, and J.A. Hubbell, *In vitro and in vivo performance of porcine islets encapsulated in interfacially photopolymerized poly(ethylene glycol) diacrylate membranes.* Cell Transplantation, 1999. **8**: p. 293-306.
6. Hern, D. and J. Hubbell, *Incorporation of adhesion peptides into nonadhesive hydrogels useful for tissue resurfacing.* J. Biomed. Mater. Res., 1998. **39**: p. 266-276.
7. Pathak, C.P., A.S. Sawhney, and J.A. Hubbell, *Rapid photopolymerization of immunoprotective gels in contact with cells and tissue.* Journal of the American Chemical Society, 1992. **114**: p. 8311-8312.
8. Mellott, M., A. Axel, K. Shields, and M. Pishko, *Release of protein from highly cross-linked hydrogels of poly(ethylene glycol) diacrylate fabricated by UV polymerization.* Biomaterials, 2001. **22**: p. 929-941.
9. Russell, R., A. Axel, K. Shields, and M. Pishko, *Mass Transfer in Rapidly Photopolymerized Poly(ethylene glycol) Hydrogels Used for Chemical Sensing.* Polymer, 2001. **42**: p. 4893-4901.
10. Revzin, A.R., R.; Yadavalli, V.; Koh, W.; Deister, C.; Hile, D.; Mellott, M.; Pishko, M., *Fabrication of Poly(ethylene glycol) Hydrogel Microstructures Using Photolithography.* Langmuir, 2001. **17**: p. 5440-5447.

Signal Generation from Switchable Polydiacetylene Fluorescence

Mary A. Reppy
Analytical Biological Services Inc.
Wilmington, DE 19801, U.S.A.

ABSTRACT

Chemical and biological sensors require a material component to act as a transducer from the molecular level event of interest to a discernable output measurable in the macroscopic world. One such material is polydiacetylene (PDA), a conjugated polymer that can switch from a non-emitting to a fluorescent state in response to environmental changes. This attribute can be harnessed to provide signal generation for bio-sensors and assays as a more sensitive alternative to the previously reported monitoring of PDA colorimetric shifts. While providing a more sensitive transduction mechanism the fluorescence behavior of PDA is also more complicated than the absorbance, in particular the emission profile of PDA in liposomes is strongly affected by the extent of polymerization. Incorporating small molecule fluorophores into the PDA materials further increases the overall emission of fluorescent PDA materials. The fluorophores accept energy from the excited state of the polymer and fluoresce, leading to both an overall increase in the quantum yield of the system and an increase in the Stokes shift. Basic photophysical properties of fatty acid PDA liposomes and a model assay for phospholipase A_2 are presented. The model assay results show that the fluorescence response is greater than the colorimetric, and is further enhanced by addition of fluorophores.

INTRODUCTION

Liposomes containing polydiacetylene (PDA) can be used for colorimetric bio-assays in an approach that exploits the changeable absorbance properties of the conjugated polymer backbone of PDA and also takes advantage of the biomimetic aspect of surfactant liposomes. The liposomes are formed from diacetylene surfactants and the diacetylene tails are photopolymerized to form PDA in the alkyl regions of the liposomes. Changes in the conjugation state of the double and triple bonds of the PDA backbone due to external perturbations lead to shifts in the absorption maxima, typically causing a color change from blue to red. Charych et al photopolymerized diacetylene fatty acid liposomes with ligands or enzymatic substrates incorporated, to form PDA liposomes [1]. Exposure of the liposomes to solutions of a target analyte caused a gradual change in the color from blue to purple or red. Charych used PDA liposomes and films with sugars, gangliosides and phosphotidylcholines incorporated as colorimetric sensors for influenza virus [2], cholera toxin [3], and phospholipases [4]. Subsequently, other researchers have developed similar colorimetric assays using PDA liposomes and films [5]. For all these colorimetric assays the liposomes or films were prepared in the blue state and upon interaction with the analyte turned red. The change in the absorption properties is quantified by calculation of the "colorimetric ratio" (CR); the ratio of the intensity of the "blue" maximum absorbance peak (650nm) over the sum of the intensities of the "blue" and "red" (550 or 490nm) absorbance peaks.

The work presented here uses the changeable fluorescence of PDA rather than the colorimetric properties for signal transduction [6]. The emissive properties of PDA are also

dependent on the conjugation length of the backbone; PDA assemblies with long conjugation lengths (i.e. blue PDA) are non-fluorescent. If the conjugation lengths are shortened (i.e. red or yellow PDA) the materials become fluorescent. The fluorescence of red PDA and the non-fluorescence of blue PDA is well established and has been noted in liposomes [7], however, the ability of PDA to change from non-fluorescent to fluorescent has not been previously exploited for sensing or assay development purposes to any significant extent. A model assay based on the colorimetric assay for phospholipase A$_2$ (PLA$_2$) developed by Charych et al [4] was run for the purpose of comparing the colorimetric response to the fluorescence response.

EXPERIMENTAL DETAILS

10,12-pentacosadiynoic acid (PCDA) and 10,12-tricosadiynoic acid (TRCDA) were purchased from GFS and recrystallized once from hexane. Dimyristoyl phopsphotidylcholine (DMPC) and phospholipase A$_2$ (PLA$_2$) were from Sigma; buffer salts and solvents were from Fisher. Organic fluorophores, 5-(((4-(4,4-difluoro-5-(2-thienyl)-4-bora-31,41-diaza-s-indacene-3-yl)phenoxy)acetyl)amino)pentylamine hydrochloride (1) and 1,1'-dioctadecyl-3,3,3',3'-tetramethylindodicarbocyanine 4-chlorobenzenesulfonate salt (2), **Figure 1**, were obtained from Molecular Probes and incorporated at a ratio of 1 fluorophore:200 surfactants. H$_2$O was purified by ultra-filtration through a Millipore Milli-Q Plus system and dispensed with a resistance of 18.2 MΩcm. Photopolymerization was performed in a Fisherbrand cross-linking oven capable of delivering controlled energy doses of UV light at 254nm.
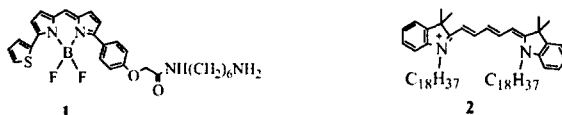
Figure 1. Fluorophores **1** and **2**

Polymerization and Emission

TRCDA liposomes and TRCDA liposomes with fluorophores **1** and **2** were prepared by sonication of surfactants in water, chilled (10 °C) and polymerized with 200mJ/cm^2 of irradiation to give deep blue solutions [6]. PCDA liposomes with and without fluorophores **1** and **2** were prepared and individual 100μL portions were polymerized with increasing doses of UV at 254nm, also giving blue solutions. The polymerized liposome solutions were then diluted 1:9 with water and heated at 70 °C for 15m; the heating step converts the PDA irreversibly to the red fluorescent form [1]. The emission and absorbance spectra of the heated liposomes were collected and the ratios of the intensities of the fluorophore fluorescence peaks (630nm for **1** and 665nm for **2**) to the PDA fluorescence peak at 560nm were calculated.

Phospholipase A$_2$ Assay [4]

Liposomes were prepared from a mixture of 10,12-tricosadiynoic acid (TRCDA) and dimyristoyl phosphatidylcholine (DMPC) in a 7:2 molar ratio with and without fluorophore **1**. The liposomes were polymerized with 200mJ/cm^2 of UV energy at 254nm forming blue solutions. Phospholipase A$_2$ (PLA$_2$) was dissolved in water at 1.0mg/mL. A mixed buffer solution was

prepared of TRIS (50mM) and NaCl (150mM) at pH 7.7 and combined with the PLA_2 solution at 9 parts buffer to 1 part PLA_2 solution. This solution was added to the liposome solution, diluting it to 0.091mM in liposomes. A control sample (CTRL) was prepared using 9 parts mixed buffer to 1 part H_2O in lieu of the PLA_2 solution. The fluorescence of the samples was read at intervals over 30m. Photobleaching of the liposomes during the assay was not observed. An equivalent assay was run with the absorbance at 650nm and 550nm measured. The colorimetric ratio (CR) was calculated at each time point and the percentage changes from the initial values of the CR and of the emission were also calculated. It should be noted that **1** has negligible absorbance at both 650nm and 550nm.

RESULTS AND DISCUSSION

Both fluorescent poly(PCDA) and poly(TRCDA) liposomes have two emission maxima, however, the relative intensities are different as can be seen in **Figure 2**. It was hypothesized that relative intensities are dependent upon the extent of polymerization of the diacetylene in the liposomes, with the peak at 550nm dominating when the PDA chains are few and relatively isolated and the 625nm peak increasing as the amount of polymer increases. TRCDA liposomes are more readily polymerized than PCDA liposomes and hence have a higher density of polymer chains. After a UV dose of $200mJ/cm^2$ the heated poly(TRCDA) liposomes have an absorbance at 550nm of 0.35 while the heated poly(PCDA) liposome absorbance is only 0.06. Changes in emission profile with inter-chain distance and/or extent of polymerization are precedented in other fluorescent polymer systems [8].
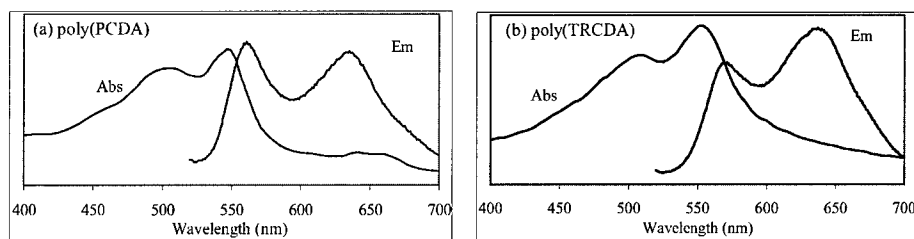
Figure 2. Absorbance (Abs) and emission (Em) spectra (arbitrary units) for (a) poly(PCDA) liposomes (heated) and (b) poly(TRCDA) liposomes (heated).

A study was performed to examine the effect of UV dose (and hence polymerization extent) on the emission profile of poly(PCDA) liposomes. After exposure to low UV doses, with the PDA chains surrounded by monomeric diacetylenes, the first emission peak of the liposomes (560nm) dominated; as the overall extent of polymerization increased the second emission peak (620nm) grew in. The absorbance spectra of the fluorescent liposomes also had two peaks at 550nm and 500nm, however, the relative intensities remained similar even as the overall absorbance increased with further polymerization (**Figure 3**). The differing effects of increased polymerization on the profiles of the absorption and emission spectra suggested that the increase in the 625nm PDA emission peak with higher UV doses did not simply arise from an increase of PDA chains with a specific conjugation length leading to the 625 emission peak, but from interactions of multiple PDA chains. This is consistent with earlier studies performed on PDA

chains in solution: fully solubilized PDA had only one emission peak while aggregated or colloidal PDA showed two emission peaks [9].
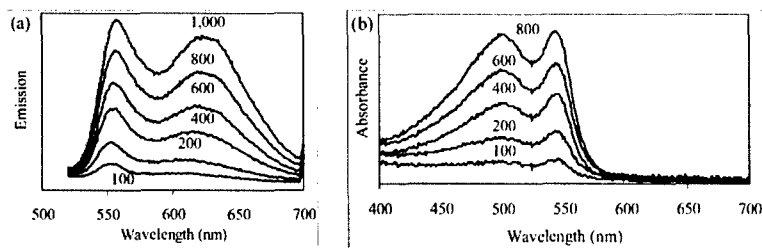

Figure 3. (a) Emission (Em.) and (b) absorbance spectra for fluorescent poly(PCDA) liposomes, (arbitrary units) at UV irradiation doses of 100, 200, 400, 600, 800 and 1000 (Em. only) mJ/cm^2.

Fluorescent polymers often have low quantum yields because the conjugated chains can act as excited state traps and provide mechanisms for non-radiative relaxation of the excited state, leading to quenching of the fluorescence [10]. Lipophilic fluorophores 1 and 2 were incorporated in the liposomes. The excitation spectra of these fluorophores overlapped with the emission spectrum of fluorescent PDA. When the liposomes, in the fluorescent state, were exposed to a wavelength that excited **only** the PDA the majority of the emission occurred at the fluorophore's emission wavelength and the overall emission was much higher than for equivalent PDA liposomes without the fluorophores (**Figure 4**). The overall rise in the emission suggested that the energy transfer from the PDA to the fluorophores competed with non-radiative decay of the PDA excited state. It should be noted that for liposomes with 1 the fluorophore emission and the 625nm emission peak of PDA overlapped, however, the fluorophore emission was much greater than the PDA emission (**Figure 4a**). The addition of the fluorophores to the PDA liposomes did not make the liposomes fluorescent when the PDA chains were in the non-fluorescent, blue, state. The emission profile of the fluorescent PDA liposomes affected whether the PDA could transfer energy to incorporated fluorophores. Poly(PCDA) underwent energy transfer with several fluorophores including both 1 and 2, while poly(TRCDA) liposomes underwent effective energy transfer only with 1. A second practical benefit from incorporating fluorophores in the PDA liposomes was that monitoring the emission of the system at the fluorophores' maximum emission during assays increased the effective Stokes shift of the system. Increase of the Stokes shift reduced the background fluorescence caused by reflection and scatter of the excitation light.

It was noted in early experiments that the extent of energy transfer seemed to decrease when larger UV doses were used for polymerization of the liposomes. This prompted a study on the effect of polymerization energy on energy transfer efficiency with PCDA liposomes incorporating 1 and 2. As seen in **Figure 4(b)**, at first the fluorophore emission increased relative to the PDA emission 560nm as the diacetylene/fluorophore liposomes were exposed to increasing doses of UV. Above a UV dose of 20-30mJ/cm^2, however, the fluorophore emission decreased relative to the emission of the PDA. This suggested that as the population of PDA chains in the liposomes increased inter-chain interactions competed with energy transfer to the fluorophores. When preparing PDA/fluorophore liposomes for use in assays a balance needed to be struck between increasing the extent of polymerization to improve the stability of the

liposomes and keeping the extent of polymerization low to optimize the energy transfer to the incorporated fluorophore.
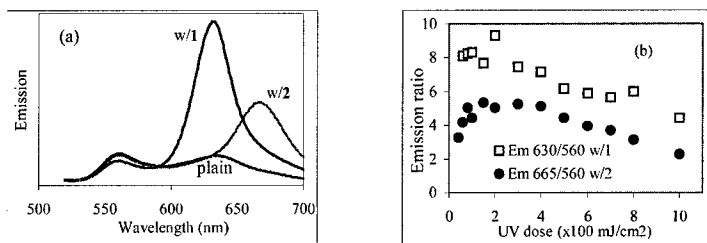
Figure 4. (a) Emission spectra of fluorescent poly(PCDA) liposomes, plain and with **1** and **2**. (b) Ratios of **1** and **2** emission (Em) (630nm and 665nm respectively) to PDA emission at 560nm vs. UV dose.

Example Assay

The same general PDA liposome formulations that have been used for colorimetric bio-sensing can also be used for fluorescence based sensing [1]. An assay for PLA_2 activity based on a literature assay [4] using poly(TRCDA)/DMPC liposomes and poly(TRCDA)/DMPC liposomes with **1** incorporated was run and monitored by emission and absorbance. The incorporation of **1** for signal enhancement did not appear to appreciably affect the stability of the liposomes. The assay results, presented as absolute percent change from the initial values of the emission and the CR, are shown in **Figure 5**. It can be seen that the overall changes in the emission were greater than the changes of the CR and that the distinction between the PLA_2 sample and the control sample was also greater. Addition of **1** also increased the change in the emission, while not significantly affecting the CR. Comparison of the slopes of the PLA_2 data and the control data indicated that the majority of the PLA_2 activity occurred within the first 10m of the assay and the changes thereafter were from the action of the buffer on the liposomes. The trend and the extent of the change in CR were consistent with the results previously obtained by Charych et al. Assays run with poly(PCDA)/DMPC liposomes gave similar results although the percent changes in emission and CR are both lower. Subsequent work on other assays has shown that changing to a lower ionic strength buffer and using a different buffer salt can reduce the background activity of the control sample.
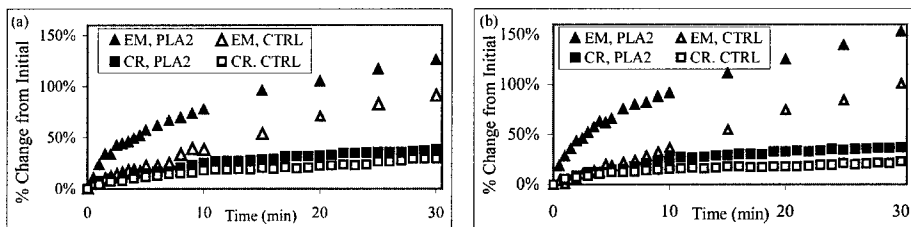
Figure 5. Percent change relative to initial values of emission (Em) and CR values of PLA_2 samples and buffer control samples versus time for the PLA_2 assay with (a) poly(TRCDA)/DMPC liposomes, and (b) poly(TRCDA)/DMPC liposomes with **1**.

Conclusions

The conversion of polydiacetylene (PDA) in liposomes from non-fluorescent to fluorescent can be exploited for signal generation in bio-assays. The changes in the emissive and absorbance properties of the PDA liposomes arise from changes in the conjugation length of the PDA backbone π bonds, however, the emissive behavior is more complex and appears to be affected by interactions between polymer chains. The emission of fluorescent PDA liposomes can be enhanced by addition of fluorophores that participate in energy transfer from the excited PDA to the fluorophore. A comparison of equivalent emission and absorbance assays for PLA_2 with polymerized diacetylene fatty acid/DMPC liposomes showed that the change in emission of the liposomes during the assay was greater than the change in absorbance. Using liposomes with a fluorophore incorporated in the assay further increased the change in emission in response to PLA_2. The results from these model assays suggest that fluorescent assays with PDA liposomes may allow detection of analytes at lower levels than the previously described colorimetric assays.

ACKNOWLEDGMENTS

REFERENCES

1. Okada S., Peng S., Spevak W., Charych D. *Acc. Chem. Res.* **1998**, *31*, 229-239.
2. Spevak W., Nagy J. Charych D. *Adv. Mater.* **1995**, *7(1)*, 85-89.
3. Pan J., Charych D. *Langmuir* **1997**, *13*, 1365-1367.
4. Okada S., Jelinek R., Charych D. *Angew. Chem. Int. Ed Eng.* **1998**, *38*, 655-659.
5. (a) Cheng Q. and Stevens R. C., *Adv. Mater.* **1997** *9(6)*, 481-483. (b) Ma Z., Li J., Liu M. Cao J., Zou Z., Tu J., Jiang L. *J. Am. Chem. Soc.* **1998**, *120*, 12678-12679. (c) Kolusheva S., Shahal T., Jelinek R. *J. Am. Chem. Soc.* **2000**, *122*, 776-780. (d) Kolusheva S., Boyer L., Jelinek R. *Nat. Biotechnol.* **2000**, *18*, 225-227. (e) Kolusheva S., Kafri R., Marina K., Jelinek R. *J. Am. Chem. Soc.* **2001**, *123*, 417-422.
6. Reppy M. A., Sporn S. A., Saller C. F., "Method for detecting an Analyte by Fluorescence", PCT International Patent WO/00171317 (March 20, 2001).
7. Singh A., Thompson R.B., Schnur J.M. *J. Am. Chem. Soc.* **1986**, *108*, 2785-2787.
8 . (a) Bazan G. C., Miao Y-J; Renak M. L., Sun B. J. *J. Am. Chem. Soc.* **1996**, *118*, 2618-2624. (b) McQuade D. T., Kim J., Swager T. M. *J. Am. Chem. Soc.* **2000**, *122*, 5885-5886.
9 . (a) Bloor D., Batchelder D.N., Ando D. J. *J. Polym. Sci.* **1981**, *19*, 321-334. (b) Kotaka T., Ohnuma H. *Chem. Phys. Lett.* **1985**, *114*, 446-450. (c) Rumbles G., Brown A. J., Phillips D., Bloor D. *J. Chem. Soc. Faraday Trans.* **1992**, *88(22)*, 3313-3318.
10. Barashkov N.N.; Gunder O.A. *Fluorescent Polymers*; Ellis Horwood: New York, 1994; Chapter 1.

Sensing With Silicon

Photochemical Enzyme Co-Factor Regeneration: Towards Continuous Glutamate Monitoring with a Sol-Gel Optical Biosensor

Jenna L. Rickus[1], Allan J. Tobin[2], Jeffrey I. Zink[3], Bruce Dunn[4]

[1]Neuroscience IDP, Neuroengineering Program
[2]Brain Research Institute
[3]Department of Chemistry and Biochemistry
[4]Department of Materials Science and Engineering

ABSTRACT

Sol-gel encapsulation has recently surfaced as a successful approach to biomolecule immobilization. Proteins, including enzymes, are trapped in the pores of the sol-gel derived glass while retaining their spectroscopic properties and biological activity. Our current work extends the unique capabilities of biomolecule-doped sol-gel materials to the detection of glutamate, the major excitatory neurotransmitter in the central nervous system. We are developing an *in vivo* fiber optic biosensor for glutamate along with methods to achieve continuous monitoring. In our research to date we have encapsulated GDH in a silica sol-gel film on the tip of an optical fiber. GDH catalyzes the oxidative deamination of glutamate to α-ketoglutarate and the simultaneous reduction of NAD^+ to NADH. To quantify the glutamate concentration, we observe the rate of change of NADH fluorescence as a function of time. An important consideration for continuous *in vivo* monitoring is the incorporation of a self-sustaining NAD^+ source. We have adopted a photochemical means of regenerating NAD^+ from NADH, by irradiating thionine (3,7-diaminophenothiazin-5-ium) which we incorporate into the sol-gel sensor material. When excited with visible light ($\lambda_{abs} \sim 596$ nm), thionine undergoes a reaction with NADH resulting in a non-fluorescent form of thionine and NAD^+. We have characterized the kinetics of this reaction in the sol-gel matrix, and have shown that the reaction results in regenerated co-factor that is usable by GDH for the oxidation of glutamate.

INTRODUCTION

Glutamate is the most prominent excitatory neurotransmitter in the central nervous system. It is present throughout the entire brain, but acts locally to produce different types of signals that vary in their spatial and temporal characteristics. Glutamate signaling is an important component of networks involved in attention, learning and memory, and motor control. Current detection techniques are limited in their ability to achieve the required resolution to observe these signals. New types of sensors are needed; optical sol-gel sensors could help to fill the gap.

Enzymes are commonly employed in biosensors because they provide both biochemical recognition and transduction of the recognition event into a reaction. Redox enzymes in particular are convenient because the electron transfer provides a measurable current or a measurable change in the spectroscopic properties of the substrate or co-factor. Dehydrogenases are the largest class of redox enzymes, but their requirement of an enzyme co-factor has hindered their use in continuous sensors [1,4,10]. Because the co-factor serves as an electron acceptor or donor, a replenishing source of co-factor is required.

In our studies, we use the enzyme glutamate dehydrogenase (GDH) to detect and measure glutamate. GDH catalyses the oxidative deamination of glutamate to form α-ketoglutarate. NAD^+ is an obligatory co-factor and serves as the electron acceptor in the reaction. The resulting reduced co-factor, NADH, fluoresces when excited with UV light. The NADH fluorescence as a function of time provides an optical output that is directly related to the glutamate concentration [6].

To create the sensor material, the GDH is encapsulated in a silica sol-gel glass. The silica forms a porous three-dimensional matrix around the enzyme, providing immobilization without covalent attachment [2,5]. The enzyme-doped material is transparent in the UV and visible spectrum making it ideal for spectroscopic measurements. With this method of encapsulation, we see no measurable leaching of enzyme from the gel and the enzyme maintains its activity for many weeks [6].

To create the sensor, GDH doped sol-gel glass is coated onto the tip of an optical fiber. In this form, the sensor functions as a dosimeter, making individual measurements in a sample well that also contains the required co-factor NAD^+. To transform this dosimeter into a continuous sensor, a method of regenerating NAD^+ from NADH is required.

One means of achieving co-factor regeneration is through photochemical reactions. When excited with visible light, the organic dye thionine undergoes a reaction with NADH resulting in relaxed thionine and NAD^+ [7,8]. Because it is the excited form of thionine that reacts with NADH, NAD^+ regeneration only occurs when the sample is irradiated with visible light. By combining enzymatic reactions with thionine excitation, it should be possible to control the regeneration reaction for continuous sensor function.

In this paper, we determine if NADH can be photochemically converted to NAD^+ for use in the oxidative deamination of glutamate by GDH. The effect of thionine concentration on NADH conversion rate is explored. In addition we determine if NADPH can undergo a similar reaction. Finally we observe the effects of sol-gel encapsulation on the rate of NADH conversion.

EXPERIMENTAL

Materials Synthesis

Tetramethoxysilane (TMOS) and thionine acetate were purchased from Fluka. NADH, NAD^+, glutamate dehydrogenase, and glutamate were purchased from Sigma. All materials were used as purchased. All solutions were made with phosphate buffer (0.02 M pH 7.0, 0.02 M NaCl).

Photochemical Regeneration of NAD^+ from NADH

NADH conversion rates in solution were determined by following the NADH fluorescence over time in samples exposed to different concentrations of excited thionine. Thionine was dissolved in phosphate buffer and sonicated for 15 minutes to form a stock solution of 100 μM. The thionine solution was diluted with phosphate buffer and added to 8 wells of a 96 well plate (NUNC N-167008) at varying concentrations. Fluorescence measurements were taken with a Labsystems Fluoroskan Ascent microplate reader. Background fluorescence at 355nm excitation and 460nm emission was taken for 20 counts with a 100 ms integration time. NADH was then injected in the well and an initial NADH fluorescence baseline was measured (40 counts, 100 ms integration time, 355nm excitation, 460 nm

emission). Thionine excited at 584nm and the NADH fluorescence was periodically measured over time. The thionine concentrations after NADH injection were 1μM, 10μM, 20μM, and 50μM each in duplicate. The initial NADH concentration in each well was 100 μM.
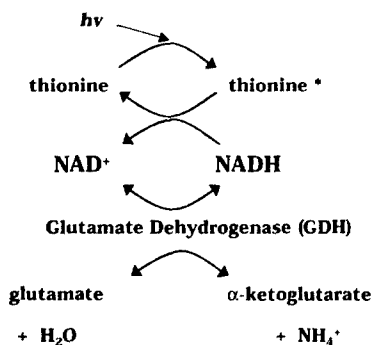
To confirm that NAD^+ was produced in the reaction of NADH with excited thionine, we determined if the reaction product could serve as a co-factor in the GDH reaction. GDH (8.8 mg/mL) and NADH (3 mM) solutions were combined in the wells of a 96 well plate (NUNC N-167008) either with or without the addition of thionine (50 μM). Each sample was excited with visible light at 584nm for 3 minutes. Then glutamate (500 μM) was injected into each well and the NADH fluorescence (1000counts, 100 ms integration time, 355nm excitation, 460 emission) was measured for 3 minutes.

Photochemical Regeneration of $NADP^+$ from NADPH in solution and in sol-gel monoliths

TMOS was hydrolyzed under acidic conditions (1.2% by volume 0.04N HCl) and a 1:2 TMOS:water molar ratio. The solution of TMOS, water, and acid was sonicated for 15 minutes. The resulting sol was filtered using 0.2μm HT Tuffryn membrane. NADPH gels were produced by combining 60μL NADPH solution of varying concentration with 40μL hydrolyzed TMOS sol in the well of a microplate. Solution samples were prepared by combining 60μL NADPH solution of varying concentration with 40 μL phosphate buffer. Gel and solution samples with final NADPH concentrations of 33 μM, 66 μM, and 100 μM were produced in triplicate. The samples were aged for 1 hour at room temperature with 20μL of phosphate buffer to prevent drying of the gels. Samples were analyzed using a Fluorskan Ascent microplate fluorometer. At time zero, 20 μL of 60 μM thionine were injected into each sample. Thionine was excited at 584 nm over five intervals of 200 seconds. Thionine fluorescence emission at 620 nm (integration time 100 ms) was collected during these intervals as well. NADPH fluorescence was measured at 460 nm (excitation 355nm, 20 ms integration time, 5 measurements) before and after each thionine excitation interval.

RESULTS AND DISCUSSION

The goal of these experiments was to demonstrate that excited thionine can be used in the sol-gel environment to convert NADH to the oxidized form, NAD^+, that is required for the GDH reaction. It was previously demonstrated that excited thionine reacts with NADH to form NAD^+ and relaxed thionine in solution [7,8]. Our objective is to couple this reaction to the GDH reaction, as illustrated in figure 1, within the sol-gel matrix. In addition, we want to characterize the kinetics of the thionine reaction, so that we can properly design and control the regeneration rate in the functioning fiber optic sensor.

hv

thionine → thionine *

NAD^+ → NADH

Glutamate Dehydrogenase (GDH)

glutamate → α-ketoglutarate

+ H_2O → + NH_4^+

Figure 1: Reaction scheme of NAD^+ regeneration coupled to the GDH reaction. NADH is produced during the oxidation of glutamate. This NADH reacts with excited thionine, thionine*, to form ground state thionine and NAD^+. The regenerated NAD^+ can then serve as the electron acceptor in another round of glutamate oxidation.

Excited thionine reacts with NADH to produce NAD^+ for participation in the GDH reaction.

First, we demonstrate that NADH can be regenerated through a reaction with excited thionine to a form that can be used by GDH. In this experiment samples of GDH and NADH with and without thionine were exposed to light at 584 nm. After exposure, glutamate was injected to each sample well and the NADH fluorescence was measured over time. Figure 2 shows the fluorescence change due to NADH production from the GDH reaction over time.
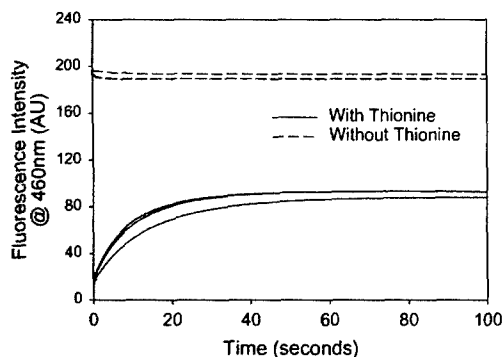
Figure 2: After reaction with excited thionine, NADH is regenerated to a form that is usable by glutamate dehydrogenase. The GDH reaction is measured by the observing NADH fluorescence as a function of time in samples containing GDH and NADH. The samples have been exposed to light in the presence (solid lines) or absence thionine (dashed lines) prior to glutamate injection at t=0. No NADH production is seen in samples without thionine. Samples that did contain thionine show an NADH production due to the enzyme reaction.

158

Glutamate was injected at t = 0. The samples without thionine show constant NADH fluorescence, corresponding to the concentration of NADH that was initially added to the well. No NAD^+ is present in these sample, so we see no enzymatic NADH production after glutamate is added. Samples containing thionine, however, show a reduced fluorescence at t=0, indicating that the NADH was consumed during the light exposure period. After addition of glutamate to these samples, there is an increase in NADH fluorescence from the GDH reaction. Because NAD^+ is required for the GDH reaction, this observance of GDH activity indicates that NAD^+ was present at t = 0. Since no NAD^+ was added to the well, the initial NADH must have been converted to NAD^+ during the light exposure period. This is consistent with previous findings [9].

This experiment demonstrates that the photochemical oxidation of NADH can be coupled to the GDH reaction for co-factor regeneration purposes. While this experiment was conducted in solution, experience has shown that photochemical reactions that occur in solution also occur in the wet gel [3].

The conversion rate of NADH to NAD^+ is controlled by thionine concentration.

Next we set out to better understand the kinetics of the reaction between thionine and NADH. Samples of NADH in phosphate buffer were exposed to varying concentrations of thionine ranging from 1μM to 50 μM. The thionine was excited at 584 nm and NADH fluorescence measurements were taken periodically to follow the reaction of NADH with excited thionine over time. As seen in figure 3A, the NADH fluorescence disappeared faster in high thionine concentrations. The initial slope of each curve was fit to a line enabling one to determine the initial rate of NADH conversion. Figure 3B shows the initial NADH conversion rate as a function of thionine concentration.
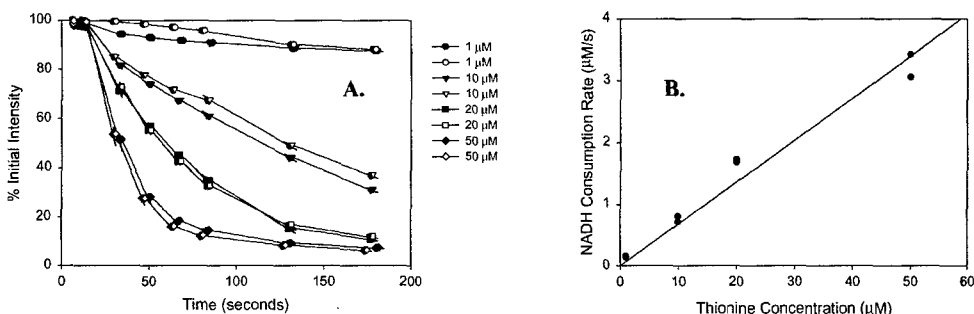
Figure 3: A. NADH fluorescence intensity is measured over time during exposure to excited thionine at varying concentrations. **B.** The initial rate of NADH consumption is a linear function of thionine concentration.

Excited thionine oxidizes NADPH in solution and in the sol-gel environment.

Some dehydrogenases preferentially use NADPH rather than NADH as a co-factor. To determine if thionine reacts with NADPH as well as NADH and to understand the affects of sol-gel encapsulation on the reaction kinetics, we compared the reaction rates of NADPH with thionine in solution with the reaction rates in sol-gel monoliths. Encapsulation did not affect the fluorescence emission spectra of the thionine when excited at 584nm (data not shown). When the samples were exposed to light at 584nm, NADPH conversion was observed in both solution and in the sol-gel. The loss of NADPH fluorescence was similar to the NADH decay in figure 3 and could be fit with a single exponential decay (data not shown). As seen in table I the NADPH decay rate constant, k_{NADPH}, was reduced by a factor of 10 in the sol-gel compared with the solution.

Table I: A comparison of NADH conversion rates in solution and in the sol-gel.

	solution	sol-gel
k_{NADPH}	9.4 ($\pm$3.3) x 10^{-3} s^{-1}	8.0 ($\pm$0.9) x10^{-4} s^{-1}

CONCLUSIONS

We have presented a photochemical method of NAD^+ regeneration by reaction of NADH with excited thionine. Excited thionine reacts with NADH to form NAD^+ that can be used by glutamate dehydrogenase for oxidation of glutamate. The rate of NADH conversion to NAD^+ can be controlled by the thionine concentration. A similar reaction occurs between NADPH and excited thionine in solution and in the sol-gel environment. The reaction rate in bulk sol-gel is about 1 order of magnitude slower than in solution.

ACKNOWLEDGMENTS

REFERENCES

[1] Alvarez, N.S., Ortea, P.M., Paneda, A.M., Castanon, M.J.L., Ordieres, A.J.M. and Blanco, P.T., *Journal of Electroanalytical Chemistry*, 502 (2001) 109-117.
[2] Dave, B.C., Dunn, B., Valentine, J.S. and Zink, J.I., *Analytical Chemistry*, 66 (1994) 1120A-1127A.
[3] Dunn, B. and Zink, J.I., *Chemistry of Materials*, 9 (1997) 2280-2291.
[4] Pereira, A.C., Fertonani, F.L., Neto, G.d.O., Kubota, L.T. and Yamanaka, H., *Talanta*, 53 (2001) 801-806.
[5] Rickus, J.L., Dunn, B. and Zink, J.I., Optically Based Sol-Gel Biosensor Materials. In F. Ligler and C.R. Taitt (Eds.), *Optical Biosensors: Present and Future*, Elsevier, in press.
[6] Rickus, J.L., Lan, E., Tobin, A.J., Zink, J.I. and Dunn, B., *Materials Research Society Fall Meeting, Vol. 662*, Materials Research Society, Boston Massachusetts, 2000.
[7] Sharma, A., *Spectrochimica Acta*, 48 (1992) 647-651.
[8] Sharma, A., *Spectrochimica Acta*, 48A (1992) 893-897.
[9] Sharma, A. and Quantrill, N.S.M., *Spectrochimica Acta*, 50A (1994) 1179-1193.
[10] Tzang, C.H., Yaun, R. and Yang, M., *Biosensors and Bioelectronics*, 16 (2001) 211-219.

Nitric Oxide Sensors obtained through the entrapment of iron complexes in sol-gel matrix

Juliana C. Biazzotto, João F. Borin, Roberto Mendonça Faria[1] and Carlos F.O Graeff
Departamento de Física e Matemática-FFCLRP-USP, Av. Bandeirantes 3900, 14040-901
Ribeirão Preto, Brazil
1-Instituto de Física de São Carlos-USP, C.P. 369, 13560-970 São Carlos, Brazil

ABSTRACT

Iron(III)-diethyldithiocarbamate (Fe3DETC) or iron(III)-tetra-pentafluorophenyl porphyrin (FeTFPP) was entrapped within a silica matrix by the sol-gel process. The obtained sol-gel materials SGFeDETC and SGFeTFPP were investigated as sensors for nitric oxide (NO). UV/Vis spectra of the SGFeTFPP present a Soret band at 410 nm similar to that found in the solution. The binding of gaseous NO resulted in a red shift in the Soret absorption band (410 to 419 nm) of the FeTFPP in the matrix unlike FeTFPP:NO in solution. In the case of SGFeDETC, after addition of sodium dithionite solution and bubbling NO we have good evidence that the complex is formed. The EPR spectrum of the SGFeDETC:NO in solid form exhibited a signal similar to that found in a solution of FeDETC:NO at 77K. The UV/Vis spectrum of SGFeDETC:NO shows a band at 367 nm also found in FeDETC:NO solutions. It is observed that the FeDETC:NO is more stable entrapped in the sol-gel than in aqueous solution. In the former the EPR signal decreases by a factor of 4 after one week, in the latter in 2 days the EPR signal cannot be observed anymore.

INTRODUCTION

Nitric oxide (NO) is an important signaling molecule that acts in many tissues to regulate a diverse range of physiological processes including neurotransmission and immune defense [1,2]. Several methods for NO detection have been developed and one of the most powerful methods for directly measuring NO production in biological systems is electron paramagnetic resonance (EPR) spin trapping techniques [3]. Iron complexes with dithiocarbamates and porphyrins are used as spin traps due to the high affinity between NO and the iron complexes, however these complexes are unstable for long-term measurements. The physical entrapment of molecules using the sol-gel process [4,5] has been used for the development of NO electrochemical and optical sensors. Sensors entrapped in gels offer numerous advantages when compared with liquid based systems: they are easier to manipulate, allow species detection and concentrations measurements with less contamination of the sample, can be used for continuous sensing, and are normally more stable. In the case of silica gels a further advantage is that it is transparent in the UV/visible/near infrared range, which makes this material especially interesting for optical sensors. For EPR measurement of special interest is the fact that solutions are in general hard to measure since liquids have high dielectric losses, or in other words they absorb microwaves thus killing the Q of the resonance cavity. EPR quartz liquid cells are necessary when liquids are to be measured by EPR, which are expensive and impose restrictions in what concerns the concentration of paramagnetic species. Thus by entrapping the paramagnetic species in a solid is of great interest for EPR. In this work we report the synthesis of the NO sensors, SGFeDETC and SGFeTFPP, which consist in the entrapment of the spin

trappings iron(III)-diethyldithiocarbamate (Fe3DETC) or iron(III)-tetra-
pentafluorophenylporphyrin (FeTFPP), within an inorganic matrix by the sol-gel process.

EXPERIMENTAL DETAILS

Synthesis of SGFeDETC. Tetraethyl orthosilicate (Aldrich) (TEOS, 4,00 mL), ethanol (4,00
mL) and concentrated HCl (150 uL) was sonicated for 10 min. After that, Triton X100 (VETEC)
(50 uL) was added to a silica sol and the resultant solution added to the Fe3DETC (Aldrich) in
dimethylformamide (DMF) (ratio DETC:Fe, 2:1). The mixture was maintained under stirring for
15 hours and allowed to stand at 30° C for aging.
Synthesis of SGFeTFPP. TEOS (4,00 mL), ethanol (4,00 mL), HCl 0,1 M (50,0 uL), water (310
uL) and Triton X100 (40,0 uL) was sonicated for 10 min. The resultant solution was added to the
FeTFPP (Midcentury) in dichloromethane (DCM). The mixture was maintained under stirring
for 2 hours and allowed to stand at 30° C for aging.
NO generation. Gaseous NO was obtained in the reaction of metallic copper and aqueous
solution of HNO_3 and passed through a trap containing concentrated NaOH solution.
Preparation of the iron nitrosyl SGFeDETC:NO. Sodium dithionite ($Na_2S_2O_3$) was added to a
piece of SGFeDETC in water. After 10 min. the material was removed, added to a saturated
aqueous NO solution and allowed to stand for 5 minutes.
UV/Vis spectra (Varian, Cary 50 spectrophotometer) were recorded using a 0.2-cm path length
quartz cell with a grounded material in DCM. For sol-gel iron nitrosyl complexes, NO gas was
bubbled in a suspension of grounded sol-gel materials and degassed DCM.
EPR (computer interfaced Varian E-4 X-Band spectrometer) was performed using a quartz tube
and a cryostat for measurements at 77K and flat cell at room temperature.


RESULTS AND DISCUSSION
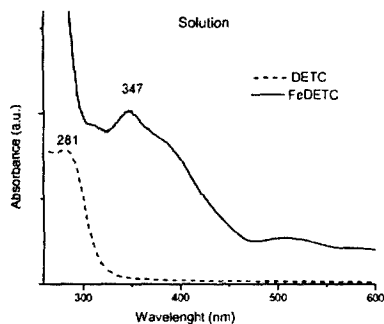
**Figure 1**. Absorption spectra of Fe3DETC and
DETC in DCM.
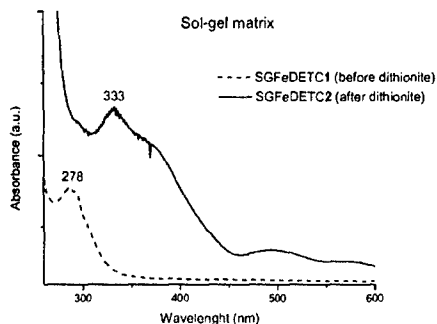
Figure 2. Absorption spectra of SGFeDETC1 and
SGFeDETC2 in DCM suspension.

The sol-gel materials containing Iron(III)-diethyldithiocarbamate (Fe3DETC) and iron(III)-tetra-pentafluorophenylporphyrin were done by adding a polymeric mixture (colloidal) to an iron (III) complexes solution. The gelation process involves the hydrolysis and condensation of ethoxyl groups of TEOS to generate siloxane bonds in the gel [6]. The evaporation of the solvents leaded to a dry solid with a glassy appearance containing the ironcomplexes caged into the pores of the silica matrix.

Fe3DETC in DMF is brown in color but after addition of the colloidal solution and stirring about 3 hours its color changes to clear yellow and remains in the final glass material. Figure 1 shows the UV/Vis spectra of the Fe3DETC and DETC in solution and Figure 2 present the spectra of SGFeDETC before (SGFeDETC1) and after (SGFeDETC2) sodium dithionite. We observed that Fe^{3+} complex exhibits three absorption bands at 347, 385 and 510 nm [7] while SGFeDETC1 a band at 278 nm. Therefore, the spectra are not similar and indicate that the iron (III) complex is formed just after the addition of sodium dithionite. A possible explanation is that the protonation of the NCS_2^- group of the complex $(CH_3CH_2)_2NCS_2^- $--$Fe^{3+}$--$^-S_2NC(CH_2CH_3)_2$ through the HCl present in the medium, leads to the iron decomplexation. In fact, SGFeDETC1 spectrum is similar to the DETC spectrum with bands at 278 and 281 nm respectively. With addition of a reducing agent, dithionite solution, to SGFeDETC1, the glass gradually changed its color to brown and the spectrum (Fig. 2) became similar to that Fe3DETC solution (Fig. 1). Thus, probably the reducing agent removed the proton of NCSH groups restoring the anion, which than can complex with Fe^{3+}, regenerating the Fe3DETC inside of the matrix. Nevertheless, it was observed a 14 nm blue shift in the optical absorption bands of the SGFeDETC2 with respect to the one found in solution, which can be attributed to changes of the molecule geometry induced by the rigid environments [8].
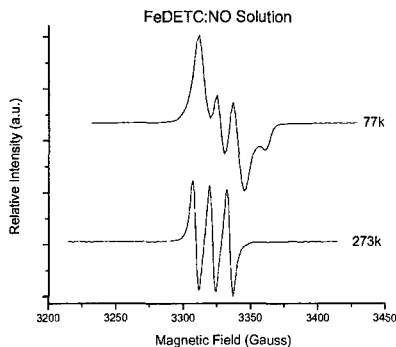
Figure 3. EPR spectra of the FeDETC:NO in DMF at 273K and 77K. Microwave power of 20 mW and modulation amplitude of 1.6 G.
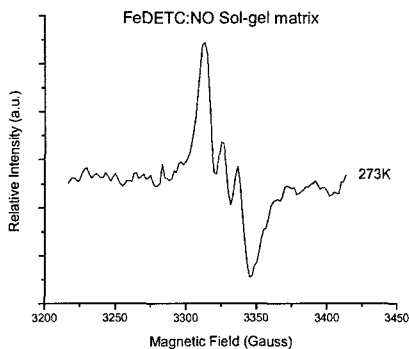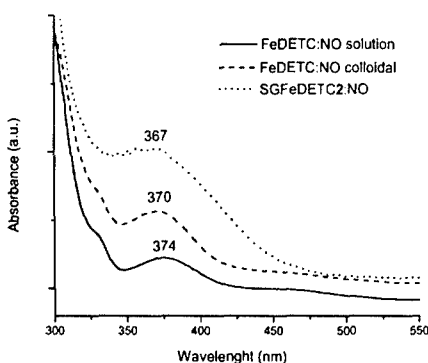
Figure 4. EPR spectra of the SGFeDETC2:NO at 273K. Microwave power of 20 mW and modulation amplitude of 1.6 G.

Although only Fe2DETC:NO shows a characteristic signal in the EPR spectrum, it was reported that diamagnetic Fe3DETCNO is gradually converted into paramagnetic Fe2DETC:NO [7]. Likewise we observed that by exposing the SGFeDETC1 to dithionite and NO, the glass changes its color from brown to green, which is the characteristic color of the iron

nitrosylcomplex. Figure 3 displays the EPR spectra of the FeDETC:NO solution (room temperature and 77K) and Figure 4 SGFeDETC2:NO spectrum at room temperature.

It's interesting to note that EPR spectrum of the FeDETC:NO in solution gave a characteristic three line signal at room temperature (g = 2,035) while ironnitrosyl complex caged in the matrix exhibit an EPR signal analogous to that FeDETC:NO at 77K (axial symmetry). This result indicates, in good agreement with the UV\VIS observations that the rigid environment of the silica matrix has important effects on the electronic properties of FeDETC:NO. The fact that the complex in the gel behaves like the freeze solution is a clear indication that the molecule rotations are hindered when encaged.

Further evidence for the formation of FeDETC:NO complex inside the gel can be obtained from the UV\VIS spectra. In Figure 5 the absorption spectrum of FeDETC:NO in solution, in the colloid as well as in the glass are shown. Notice the bands at 318, ~374 (more intense) and 498 nm are present in all spectra, however for the glass the band at ~367 nm is more prominent.

Figure 5. Optical absorption spectra of FeDETC:NO solution, FeDETC:NO colloidal and SGFeDETC2:NO (after addition of dithionite and NO).

The stability of the SGFeDETC2:NO is enhanced when compared to FeDETC:NO solutions. As can be seen in Figure 6 the EPR signal found in SGFeDETC2:NO can be measured even after seven days, with a decrease of a factor 4 in its intensity. On the other hand the EPR signal of FeDETC:NO aqueous solution kept at room temperature, is absent after two days, which means a decrease by at least a factor of 20 in the period. In fact the behavior of the SGFeDETC2:NO EPR signal is more complex, it increases at first, followed by a decrease. The increase in stability is not clearly understood, however it may be related to the rigidity of the complex environment as revealed by the EPR spectra, see figure 4. A more comprehensive discussion of the dynamics of NO in this hybrid material shall be discussed elsewhere.
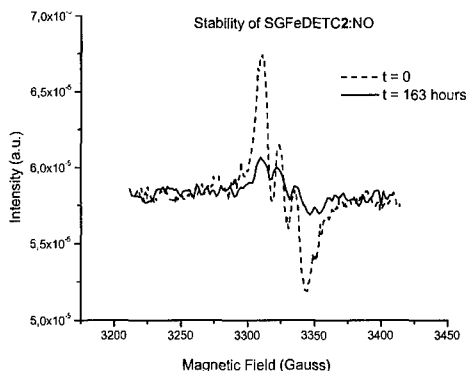
Figure 6. EPR spectra of the SGFeDETC2NO in t = 0 and after t = 163 hours. Microwave power of 20 mW and modulation amplitude of 1.6 G at 273K.

The absorption spectra of FeTFPP in solution and in sol-gel matrix are shown in Figure 7 and Figure 8, respectively. No changes in the band at 355 nm, Soret band (411 nm) and Q-band (509 nm) were observed for FeTFPP entrapped in the sol-gel matrix compared to the solution. Upon addition of NO, the Soret absorption of FeTFPP solution is red shifted to 424 nm and the band at 540 nm replaces that one at 509 nm. For SGFeTFPP:NO we observed a smaller displacement of the Soret band (411$\longrightarrow$419 nm) than in solution (Fig. 8) and the appearance of the band at 540 nm. This suggests that either a change in the binding affinity occurred due the entrapment or that the concentration of NO we have used was not enough to saturate the Fe complex inside the sol-gel material.
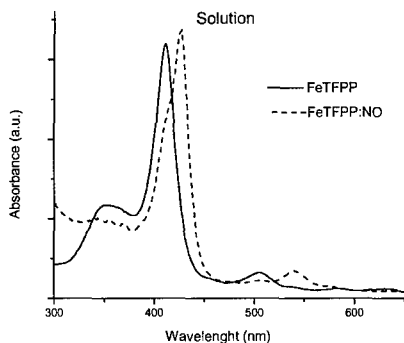
Figure 7. Optical absorption spectra of FeTFPP and FeTFPP:NO in DCM.
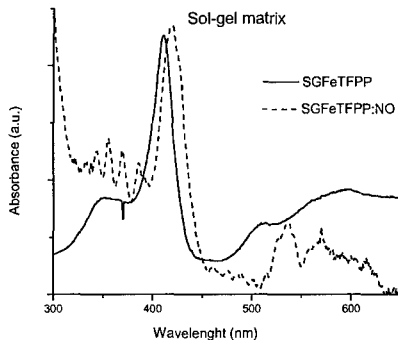
Figure 8. Optical absorption spectra of SGFeTFPP and SGFeTFPP:NO in DCM.

Notice that the changes in the band at 355 nm are inconclusive due to the fact that NO_2 molecules also absorb in this same region of the spectrum [9]. Thus its is hard to separate the effects of NO to this band, since we certainly have NO_2 in our sample too.

CONCLUSIONS

A new solid material containing the spin trap FeDETC entrapped in the silica matrix was obtained with interesting characteristics for EPR applications. The formation of this new hybrid material was done by adding FeDETC to the silica colloidal solution. Nevertheless it was found from UV/Vis analysis that in this stage the iron decomplexes probably due to acidic medium. It is necessary to add a reducing agent, in our case sodium dithionite, to restore the ironcomplex inside the matrix. Both SGFeTFPP and SGFeDETC can be used to bind NO as observed by UV/Vis and EPR results. SGFeDETC after NO binding gave, at room temperature, an EPR signal, which was found to be more similar to that in FeDETC:NO solutions at 77K than at room temperature. This effect was attributed to the rigid environment found in the gel, which changes the electronic properties of the complex. The stability of the FeDETC:NO complex was enhanced when entrapped. It was observed that SGFeDETC:NO can be kept at room temperature for many days with a small effect in the EPR signal, contrary to what is found in the solution. The results demonstrated that the hybrid material comprised of the sol-gel and spin traps are promising for NO EPR based or optical sensors.

ACKNOWLEDGEMENTS

REFERENCES

1. J. Garthwaite and C.L. Boulton, Annu. Rev. Physiol. **57**, 683 (1995).
2. J.B. Hibbs Jr., R.R. Taintor and Z. Vavrin, Science **235**, 473 (1987).
3. Y. Kotake, Methods Enzymol. **268**, 222 (1996).
4. S. Trévin, F. Bedioui and J. Devynck, J. Electroanal. Chem. **408**, 261 (1996).
5. D.J. Blyth, J.W. Aylott, J.W.B. Moir, D.J. Richardson and D.A. Russell, Analyst **124**, 129 (1999).
6. R.J.P. Corriu and D. Leclercq, Angew. Chem. Int. Ed. Ingl. **35**, 1420 (1996).
7. A.F. Vanin, X. Liu, A. Samouilov, R.A. Stukan and J.L. Zweier, Biochim. Biophys. Acta **1474**, 365 (2000).
8. Maruszewski, J. Mol. Struct. **479**, 53 (1999).
9. A.F. Vanin, Biochemistry **60**, 441 (1995).

O6.7

A SELF-LOCKING TECHNIQUE WITH FAST RESPONSE AND HIGH SENSITIVITY FOR MICRO-CANTILEVER BASED SENSING OF ANALYTES

A. Mehta, G. Muralidharan, A. Passian, S. Cherian T.L. Ferrell and T. Thundat.[*]
Life Sciences Division, Oak Ridge National Lab, Oak Ridge, TN 37831

ABSTRACT

MEMS based microcantilevers have been employed as sensors in both liquid and ambient conditions. One scheme for detection is based upon monitoring the change in microcantilever resonant frequency as a function of the adsorbed analyte concentration. However, the sensitivity is limited by the accuracy of the frequency measurements, which is a function of the Q-factor of the vibrating element and the measurement bandwidth. In this paper, we present a feedback scheme for self-locking amplification of the small-amplitude thermal oscillations of the microcantilever. Using this approach, we demonstrate an improvement in the Q-factor by two to three orders of magnitude as compared to that of the undriven microcantilever. Use of this technique eliminates the need for lock-in detection and results in improved response times for sensor applications. Experiments using the proposed feedback amplification technique show improved sensitivity for the detection of biological molecules in liquids, and for adsorbed vapors under ambient conditions.

INTRODUCTION

The field of chemical and biological sensing is increasingly turning to microelectromechanical systems (MEMS) based devices to perform rapid measurements of specific chemical species with high selectivity and sensitivity. Microcantilevers used for imaging in atomic force microscopes show a response because of interatomic forces between the surface and the cantilever tip. This phenomenon has been exploited to use the cantilever as a sensor/transducer giving birth to a new class of chemical and biological sensors [1,2,3,4]. In such sensors, the microcantilever surface is treated with a specific coating or receptor molecules. On exposure to the sample, the target molecules bind to the surface. This step can be detected by either monitoring the deflection of the cantilever (DC detection) or by measuring the change in its resonant frequency (AC detection). Various techniques such as optical beam deflection, variation in piezoresistive, capacitive or piezoelectric response are used to quantify the amount analyte bound. Microcantilever sensors developed for gas phase environments have been demonstrated to have a picogram mass resolution [5]. For many applications, especially for biological samples, sensors need to function in a liquid environment. The development of microcantilever based sensors for detection in liquid faces two drawbacks: (i) a drift in the cantilever deflection due to thermal fluctuations in the flow chamber[6] and (ii) the reduction in the quality factor (Q) of the microcantilever when it is immersed in liquids [7,8] Cantilevers exhibit a measurable amplitude of vibrations due to thermal or ambient induced oscillations [9,10]. With an increasing trend towards miniaturization, manipulation and control of thermal motion of microcantilevers can result in simpler, cheaper and portable devices.

---

[*] Author to whom correspondence should be addressed

Typical amplitude of vibration of a microcantilever with a spring constant of 0.1 N/m is approximately 0.1 nm. This amplitude is too small which limits its applicability in detection, imaging and sensing. For typical microscopy and sensing applications, such cantilevers are used with a piezoelectric bimorph, which are driven with a frequency close to the natural resonant frequency of the cantilever thus enhancing the amplitude of vibrations [9]. Recently, various methods have been attempted to control the dynamics of cantilever vibrations in an effort to improve the sensitivity of the cantilever of both imaging and sensing applications [11,12,13]. It has been shown recently that by modifying the input signal to the piezoelectric bimorph, the vibrating characteristics of the cantilever can be favorably modified. Alternatively, it has also been shown that the thermal vibrations of the cantilever can be amplified and used to drive the cantilever in a feedback mode with a resultant large increase in the Q factor of the cantilever [8]. In this paper, we utilize the self tuning amplification phenomena of the phase shifted feedback signal to demonstrate its applicability in sensing applications in gas and liquid environments. This technique improves the minimum detectable frequency shift thus improving the sensitivity of detection. By eliminating the need for external excitation of the cantilever using frequency sweep generator, fast kinetics of adsorption and binding to surfaces can also be studied.

EXPERIMENTAL METHOD

Commercially available V-shaped silicon nitride and silicon cantilevers (Thermomicroscopes) were used without any modifications for these studies. Typical dimensions of the cantilevers were, length: 100-200 μm; width: 20-40μm; and thickness: 0.7-1μm. These were mounted in a cantilever holder used for tapping mode atomic force microscopy with a built-in piezoelectric bimorph that drives the cantilever (Digital Instruments). The motion of the cantilever was detected using a laser beam reflected off the free end of the cantilever into a split-quadrant photo-diode. Figure 1 shows a schematic diagram of the experimental setup used. Briefly, The vertical difference output from the photo-diode was routed through a variable gain amplifier and phase shifter before it was applied to the piezoelectric bimorph of the cantilever holder. The vertical difference signal was analyzed in the frequency domain using an FFT spectrum analyzer.
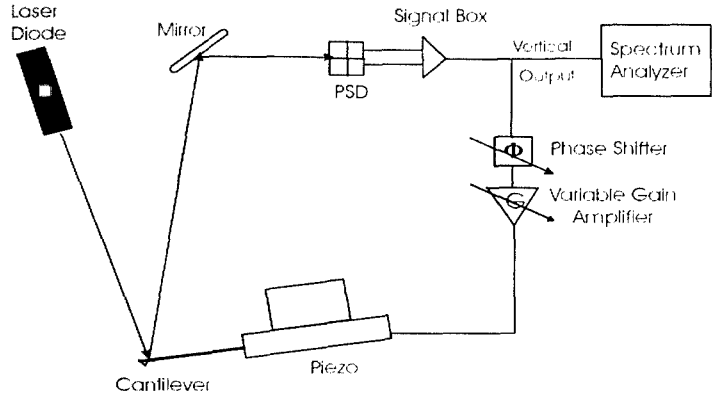

FIGURE 1. Schematic diagram of the experimental setup for measurements of cantilever resonance with a feedback loop. The laser diode, position-sensitive detector and associated electronics were housed in a commercially available head used for atomic force microscopy.

For gas phase experiments, silicon cantilevers were exposed to TNT vapors by placing a piece of solid TNT 2-3 cm below the cantilever surface. The vapor pressure of TNT near the cantilever was varied by changing the temperature of the solid piece of TNT placed in the oven. A shutter was used to control the start and end of exposure. Experiments in liquids were done in a fluid cell (Digital Instruments) with a reservoir volume of 300 µl. The cantilever was placed in phosphate buffered saline (PBS) and allowed to equilibrate for two hours. A syringe pump (IITC Inc.) was used to pump buffer solution and the analytes through the flow cell. After equilibration 1 ml of biotin (0.2 mg/ml) was injected through a multiport injection valve (Upchurch Scientific), and approximately 2 h later 1 ml of neutravidin (0.2 mg/ml) was injected. The resonant frequency was monitored as a function of time under feedback driven conditions.

RESULTS AND DISCUSSION

Figure 2 shows the frequency response of the cantilever in air (A) and in liquid (B) to thermally induced vibrations. Typical amplitudes of cantilever due to thermal oscillations in air and water range from 0.01 to 0.1 nm (shown as solid lines in Figure 2). The fundamental resonant frequency of the cantilever is reduced due to the increased viscous drag effects in water. Secondly, and more importantly the Q factor decreases dramatically from approximately 20 in air to 1.8 in water. This is due to the hydrodynamic damping between the cantilever and the liquid environment. The amplitude of the oscillations is of the order of a few hundred microvolts. The frequency response of the feedback driven cantilever is shown in solid lines in Figure 2. The amplitude of cantilever oscillations was three orders of magnitude higher in both air and liquid. More significantly, the Q factor improved to 2975 (in air) and 20 (in water). In liquid medium detection of the fundamental frequency using a piezo bimorph by external sweeping is complicated by the appearance of multiple peaks due to excitation of acoustic waves in the reservoir. The feedback amplification technique eliminates the need for an external frequency sweep signal as it locks to the fundamental resonant frequency of the vibrating cantilever.
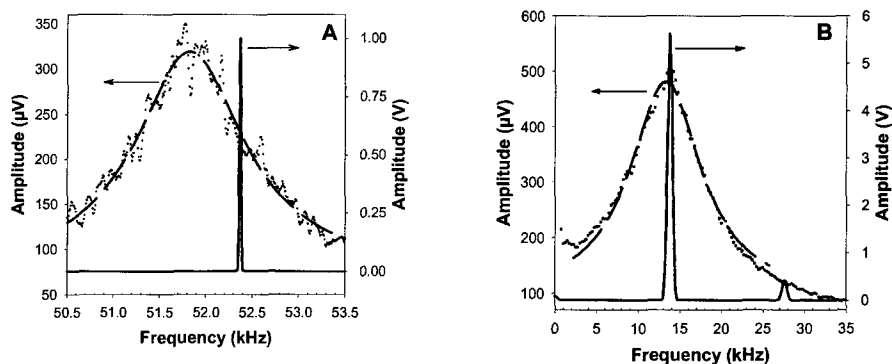
FIGURE 2. Frequency spectra for a Si_3N_4 cantilever (length = 100 µm; spring constant, k = 0.32 N/m) in (A) air, and (B) water. The raw data for undriven vibrations is shown by solid circles, the Lorentzian fit is shown by the dashed lines and the phase shifted feedback driven response is shown by solid lines.

For thermally induced (undriven) vibrations the resonance peak appears as a very broad peak with full width at half maximum (FWHM) = 8.5 kHz, (Figure 2B, dashed line). The vibrations due to the phase shifted and amplified feedback drive signal in liquid exhibited a significantly sharper peak with FWHM = 0.65 kHz, as shown in Figure 2B (solid line). The amplitude was amplified by three orders of magnitude, and the Q-factor improved from 1.8 to 19. Due to the smaller FWHM, frequency measurements can be made at a smaller linewidth setting for the spectrum analyzer. This improves the minimum detectable frequency shift ($\Delta\omega$) from 15 Hz for the undriven motion to 1 Hz for the feedback driven cantilever. Similar results were also observed for rectangular, silicon cantilevers.

For detection in gas phase environments, the adsorption of TNT vapors on the cantilever surface was studied. Figure 3 shows the variation in resonant frequency of the microcantilever as a function of time when its surface was exposed to TNT vapors by opening the shutter. As increasing amounts of TNT were adsorbed on the surface of the cantilever, the increase in its effective mass resulted in a drop in the fundamental resonant frequency (ω_0). The minimum detectable shift in frequency, $\Delta\omega$, is approximately ω_0/Q. Thus, an increase in the Q factor by 2-3 orders of magnitude improves the resolution of detection significantly. Figure 3 (inset) shows that feedback driven technique allows rapid frequency shift measurements. When employing the traditional frequency sweep method to detect small shifts in resonant frequency, the resolution bandwidth of the frequency detection device needs to be reduced which increases the sweep time for each acquisition cycle. Since the feedback drive signal is always locked to the fundamental resonant frequency of the vibrating cantilever, this problem is circumvented, allowing for rapid measurements. Thus, this technique could be used for kinetic measurements of adsorption/desorption studies.
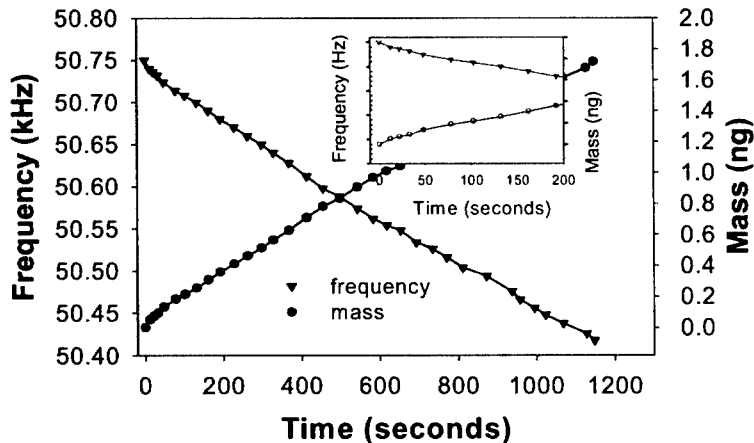
Figure 3. Variation in the resonant frequency of the feedback driven microcantilever and the adsorbed mass as a function of time during adsorption of TNT. Inset shows data for the first 200 sec.

to bind to the gold-coated side of the cantilever. The resonance frequency of the cantilever dropped as a function of biotin binding from 9.67 kHz to 9.35 kHz, as shown in Figure 3. Subsequent injection of neutravidin, which binds to the biotin on the cantilever, showed a further drop of 1.7 kHz in the fundamental resonance frequency. The sensitivity of feedback driven cantilever sensors is improved due to the higher Q factor. The minimum detectable mass (Δm_{min}) for a cantilever is proportional to $\Delta\omega/\Delta\omega_0$. Since the minimum detectable frequency shift is markedly improved with the feedback, the sensitivity improved by an order of magnitude. By attaching specific receptors or antibodies to the surface of the cantilever, these sensors can designed to exhibit selectivity for specific analytes.
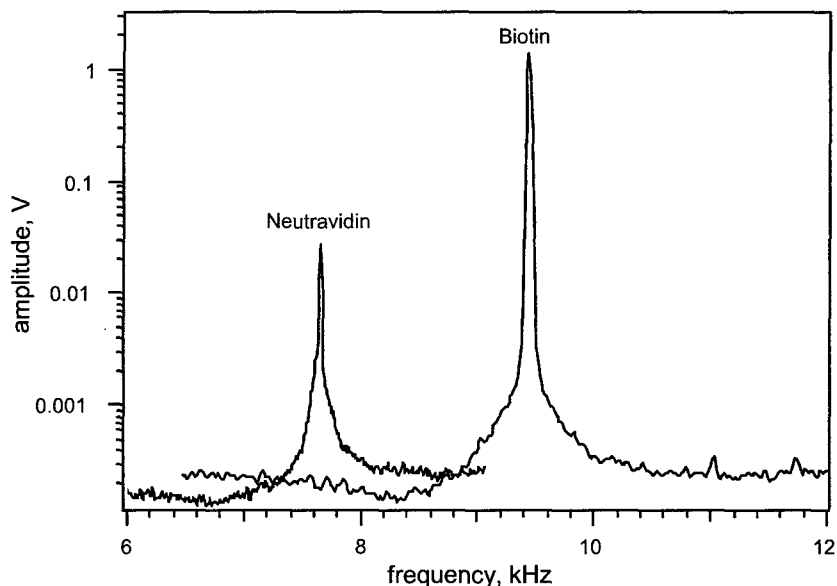
FIGURE 4. Resonant frequency shift of a feedback driven Si_3N_4 cantilever in PBS during binding with biotin and neutravidin at different times (1) 25 min, $\omega_0 = 9.656$ kHz, (2) 30 min., $\omega_0 = 9.437$ kHz, (3) 60 min., $\omega_0 = 9.434$ kHz. After two hours, neutravidin was injected and allowed to bind with the same cantilever. (4) 15 mins. after neutravidin injection, $\omega_0 = 7.648$ kHz.

CONCLUSIONS

The applicability of feedback enhanced amplification of thermal oscillations of microcantilevers for use in sensors has been demonstrated in ambient and liquid environments. The sensitivity of detection is significantly improved due to the increase in the Q factor of the cantilever. The

improvement in the resolution bandwidth for frequency shift measurements also makes this technique applicable for kinetic studies of adsorption.

ACKNOWLEDGEMENTS

REFERENCES

1. Chen, G. Y., Thundat, T., Wachter, E. A., and Warmack, R. J., Journal Of Applied Physics. 77, 3618-3622 (1995).
2. Thundat, T., Warmack, R. J., Chen, G. Y., and Allison, D. P., Applied Physics Letters. 64, 2894-2896 (1994).
3. Fritz, J., Baller, M. K., Lang, H. P., Rothuizen, H., Vettiger, P., Meyer, E., Guntherodt, H. J., Gerber, C., and Gimzewski, J. K., Science. 288, 316-318 (2000).
4. Raiteri, R., Nelles, G., Butt, H. J., Knoll, W., and Skladal, P., Sensors and Actuators B-Chemical. 61, 213-217 (1999).
5. Thundat, T., Wachter, E. A., Sharp, S. L., and Warmack, R. J., Applied Physics Letters. 66, 1695-1697 (1995).
6. Butt, H. J., Journal of Colloid and Interface Science. 180, 251-260 (1996).
7. Tamayo, J., Humphris, A. D. L., Malloy, A. M., and Miles, M. J., Ultramicroscopy. 86, 167-173 (2001).
8. Mehta, A., Cherian, S., Hedden, D., and Thundat, T., Applied Physics Letters. 78, 1637-1639 (2001).
9. Sarid D, Oxford Series on Optical Sciences, (1991).
10. Vig, J. R. and Kim, Y., Ieee Transactions On Ultrasonics Ferroelectrics And Frequency Control. 46, 1558-1565 (1999).
11. Durig, U., Steinauer, H. R., and Blanc, N., Journal of Applied Physics. 82, 3641-3651 (1997).
12. Albrecht, T. R., Grutter, P., Horne, D., and Rugar, D., Journal of Applied Physics. 69, 668-673 (1991).
13. Tamayo, J., Humphris, AD L., and Miles, M. J., Applied Physics Letters. 77, 582-584 (2000).

Chemical Sensing With Resistive Microcantilevers

G. Muralidharan[1], A. Wig[1], L. A. Pinnaduwage[1], D. L. Hedden[1], P. G. Datskos[1], T. Thundat[1], and R. T. Lareau[2]
[1]Oak Ridge National Laboratory, Oak Ridge, TN-37831-6123.
[2]Federal Aviation Administration, Atlantic City, NJ 08405.

ABSTRACT

MEMS-based microcantilevers have been proposed for a variety of biological and chemical sensing applications. Measuring the magnitude of microcantilever deflection due to adsorption-induced bending, and following the variation in the resonant frequency of the microcantilevers due to the adsorbed mass are two techniques commonly employed for sensing analytes. Apart from possessing a high level of sensitivity to small changes in mass, microcantilevers are also very sensitive to small changes in temperature and hence the flow of heat. One way of achieving high sensitivity in thermal measurements is by using a bimaterial microcantilever and measuring its deflection as a result of thermal fluctuations. Commercially available piezoresistive microcantilevers are an example of bimaterial cantilevers and in this study, we propose the use of such cantilevers for sensing explosives. We show that sensing can be accomplished by following the differences in the thermal response of the cantilevers introduced by the presence of explosives adsorbed from the vapor phase onto the surface of the cantilever. We discuss the issues involved in determining the sensitivity of detection and selectivity of detection.

INTRODUCTION

Real-time detection of explosives is important for practical applications ranging from passenger baggage-screening to the disarming of landmines. With their compactness and potential low cost, detection techniques based on Silicon-based Micro Electro-Mechanical Systems (MEMS) provide a path for the development of miniaturized sensors. One method for detecting explosives is through the detection of vapors in equilibrium with the solid explosive [1]. To design devices that would detect explosive chemicals such as TNT through detecting the presence of their vapors, a detailed understanding of the physical chemistry parameters involved in vapor transport, knowledge of the diffusion coefficients, molecular sticking coefficients and vapor pressures over non-ideal solid solutions are all of importance[2]. In addition, detailed knowledge of the interaction of such explosive vapors with exposed surfaces is of interest. For example, it would be of interest to know how much vapor would adsorb and stick to the sensing surface over a certain period of time under typical conditions at which the sensor would be used. Although data are available on the long-term adsorption and desorption of vapors such as TNT from surfaces of soils [3], very little data is available on the short-term behavior related to surfaces that would be common in MEMS. This information along with the known minimum detectable quantity would determine the time necessary for detection. In addition, knowledge of the relative affinities of different surfaces to these vapors would help in designing surfaces that would maximize sensitivity while minimizing detection time.

One characteristic of explosives that make detection of vapors difficult is their very low equilibrium vapor pressures at room temperature. For example, it is very well known that for TNT, this is in the range of ppb_v at room temperature. Under conditions where dilution is possible, such as in an open atmosphere, it is expected that the vapor pressures will be in the of ppt_v range [2]. Hence the technique used to measure the adsorption of TNT onto surfaces has to be sensitive to measure small changes in the amount of adsorbed analyte. Various studies in the past have shown that MEMS-based microcantilevers can be used for a wide range of chemical and biological sensing applications with very high level of sensitivites [4-8]. It has been demonstrated that sensing using cantilevers can be established either through the measurement of changes in its resonant frequency or through the measurement of bending induced by changes in surface stress. Resonant frequency changes are caused by the adsorption of the analyte onto the surfaces of the cantilever with a resultant change in the overall mass. On the other hand, bending is induced in the cantilever when the two surfaces of the cantilever have different affinities for the analyte which results in differential adsorption. Prior studies shown that pg-level mass resolution can be achieved when cantilevers are used for sensing changes in mass using the changes in the resonant frequency of the cantilever [8]. Selectivity in these experiments is achieved by coating one of the two surfaces of the cantilever with a chemical that interacts preferentially with the analyte of interest. Chemicals, self-assembled monolayers, and polymers have been used in previous studies to achieve selectivity [7,9].

In the current study, we present a method that uses uncoated piezoresistive cantilevers as the sensing element. We follow the adsorption and desorption of TNT from a Si/SiO_2-surface exposed to the vapors using the variation in the resonant frequency of the cantilever. During adsorption, the resonant frequency of the cantilever decreases due to an increase in mass while the resonant frequency of the cantilever increases during desorption since the total mass associated with the cantilever decreases. After the desired amount of TNT has been adsorbed onto the surface of the cantilever, the microcantilever is rapidly heated to induce reactions on its surface due to the presence of TNT. We show that the response of the piezoresistive cantilever to an applied voltage varies with the amount of TNT adsorbed on its surfaces. We discuss how this methodology can be used to selectively detect TNT. This technique is versatile since such studies are conducted with "real-surfaces" and at ambient conditions.

EXPERIMENTAL METHOD

Figure 1 shows a schematic of the experimental setup. The setup used for the measurements was designed to follow the time-dependent behavior of the microcantilever using light reflected from the surface of the cantilever. A red solid-state laser was used as the light source while a two-quadrant Position Sensitive Detector (PSD) converts the reflected light signal into a voltage that is proportional to the position of the light incident on the detector. Commercially available piezoresistive microcantilevers were used for these experiments since the piezoresistive layer can be used as a heating element to rapidly heat the cantilever. Figure 2 shows a Scanning Electron Microscope image of the commercially available microcantilevers.

To follow the changes in resonant frequency, the piezoresistive microcantilevers were driven using a speaker in the "feedback" mode. It has been shown previously that this method of
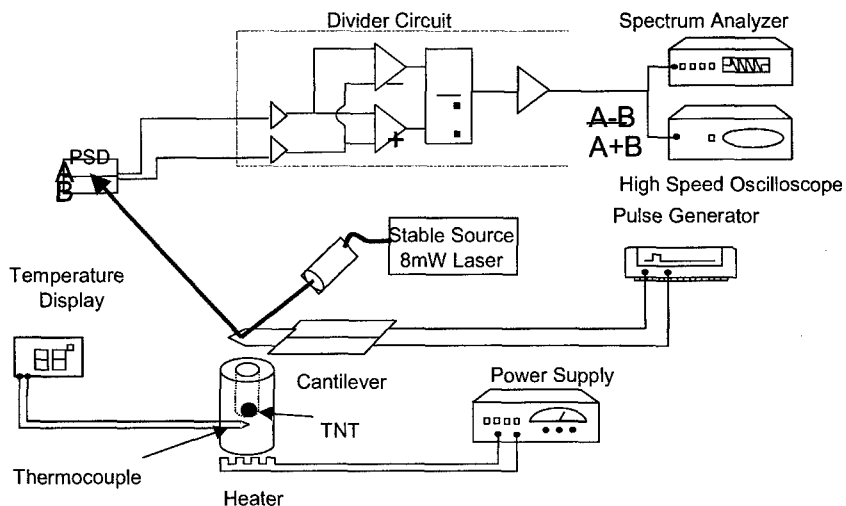
Figure 1. Schematic Showing Key Components of the Experimental Setup

excitation results in high-Q factors and hence better accuracy in real-time, fast data collection [10]. In contrast to the case where the cantilever is driven using an external signal generator source, this method is quicker since the cantilever is "self-tuning" and no external tuning of drive frequency is necessary. The frequency response of the microcantilever was measured using a high-speed digitizer /spectrum analyzer. The source of TNT vapor is a solid piece of TNT positioned at a distance of about 2-3 cm directly beneath the bottom surface of the microcantilever. The vapor pressure of TNT near the cantilever is varied by changing the temperature of the solid piece of TNT placed in the oven. A shutter is used to control the start and end of exposure. After the desired amount of TNT is adsorbed on the cantilever (as indicated by the change in resonant frequencies), a single square voltage pulse of magnitude 10 Volts is applied across the cantilever and the response of the microcantilever to this voltage pulse is followed as a function of time.

RESULTS AND DISCUSSION

Figure 2. SEM Image of a Typical Piezoresistive Micro cantilever used for the Experiments.

Figure 3 shows the variation in resonant frequency of the microcantilever as a function of time when its surface was exposed to TNT vapors by opening the shutter. Before exposure to the TNT vapor, the surface was cleaned by resistively heating the microcantilever. The temperature of the oven

containing the solid TNT was maintained at 66°C while the cantilever was maintained at room temperature. This temperature of TNT was selected to enable adsorption of TNT onto the surface of the cantilever over a reasonably short period of time. However, the technique can also be used to monitor the adsorption of TNT at lower partial vapor pressures as would be observed when the TNT is maintained at lower temperatures. Note that the frequency decreases as a function of time and that the frequency changes fairly rapidly over a period of 15 minutes. This reduction in frequency can be attributed to an increase in the total cantilever mass, showing clearly that TNT adsorbs and sticks to the cantilever surface. From a knowledge of the mass of the microcantilever, the frequency change can be correlated to a change in mass using the expression

$$\left(\frac{f_0^2}{f_1^2} - 1 \right) m_0 = \delta m , \qquad (1)$$

where f_0 denotes the resonant frequency before adsorption of TNT, f_1 denotes the resonant frequency of the microcantilever after adsorption of TNT, m_0 the initial mass of the microcantilever, and δm is the change in mass of the cantilever. The increase in mass attributable to the adsorption of TNT is calculated using equation (1) and an initial cantilever mass of 130 ng and is shown on the right axes of the figures.

Figure 4 shows the variation in frequency after closing the shutter thus shutting off the source of TNT vapor. Note that the frequency increases gradually and returns to its original frequency over a period of over six hours indicating that the TNT that had adsorbed previously, desorbs from the surface of the microcantilever. It is important to note that desorption does occur under ambient conditions. Also to be observed are the relative values of the time-scales for adsorption and desorption. Note that under typical ambient conditions, it takes a relatively long period of time (many hours) to desorb the few nanograms of adsorbed TNT.

Figure 5 shows the response (voltage output from the PSD) of the cantilever as a function of time to an applied constant voltage pulse along with the effect of adsorbed TNT on the cantilever response. It should be noted that the settling time of the applied voltage is of the order of a few microseconds while the microcantilever response time to reach maximum deflection (for this particular cantilever) is of the order of 1 millisecond. Thus, thermal equilibrium between the microcantilever and its surroundings and not the rate of application of the voltage affects the
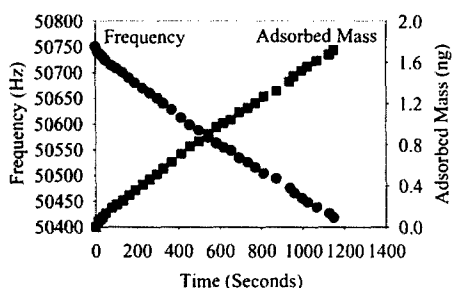
Figure 3. Variations in Cantilever Resonant Frequency and Adsorbed Mass as a Function of Time During Exposure to TNT Vapors.
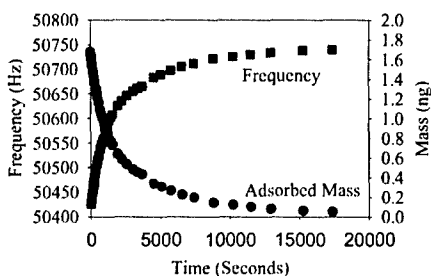
Figure 4. Variations in Cantilever Resonant Frequency and Adsorbed Mass as a Function of Time After the Removal of TNT Vapors.

rate of temperature rise within the cantilever. The variation in output voltage as a function of time shown in the figure can be understood based upon the structure of the microcantilever [11]. It should be noted that the microcantilever consists of a p-type Si-substrate and a p+-Si resistive layer protected by a thin oxide layer. As current passes through the conductive layers in the cantilever, the temperature of the microcantilever rises, and the microcantilever bends due to differential thermal expansion coefficients of the materials comprising the microcantilever (bimaterial effect). Since the coefficient of thermal expansion of Si (2.6×10^{-6} /K) is much larger than that of SiO_2 (4×10^{-7} /K), for a temperature rise ΔT, the microcantilever will bend towards the SiO_2 side (downwards in this geometry) thus resulting in a negative voltage output from the PSD as is verified experimentally from the figure.

Also evident from figure 5 is the effect of TNT in modifying the response of the cantilever. Note the presence of inflections in the curve even with small amounts of adsorbed TNT, with the inflections becoming enlarged to a clear maximum (a bump) with increasing amounts of TNT. This is illustrated clearly in figure 6, which shows the difference between the response of the microcantilever with and without adsorbed TNT for three different quantities of adsorbed TNT. Calculations show that the area under the difference curve is proportional to the amount of TNT adsorbed onto the surface of the cantilever. Thus, the effect of the presence of TNT is clearly manifested in the response of the cantilever to the heating pulse.

In summary, we have shown that explosive vapors such as TNT can be adsorbed onto microcantilever surfaces and detected through their influence on the bending behavior during rapid heating of these microcantilevers. Important factors to be considered in using this technique for detecting TNT are sensitivity and selectivity. Ability to detect about 70 picograms of TNT present on the cantilever has already been demonstrated while improvement in this value can be achieved by modifying the design of the cantilever. It has been observed that a minimum applied voltage (and hence cantilever temperature) is necessary to observe the responses shown in figure 5. This provides an avenue for obtaining selectivity in the detection of TNT vapors.
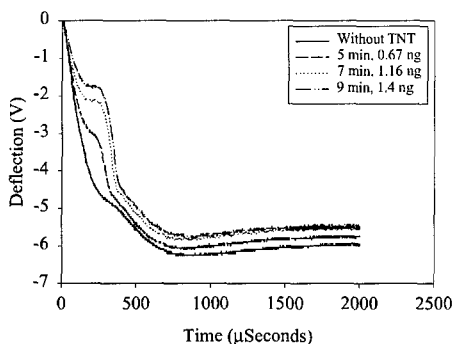
Figure 5. Effects of Varying Amounts of TNT on Cantilever Response to the Applied Voltage.
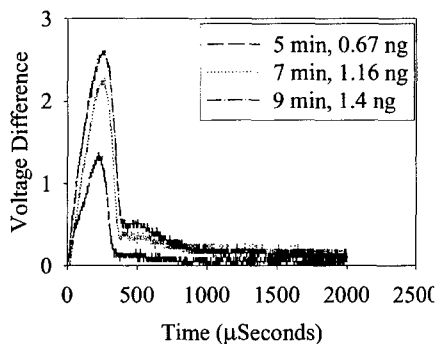
Figure 6. Differences Between the Responses of the Cantilever to the Applied Voltage in the Presence of Varying Amounts of TNT.

Preliminary analysis of the nature of the response shows that the observed effect is due to an exothermic reaction on the surfaces of the microcantilever in the presence of TNT. Further work is in progress to understand the mechanism by which the cantilever response is modified in the presence of TNT.

CONCLUSIONS

Feasibility of detecting explosives such as TNT through detecting their vapors with piezoresistive microcantilevers has been explored. Experiments clearly show that TNT vapors adsorb onto the microcantilever surface and modify the response of the piezoresistive cantilever to an applied voltage pulse that heats the cantilever. Further work is needed to map out regimes under which selectivity can be achieved in detecting TNT vapors and to establish the mechanisms of interaction and detection.

ACKNOWLEDGMENTS

REFERENCES

1. A. Fainberg, Science, **255**, 1531 (1992).
2. J. I. Steinfleid and J. Wormhoudt, Annu. Rev. Phys. Chem., **49**, 203 (1998).
3. E. Bender, A. Hogan, D. Leggett, G. Miskolczy and S. MacDonald, Journal of Forensic Sciences, **37**, 1673 (1992).
4. T. Thundat, E.A. Wachter, S. L. Sharp and R. J. Warmack, Appl. Phys. Lett., **66**, 1695 (1995).
5. T. Thundat, P. I. Oden and R. J. Warmack, Microscale Thermophys. Eng., **1**, 185 (1997).
6. T. Thundat, G. Y. Chen, R. J. Warmack, D. P. Allison, E. A. Wachter, Anal. Chem., **67**, 519 (1995).
7. Roberto Raiteri, Massimo Grattarola, Hans-Jürgen Butt, and Petr Skládal, Sensors and Actuators B, **79**, 115 (2001).
8. P. I. Oden, Sensors and Actuators B, **53**, 191 (1998).
9. Hai-Feng Ji, K. M. Hansen, Z. Hu, and T. Thundat, Sensors and Actuators B, **72**, 233 (2001).
10. A. Mehta, S. Cherian, D. L. Hedden, and T. Thundat, Appl. Phys. Lett., **78**, 1637 (2001).
11. U.S. Patent 5,595,942.

AUTHOR INDEX

SUBJECT INDEX